12

OFFICE OF NAVAL RESEARCH
Contract N00014-80-C-0213
Project NR 092-58

Technical Report
June 1987

FRACTO-EMISSION FROM POLYMERS

J. Thomas Dickinson

Washington
State University

DEPARTMENT OF PHYSICS

12

OFFICE OF NAVAL RESEARCH
Contract N00014-80-C-0213
Project NR 092-58

Technical Report
June 1987

FRACTO-EMISSION FROM POLYMERS

J. Thomas Dickinson

Department of Physics
Washington State University
Pullman, Washington 99164-2814

Approved for public release; distribution unlimited

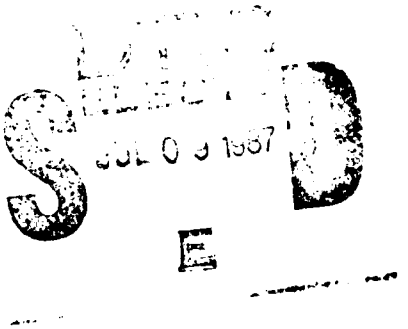

UNCLASSIFIED
SECURITY CLASSIFICATION OF THIS PAGE

AD-A183027

REPORT DOCUMENTATION PAGE

Form Approved
OMB No 0704-0188

1a REPORT SECURITY CLASSIFICATION UNCLASSIFIED	1b RESTRICTIVE MARKINGS
2a SECURITY CLASSIFICATION AUTHORITY	3 DISTRIBUTION / AVAILABILITY OF REPORT APPROVED FOR PUBLIC RELEASE; DISTRIBUTION UNLIMITED
2b DECLASSIFICATION / DOWNGRADING SCHEDULE	
4 PERFORMING ORGANIZATION REPORT NUMBER(S) FRACTO87	5 MONITORING ORGANIZATION REPORT NUMBER(S)
6a NAME OF PERFORMING ORGANIZATION FRACTURE LABORATORY DEPARTMENT OF PHYSICS 6b OFFICE SYMBOL (If applicable)	7a NAME OF MONITORING ORGANIZATION OFFICE OF NAVAL RESEARCH PROPULSION AND ENERGETICS PROGRAM
6c ADDRESS (City, State, and ZIP Code) WASHINGTON STATE UNIVERSITY PULLMAN, WA 99164-2814	7b ADDRESS (City, State, and ZIP Code) 800 NORTH QUINCY STREET ARLINGTON, VA 22217
8a NAME OF FUNDING / SPONSORING ORGANIZATION 8b OFFICE SYMBOL (If applicable)	9 PROCUREMENT INSTRUMENT IDENTIFICATION NUMBER CONTRACT N00014-80-C-0213
8c ADDRESS (City, State, and ZIP Code)	10 SOURCE OF FUNDING NUMBERS PROGRAM ELEMENT NO / PROJECT NO / TASK NO / WORK UNIT ACCESSION NO

11 TITLE (Include Security Classification)
FRACTO-EMISSION FROM POLYMERS

12 PERSONAL AUTHOR(S)
J. THOMAS DICKINSON

13a TYPE OF REPORT	13b TIME COVERED	14 DATE OF REPORT (Year, Month, Day)	15 PAGE COUNT
TECHNICAL; SUMMARY	FROM 6/1/85 TO 5/30/87	JUNE 21, 1987	171

16 SUPPLEMENTARY NOTATION

17 COSATI CODES		
FIELD	GROUP	SUB-GROUP

18 SUBJECT TERMS (Continue on reverse if necessary and identify by block number)
CRACK PROPAGATION, FRACTURE, PARTICLE EMISSION, FRACTO-EMISSION, POLYMERS, CRYSTALS, ENERGETIC MATERIALS, RDX, ELECTRON BEAM INDUCED FRACTURE, MICROCRACKING, RADIATION DAMAGE, BOND SCISSIONS

19 ABSTRACT (Continue on reverse if necessary and identify by block number)

Progress in the investigation of fracto-emission (FE) from polymers, crystalline materials, and interfaces are presented involving measurements of electron, photon, radiowave, and neutral atom and molecule emissions. We examine FE during the peeling of binder elastomer from single crystals of RDX; these emissions show FE features unique to adhesive failure. We present images of the photon emission during the peeling of adhesives. We also present mass spectroscopic measurements of the neutral particles emitted from the fractur of single crystals of MgO. In an appendix, we present results of simultaneous measurements of photon and electron emission from single crystal MgO. In addition, we present experiments on the consequences of simultaneous exposure of polymers to electron beam radiation and mechanical stress. In these studies we show that cracks can be initiated and/or propagated at stresses lower than critical stress values. The morphology of the stressed polymers plays a key role in the observed response.

20 DISTRIBUTION / AVAILABILITY OF ABSTRACT	21 ABSTRACT SECURITY CLASSIFICATION
X UNCLASSIFIED/UNLIMITED ☐ SAME AS RPT ☐ DTIC USERS	UNCLASSIFIED
22a NAME OF RESPONSIBLE INDIVIDUAL R. S. MILLER	22b TELEPHONE (Include Area Code) (202) 696-4404 / 22c OFFICE SYMBOL

DD Form 1473, JUN 86 — Previous editions are obsolete — SECURITY CLASSIFICATION OF THIS PAGE

UNCLASSIFIED

TABLE OF CONTENTS

I. TECHNICAL SUMMARY

The deformation and fracture of insulating materials and interfaces between dissimilar materials can produce excitations within materials and on fracture surfaces that lead to the emission of particles. The types of particles observed include charged particles such as electrons and ions, neutral species (atoms, molecules, and radicals), and photons (of radio, IR, and visible wavelengths). Taken together, we call this emission *fracto-emission* (FE). Our studies to date have emphasized measuring the characteristics of this emission, determining emission mechanisms, and to examine the relations between FE and the nature of the fracture event (locus of fracture, crack velocity, charge separation and bond breaking phonomena, etc.).

In this report we present results on the fracture of model propellents and measure for the first time the FE during the peeling of binder elastomer [HTPB and GAP] from single crystals of RDX. We show that these emissions exhibit FE features unique to adhesive failure. We also present images of the photon emission during the peeling of adhesives created by peeling household adhesive tapes from Poloroid Film or from optical fiber bundles in contact with the film. We present mass spectroscopic measurements of the neutral particles emitted from the fracture of single crystals of MgO where we examine the role of large concentrations of precipitates and incorporated OH in producing O containing emissions. In an appendix, we present results of simultaneous measurements of photon and electron emission from single crystal MgO including measurements on the photon emission which occurs during loading prior to failure. In addition, we present experiments on the consequences of simultaneous exposure of polymers to electron beam radiation and mechanical stress. In these studies we show that cracks can be initiated and/or propagated at stresses lower than critical stress values. The morphology of the stressed polymers plays a key role in the observed response.

II. INTRODUCTION

When a crack propagates through an insulating material or at an interface, a number of excitations and imbalances in charge stoichiometry can occur. This can result in electronic and chemical processes which result in the emission of particles, i.e., electrons ±ions, neutral species, and photons from the region of the crack and from the fracture surfaces. This emission is called *fracto-emission* (FE). Our goals are to 1) characterize in detail the properties of FE, 2) to determine the emission mechanisms for the particles observed, and 3) to examine the dependence of FE on the fracture event and materials properties. For example, we have shown previously that these emissions are sensitive to the locus of fracture, crack velocity, and various external parameters such as gaseous environment, fracture surface temperature and presence of electric fields. The interactions of fracture generated surface charge, emitted charge, and external electric fields is of some interest to propellent researchers because of the hazards of discharges to or within energetic materials.

In addition, we are exploring the interaction of radiation with materials under mechanical stress. We are determining the sensitivity of materials under stress to damage of various kinds induced by bombardment by electrons, ions, and energetic photons. For example, we are studying electron beam induced crack initiation and crack propagation.

In this report we include our recent work done in collaboration with Dr. Rena Yee on the electron and photon emission accompanying the peeling of binder elastomers directly from single crystals of RDX and compare these results from the fracture of unfilled binder and RDX filled binder which constitutes model rocket propellent (Section III). This work has been submitted to *J. Appl. Phys.*

In section IV, we examine contact prints (autographs) of the photon emission produced by another type of adhesive failure: pressure sensitive tapes peeled from surfaces. One sees direct evidence of the small electrostatic discharges which occur in this type of fracture involving interfacial failure. This work has been submitted to *J. Adhesion.*

Section V contains work on the neutral molecule emission produced from the fracture of single crystal MgO. Here we are concerned with the role of incorporated OH groups which we characterize with IR spectroscopy and accompanying precipitates with the emission of O containing gases. This work has been submitted to *J. Vac. Sci. Technol A.*

In Appendix I we include a very closely related study on single crystal MgO, work performed for the National Science Foundation, which examines the simultaneous emission of electrons and photons during the deformation and fracture of MgO. We include this work because it clearly shows the types of excitations that can occur in a crystalline material under such loading and presents mechanisms for these emissions.

In Section VI a short review paper on FE is presented which includes correlations of the emission with crack position (on a submicroseond scale), fracture surface temperature (following fracture), surface roughness as seen by fractography, and an example of photon emission due to debonding between polymer and a fiber inside a specimen. This paper is to be published in the *Proceedings of the International Society for Optical Engineering* (SPIE), Vol. 743.

Section VII includes a study of the initiation and growth of cracks in polymers created by exposing materials to mechanical stress and electron beam irradiation. Here we are interested in possible synergisms between these stimuli that result in microcracking and crack propagation. This work has been submitted to *J. Vac. Sci. Technol. A.*

Section VIII is a similar study of stressed polymers undergoing bombardment by energetic neutral atoms, in this case several keV Xe atoms, which also shows that microcracking can result. This work will be published in the *ASTM Proceedings for Radiation Effects on Materials.*

PARTICIPANTS IN THIS WORK

J. Thomas Dickinson, Principal Investigator
L. C. Jensen, Research Physicist
E. E. Donaldson, Professor of Physics
M. H. Miles, Associate Professor of Physics
M. K. Klakken, Ph.D. Student (Currently with Hercules, Inc.)
Steve Langford, Ph.D. Student
Russell Cory, M.S. Student
Fan Jaiwan, M.S. Student, Pursuing Ph.D.
Ma Zhenyi, M.S. Student, Pursuing Ph.D.

VISITORS CONTRIBUTING TO WORK

Dr. Rena Yee, Naval Weapons Center, China Lake, CA.
Dr. Ron Rabe, Los Alamos National Labs, Los Alamos, NM
Dr. Friedemann Freund, Institute of Geochemistry, U. Koln

III. FRACTO-EMISSION ACCOMPANYING ADHESIVE FAILURE BETWEEN ROCKET PROPELLENT CONSTITUENTS

J. T. Dickinson, L. C. Jensen, M. H. Miles
Washington State University
Pullman, WA 99164-2814

and

R. Yee
Navy Weapons Center
China Lake, CA 93555-6001

ABSTRACT

In past studies, we have shown that fracto-emission (the emission of electrons, ions, photons, and neutral species) is observable during and following the fracture of simulated model propellent composites. In this paper we examine the electron, photon, and radio frequency emissions from two situations that lead to interfacial or adhesive failure: the fracture of model propellents loaded with cyclotriethylene - trinitramine (RDX), and the peeling of binder material from macroscopic single crystals of RDX. Two binder materials are examined: hydroxy-terminated polybutadiene/isophorone diisocyanate and polyglycidyl azide prepolymer cured with a multifunctional isocyanate.

Keywords: propellent, elastomer, polymer, energetic materials, composites, adhesion, fracture, peeling, detachment, dewetting, electron emission, photon emission, triboluminescence, charge separation, fracto-emission.

I. INTRODUCTION

When fresh free surfaces are formed during the fracture of non-metals, the emission of a number of particles have been observed [1-21]. These emissions include the release of electrons, ions, neutral atoms and molecules, photons (frequently called triboluminescence), and long wavelength electromagnetic radiation (radiowaves). These emissions are known collectively as "*fracto-emission*". We have reported previously the observation of electron emission and photon emission during the fracture of simulated rocket propellents [2,3,11,12,14,15] and single crystals of energetic materials [19-21]. One reoccurring observation involves the striking consequences of fracture involving interfacial or adhesive failure between polymers and materials such as glass, metals, or dissimilar polymers: the emission intensities often exceed cohesive failure signals by orders of magnitude, the energy distributions are considerably higher, and the durations of the emission after fracture are often many hundreds of seconds as compared with only a few seconds or less for the cohesive cases. As previously discussed, the key physical phenomenon that is responsible for these unique emission characteristics is the separation of charge when interfaces between dissimilar materials fail [e.g. 12, 14-16].

Since rocket propellents consist generally of elastomeric binders filled with high concentrations of small, crystalline explosive material, it was of interest to determine if during the fracture of rocket propellents, fracto-emission characteristic of interfacial failure occurred *and*, in particular, if detachment between macroscopic surfaces of binder and explosive crystal would be emissive in comparison with the emission from the fracture of neat binder. The physical and chemical consequences of the fracture of energetic materials is of importance due to possible connections with undesirable instabilities that occasionally arise during handling and combustion of these materials.

II. EXPERIMENTAL

Samples of model rocket propellent were produced at the Naval Weapons Center (NWC) as part of a larger study directed by one of us (R.Y.Y.) on the mechanical properties of a variety of propellent formulations. This work will be published elsewhere. For this study we examine the emission for systems involving the binder materials:

a) HTPB: hydroxy-terminated polybutadiene/isophorone diisocyanate (R45M/IPDI), and

b) GAP: polyglycidyl azide prepolymer cured with a multifunctional isocyanate.

Two types of specimens were tested: tensile specimens (see Fig. 1a) and macroscopic, interfacial failure specimens (see Fig. 1b). The tensile specimens were prepared both neat and filled with cyclotriethylene-trinitramine (RDX) crystallites (mixtures of Class A and Class E RDX which represent crystallites of different particle sizes distributions; e.g., A contains larger particles -- typically 200 microns, and E contains typically 4 micron particles). The filled HTPB contained 75% and the GAP samples contained 68.6% by weight RDX. Both the filled and unfilled elastomers were tested in the form of rectangular 2 mm x 9 mm x 5 mm tensile specimens which contained a 1 mm notched in the center. The tensile specimens were strained at either 2.5 mm/s or 30 mm/s. The notched unfilled HTPB specimens typically elongated to 250% before failure, while the notched GAP samples elongated to approximately 60%. Both notched elastomers had a load at fracture of 6 N.

For the macroscopic "peel" experiments, large single crystals of RDX were grown from a carefully prepared acetone solution. Crystals of high optical quality of dimensions of approximately 1 cm in length and a few mm in thickness. The largest of the exposed crystal planes were chosen for attachment by a "tape" using the binders for

adhesive. The tape was made by first mixing and degassing the prepolymer, catalyst and curative. The uncured polymer was then spread out to form a layer about one mm thick on a piece of polyester cloth on aluminum foil which, in turn, was supported by an aluminum plate. The RDX crystal was then laid on top of the uncured binder with the the desired crystal plane facing down onto the uncured polymer. The whole assembly was then covered with aluminum foil and heated in an oven at 60 C under atmospheric pressure to cure. The curing time was five days for the R45M system and three days for the GAP system. The binder/crystal interfaces were irregular in shape with an average contact area of 1.2 cm^2 for GAP/RDX and 0.6 cm^2 for the HTPB/RDX system. The T-peel test was conducted at a peel rate of 1.2 mm/s.

All experiments were conducted in a diffusion pumped vacuum system at 10^{-4} - 10^{-5} Pa. Electrons were detected with a Galileo Electro-Optics channel electron multiplier model 4821. Visible photons were detected with a Thorn EMI 9924QB photomultiplier tube with a quartz window and bialkali cathode. Both detectors produced narrow 10 ns pulses which were amplified, discriminated, and counted in a multichannel scaler. The sample load was measured with a Sensotec Model 51 Load Cell, the output of which was digitized.

Figure 1 shows schematically the testing arrangements for a) the tensile specimens and b) the macroscopic "peel" experiments. In the latter experiments, great care was taken to minimize the forces applied to the interface prior to testing, thus the use of a light weight cord to attach to the "tape". This cord was attached to a force transducer mounted on a rod that could be translated from outside the vacuum system at a uniform rate. The measured force was thus the total force applied to the "tape" and was approximately equal to the peel force. In the data presented, the emission curves are plotted on a semilog scale and the load curves shown are on linear scales.

III. RESULTS AND DISCUSSION

We first examined the electron emission (EE) from the tensile fracture of the filled and unfilled elastomeric binders. Fig. 2 shows the electron emission (EE) from the tensile fracture of RDX filled HTPB strained at 2.5 mm/s. The vertical arrows mark the time interval when crack growth was occurring. The emission consists of a build up of intensity *during* crack growth, peaking at the final separation of the two surfaces. The after-emission following fracture is a decaying signal which lasts a few seconds. Attempts to detect the photon emission (phE) from fracture produced at this strain rate showed no detectable signal above the noise level of our photomultiplier.

Figures 3a and 3b show the simultaneous EE and phE, respectively, from the tensile fracture of the same material (RDX filled HTPB) where the strain rate has been increased to 30 mm/s. The EE has increased by an order of magnitude, with a significantly longer tail in the after-emission. The phE, although small, is now evident as a short burst (duration < 1 s) above the detector noise. Such emission is typical of the fracture of elastomeric composites where interfacial failure and a high degree of charge separation occur [2,14,15].

Similar experiments were carried out on RDX filled GAP. Figures 4a and 4b show the EE and phE, respectively, from the tensile fracture of the filled GAP samples strained at 30 mm/s. At this relatively high strain rate, there are large bursts of EE and phE at fracture followed by a long decay in the electrons and a distinctly observable decay in the photon emission. When compared with lower strain rates, the higher strain is found to produce an order of magnitude more EE and easily detectable phE with a distinct decay curve following fracture.

The ratio of EE/phE intensities as well as the details of the long time scale decay in the EE and phE are very much material dependent. The HTPB/RDX composite

samples yield considerably more electrons than photons, whereas the GAP/RDX samples yield relatively smaller EE/phE ratios due to the more intense phE.

Figures 5a and 5b show the EE from the tensile fracture of the unfilled HTPB and GAP binders without the RDX filler, fractured at a strain rate of 2.5 mm/s. The fracture of the neat binders produces very few electrons. Table I presents a summary of the total detected emission (the integrated emission curves) for the various types of tests.

The striking differences between unfilled vs filled binders are attributed to the occurrence of the failure of the interfaces between the filler particles (RDX) and the elastomer matrix. At the strain rates studied here, the possibility of fracturing individual RDX crystals does not seem very likely. Such small crystals would tend to move with the matrix as the matrix was strained and detach (dewet) at stresses well below the strength of the crystals. Furthermore, we have previously reported on the electron emission from the fracture of single crystals of RDX loaded in three point bend 20]. The most typical emission curve was a burst of electrons of a few hundred counts/sec which then decayed in just a few seconds. Clearly the fracture of the *components* of the composite system alone does not produce the characteristics of the signals seen accompanying fracture of the composites.

The basic concepts of the model we have proposed to explain the characteristics of emission accompanying interfacial failure involves the intense charge separation accompanying this form of fracture. The charging process which creates this charge separation is due to contact charging that occurs when dissimilar materials are placed in contact with one another. In order for the Fermi level to be a continuously smooth function at the interface between the two materials, charge exchange must occur at the boundary. The charging process in insulators is typically a slow process, ranging from minutes to days. However, when these surfaces are separated "rapidly", the low mobility of charge in insulators prevents recombination of charge on the separated surfaces.

Thus, patches of charge in the vicinity of the crack tip yield electric fields across relatively small dimensions. The desorption of gases and release of fracture products near the crack tip provide sufficient pressure in the region of high E fields that microdischarges can occur in the crack. This produces charged particles, detectable long wavelength electromagnetic radiation, and photon emission. Electrons and ions formed in the discharge may excite the crack walls via bombardment, creating excitations, usually explained in terms of electron-hole pair production. The relevant charge states are quickly trapped, e.g., electrons falling into traps near the conduction band, which then may undergo thermally stimulated migration until recombination occurs. This recombination can yield an emitted electron (thermally stimulated electron emission), via an Auger process, or a photon via a radiative transition (thermally stimulated luminescence) [22].

In order to provide further evidence that such a mechanism is occurring in the RDX-binder systems, we designed a "peel" experiment, wherein macroscopic surfaces of binder and RDX could be separated in a controlled manner, and the fracture surfaces examined to verify that at least visually adhesive vs cohesive failure had occurred. As previously described, a large RDX crystal had one crystal face covered with a "tape" of HTPB or GAP elastomer bonded to the crystal which could then be "peeled" off the crystal by application of a force to the relatively rigid backing.

Figures 6a and 6b show on slow time scales the resulting electron emission accompanying the peeling of HTPB and GAP binders from RDX crystals. The onset and completion of peeling are marked with vertical arrows as shown. When compared with the emission from fracture of the binder alone and from cleavage fracture of RDX these curves clearly are characteristic of interfacial failure. The emission is intense and very long lasting. From previous studies, such curves are indicative of considerable electrical activity (microdischarges) during the fracture process which creates elementary excitations on the fracture surfaces (e.g., the elastomer, the crystal, or both). The

thermal stimulation of these excitations result in recombination events (such as electron-hole pair annihilation), thereby radiating a photon or ejecting an electron from the material.

Figures 7a and 7b show on the same time scales the simultaneous measurement of the applied load and electron emission during the peeling of HTPB from an RDX crystal as the end of the tape was pulled at 1.2 mm/s. The onset of emission is about half way up the observed rise in load, indicating that the onset of peeling was not at the maximum applied force. This may have been due to a slight debonding of a small portion of the binder from the crystal during handling, resulting in weaker adhesion. The highest emission rate occurs during the peeling of the binder from the crystal which corresponds to the time when the applied force is large and fluctuating. Fig. 7c shows the rise in the emission curve (same data as Fig. 7b) at 10 ms/channel. At this higher time resolution, we can see flucuations in the emission rate that are due to the uneven crack velocity during the peel. The arrow indicates where separation of the two surfaces was complete.

Figures 8a and 8b are the corresponding load and EE curves during the peeling of the RDX/GAP system. Here a slight drop in load is observed coinciding with the onset of EE, but again the load rises during the remaining peel. The final detachment (which frequently can happen very quickly) yielded the spike in emission shown. Fig. 8c shows the rise in emission (same data as Fig. 8b) at 10 ms/channel, again showing the fluctuations in emission during peeling. Note that here the burst at the end of the peel (vertical arrow) has a short decay visible on this time scale.

The fracture surfaces under visual, low magnification inspection were very smooth, with a very slight residue visible on the RDX crystal surfaces. There was never any evidence of cohesive fracture either in the elastomer or the RDX crystals.

In some of our experiments the motion of the backing/elastomer surface following separation gave us some interesting information. Fig. 9a shows the emission of

an HTPB/RDX peel experiment where immediately after separation (indicated by the arrow), the backing fell to the bottom of the chamber, several cm from the RDX crystal which remained in front of the detector. The fact that the emission continues indicates that the exposed crystal surface is *one* of the emitting surfaces.

In Fig. 9b the EE from an HTPB peel experiment shows a typical rise and fall at the first peak on the left due to the peeling. The second peak occurred when the "tape" was pulled further causing it to twist the detached elastomer surface towards the detector. The third peak occurred when additional motion resulted in the elastomer surface moving closer and in full view of the detector. The increases indicate that the HTPB elastomer surface is also an emitter following detachment. In general, the elastomer surface was more emissive for the HTPB/RDX system than for the GAP/RDX system.

Fig. 10 shows the EE accompanying the peeling of GAP from RDX (first peak). After a few seconds of decay with the backing/elastomer surface being held a few mm from the crystal surface, the backing fell to the bottom of the chamber at the instant shown by the vertical arrow. The remaining crystal surface alone produced an increasing amount of detected emission. The electrostatics of the original arrangement (narrowly separated surfaces) apparently discouraged collection of the emitted charges by the electron detector. Also, these results show that the RDX crystal surface is a major contributor to the emission after fracture. In general, the RDX crystal surface was more emissive in the GAP/RDX system than the HTPB/RDX system.

In Figures 11a and 11b we show the simultaneous RE and EE during the peeling of a HTPB/RDX peel system. A number of RE bursts are seen only during the peeling of the elastomer from the RDX crystal. The accompanying EE is not a smooth response but consists of several bursts in emission, many of which correlate with RE bursts. This type of emission is consistent with the occurrence of microdischarges in the crack tip during the propagation of the "crack", i.e., during the peeling process. Note that this is

occurring in a vacuum. Such breakdown requires gases with reasonably low breakdown potentials to be present in the crack tip. We always see the release of gases such as H_2O, CO, and CO_2 during the cohesive fracture of polymers such as polybutadiene although we have not yet determined the gases released during adhesive failure. It should be noted that the phE and RE bursts observed during peeling of pressure sensitive adhesives are considerably more intense in vacuum compared to air, suggesting that the gases *from* the sample can be conducive to breakdown.

IV. CONCLUSIONS

We have shown that the fracture of HTPB/RDX and GAP/RDX composites as well as the separation of adhesively bonded macroscopic surfaces of HTPB and GAP bonded adhesively to single crystals of RDX show the characteristics of fracto-emission accompanying interfacial failure when compared with the signals from the unfilled binder or the fracture of *single crystal* RDX. These features include intense, long lasting emission with non-first order decay kinetics, as well as the occurrence of discharge activity (RE) during the peeling process.

Both the HTPB/RDX composite and interface systems typically yielded higher electron emission rates than the GAP/RDX system, approximately a factor of 5 more intense. The HTPB/RDX composite emission was dominated by EE, with the HTPB surface being the most emissive. The GAP/RDX composite system had larger phE emission and exhibited a more active RDX surface for emission than the corresponding experiments in the HTPB/RDX system. Also, in some cases the charge present on the separated surfaces was shown to influence the trajectories of the emitted particles to the detector. Topics of further study include measurements of the energies of the charged particles, emission intensity vs separation velocity, a careful search for and identification

of possible ionic species, and determining in more detail the role of the polymer/crystal interface in determining the intensity of these emissions.

V. ACKNOWLEDGMENTS

This work was supported by the Office of Naval Research Power Program under Contract N00014-80-C-0213, NR 659-803 (Washington State University) and Task Numbers AARR024-02 and AARR014-11 (Naval Weapons Center) and NAVSEA Task No. SRO2403.

REFERENCES

1. J. T. Dickinson, E. E. Donaldson, and M. K. Park, J. Mat. Sci. 16, 2897-2908 (1981).

2. J. T. Dickinson, L. C. Jensen, and A. Jahan-Latibari, Rubber Chemistry and Technology 56, 927-941 (1983).

3. J. T. Dickinson, "Fracto-Emission Accompanying Adhesive Failure," in *Adhesive Chemistry-Developments and Trends*; Edited by L. H. Lee, Plenum, New York, (1985).

4. J. T. Dickinson, A. Jahan-Latibari, and L. C. Jensen, J. Mat. Sci. 19, 1510 (1984).

5. J. T. Dickinson, L. C. Jensen, and S. K. Bhattacharya, J. Vac. Sci. Technol. A, 3 1398 (1985).

6. J. T. Dickinson, L. B. Brix, and L. C. Jensen, J. Phys. Chem. 88, 1698-1701 (1984).

7. J. T. Dickinson, L. C. Jensen, M. R. McKay, and F. Freund, J. Vac. Sci. Technol. A, 4 1648 (1986).

8. J. T. Dickinson, M. R. McKay, and L. C. Jensen, J. Vac. Sci. Technol. A, to be published.

9. S. C. Langford, J. T. Dickinson, and L. C. Jensen, to be published in J. Appl. Phys.

10. J. T. Dickinson and L. C. Jensen, J. Am. Ceramics Soc. 68, 235 (1986).

11. J. T. Dickinson and L. C. Jensen, J. Poly. Sci.: Poly. Phys. Ed., 20, 1925-1932 (1982).

12. J. T. Dickinson, M. K. Park, E. E. Donaldson, and L. C. Jensen, J. Vac. Sci. Technol. 22, 436-439 (1982).

13. L. A. K'Singam, J. T. Dickinson, and L. C. Jensen, J. Am. Ceramics Soc. 68, 510 (1985).

14. J. T. Dickinson, L. C. Jensen, and A. Jahan-Latibari, J. Vac. Sci. Technol. A, 4, 1112-1116 (1984).

15. J. T. Dickinson, and L. C. Jensen, J. Poly. Sci.: Poly. Phys. Ed. 23, 873 (1985).

16. E. E. Donaldson, J. T. Dickinson, and X. A. Shen, J. Adhesion 19, 267 (1986).

17. J. T. Dickinson and E. E. Donaldson, to be published in J. Adhesion.

18. A. S. Castro, R. Corey, J. T. Dickinson, R.V. Subramanian, and Y. Eckstein, to be published in Composites Science and Technology.

19. M. H. Miles and J. T. Dickinson, Appl. Phys. Lett. 41, 924 (1982).

20. J. T. Dickinson, M. H. Miles, W. L. Elban, and R. G. Rosemeier, J. Appl. Phys. 55, 3994 (1984).

21. M. H. Miles, J. T. Dickinson, and L. C. Jensen, J. Appl. Phys. 57, 5048 (1985).

22. R. Chen and Y. Kirsh, *Analysis of Thermally Stimulated Processes*, Pergamon, Oxford, 1981.

FIGURE CAPTIONS

Figure 1. Experimental arrangement for the detection of electrons from fracture. a) Set-up for tensile fracture of the filled and unfilled binder; b) Set-up for the peeling of the binder from single crystal RDX. In each case, the testing was performed in vacuum.

Figure 2. The electron emission (EE) from the tensile fracture of RDX filled HTPB strained at 2.5 mm/s. The vertical arrows mark the time interval when crack growth was occurring. At this strain rate, no photon emission was detected.

Figure 3. a) The electron emission (EE) and b) the photon emission (phE) from the tensile fracture of RDX filled HTPB strained at 30 mm/s. The rapid rise in the EE and the spike in the phE are coincident with the time of fracture.

Figure 4. The electron emission (EE) and b) the photon emission (phE) accompanying the tensile fracture of RDX filled GAP strained at 30 mm/s.

Figure 5. The electron emission (EE) from the tensile fracture of the unfilled binders: a) HTPB, and b) GAP. The strain rate was 2.5 mm/s.

Figure 6. Long time scale electron emission (EE) curves from the peeling of the elastomers from macroscopic RDX single crystals. a) HTPB from RDX, and b) GAP from RDX.

Figure 7. Simultaneous display of a) the peel force and b) the electron emission (EE) during and following the peeling of HTPB from single crystal RDX. c) The same EE data displayed on a faster time scale (10 ms/channel) during the motion of the crack.

Figure 8. Simultaneous display of a) the peel force and b) the electron emission (EE) during and following the peeling of GAP from single crystal RDX. c) The same EE data displayed on a faster time scale (10 ms/channel) during the motion of the crack.

Figure 9. Electron Emission (EE) accompanying and following the peeling of HTPB from single crystal RDX. a) At the vertical arrow, the backing and elastomer fell away from the detector. The remaining emission is coming from the RDX crystal surface. b) After the initial peak due to peeling additional increases in emission are due to motion of the new elastomer surface to more favorable positions relative to the detector, thus showing that the elastomer surface is also an intense emitter.

Figure 10. The electron emission (EE) from the peeling of GAP from single crystal RDX. At the instant shown by the vertical arrow, the backing/elastomer fell to the bottom of the chamber, resulting in an *increase* in emission.

Figure 11. Simultaneous measurements of a) the bursts of long wavelength radiation (RE) and b) the electron emission (EE) during the peeling of HTPB from a RDX single crystal. The detection of RE during peeling strongly suggests that microdischarges are occurring due to charge separation during the peel.

Table I. Summary of Total Electron and Photon Emission Intensities For Various Tests Performed.

Specimen Detected	Strain Rate mm/s	Total EE Detected (Counts/cm^2)	Total PhE (Counts/cm^2)
Neat HTPB	2.5	400	nm
Neat GAP	2.5	150	nm
RDX filled HTPB	2.5	12,000	40
RDX filled HTPB	30	25,000	1,000
RDX filled GAP	2.5	nm	nm
RDX filled GAP	30	80,000	7,000
PEEL: HTPB from RDX	1.2	400,000	nm
PEEL: GAP from RDX	1.2	20,000	nm

nm = not measured

a)

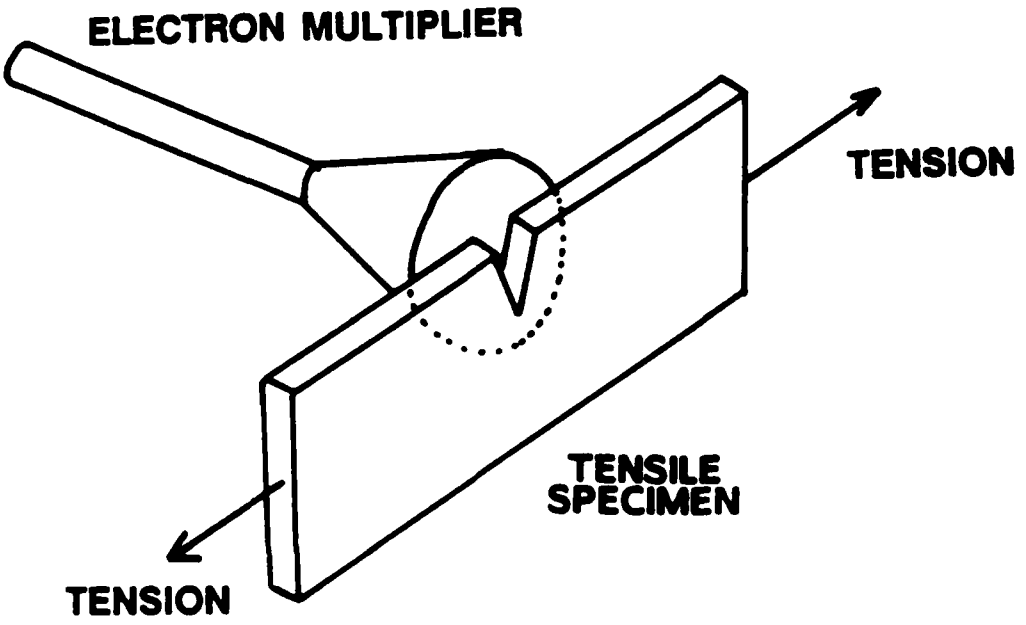

EXPERIMENTAL SET-UP FOR FRACTURE OF TENSILE SPECIMEN

Fig. 1a

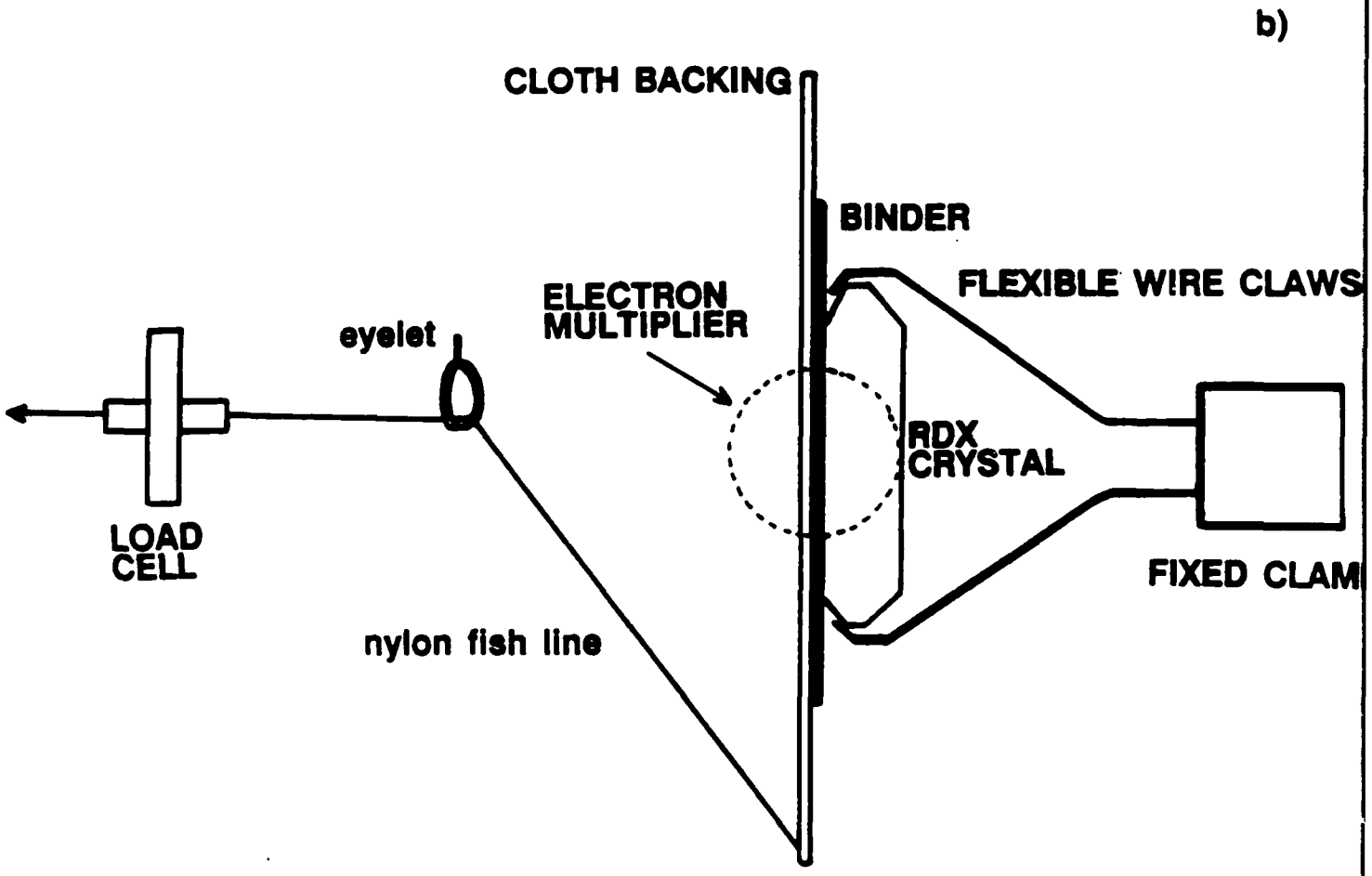

EXPERIMENTAL SET-UP FOR PEEL EXPERIMENT

Fig. 16

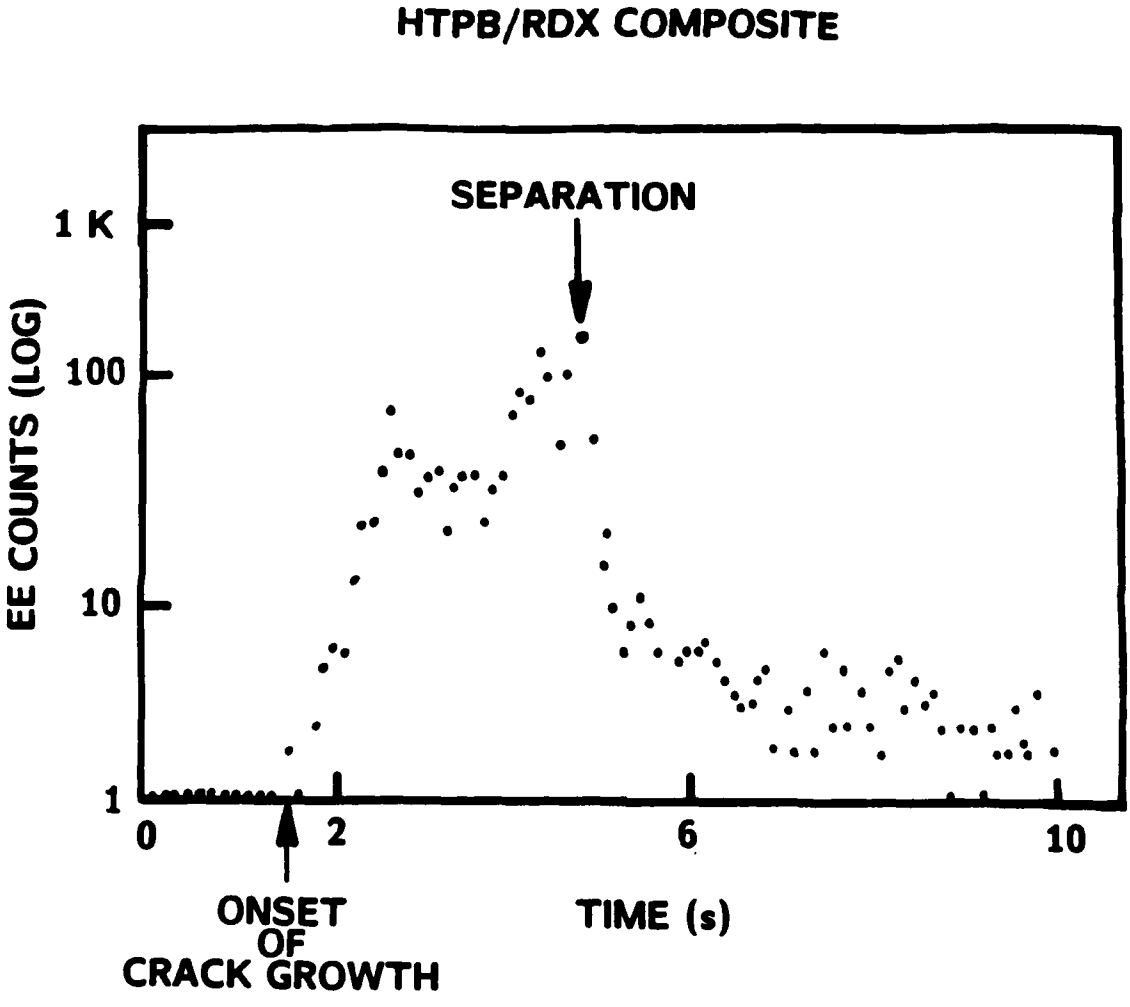
HTPB/RDX COMPOSITE
SEPARATION
1 K
100
10
1
EE COUNTS (LOG)
0
2
6
10
TIME (s)
ONSET
OF
CRACK GROWTH

Fig. 2

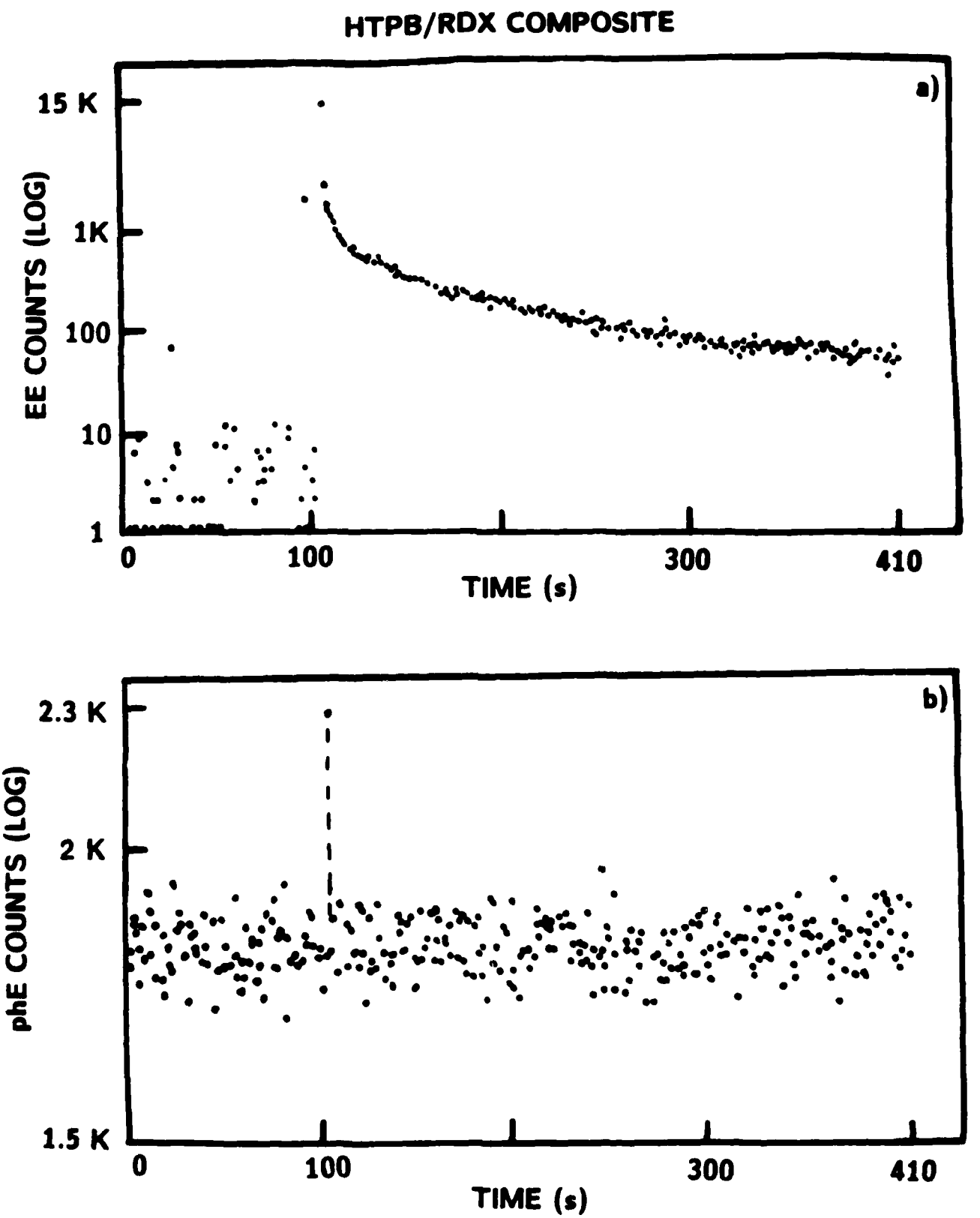
HTPB/RDX COMPOSITE
a)
15 K
1K
100
10
1
EE COUNTS (LOG)
0
100
300
410
TIME (s)
b)
2.3 K
2 K
1.5 K
phE COUNTS (LOG)
0
100
300
410
TIME (s)

Fig. 3

GAP/RDX COMPOSITE

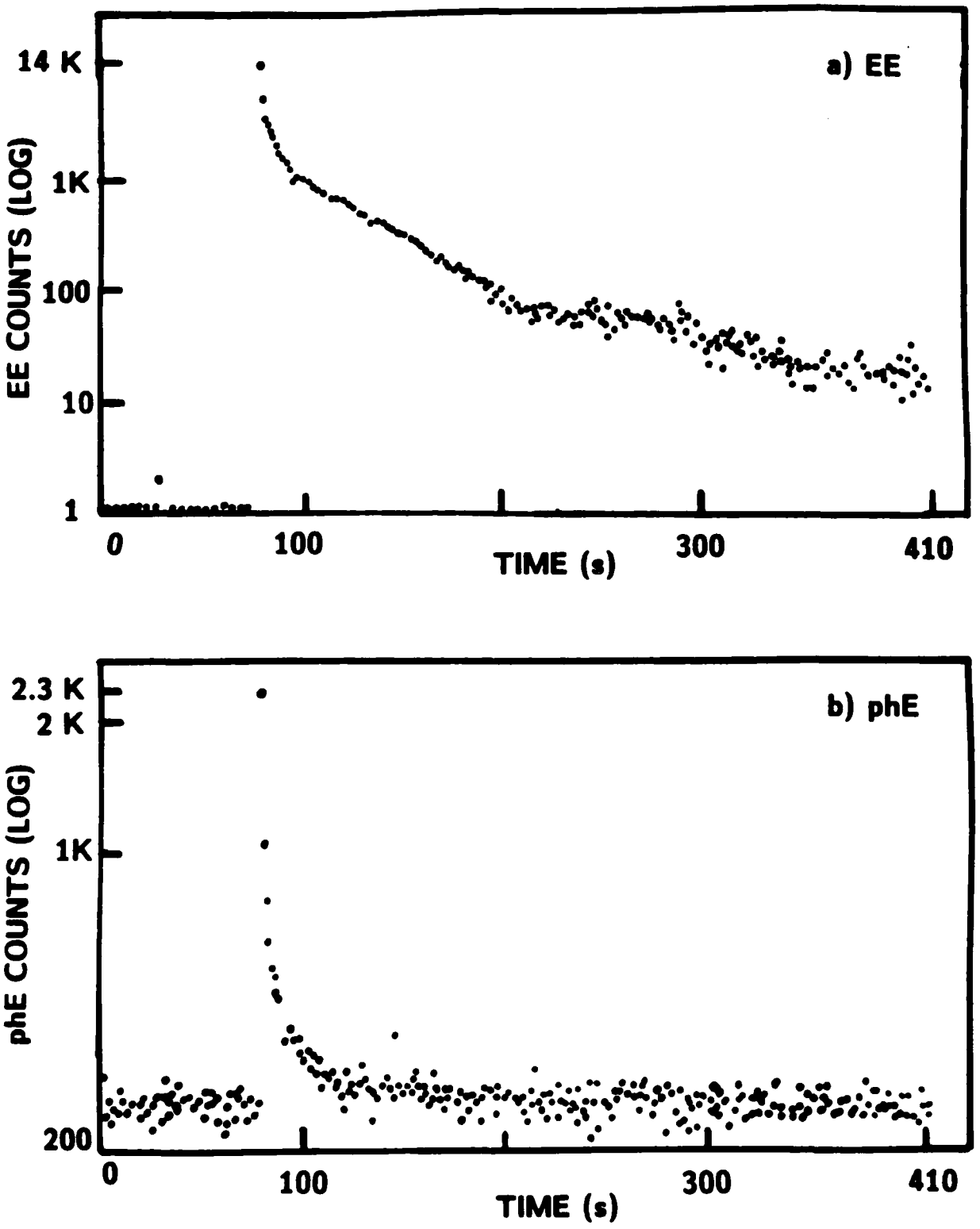

Fig. 4

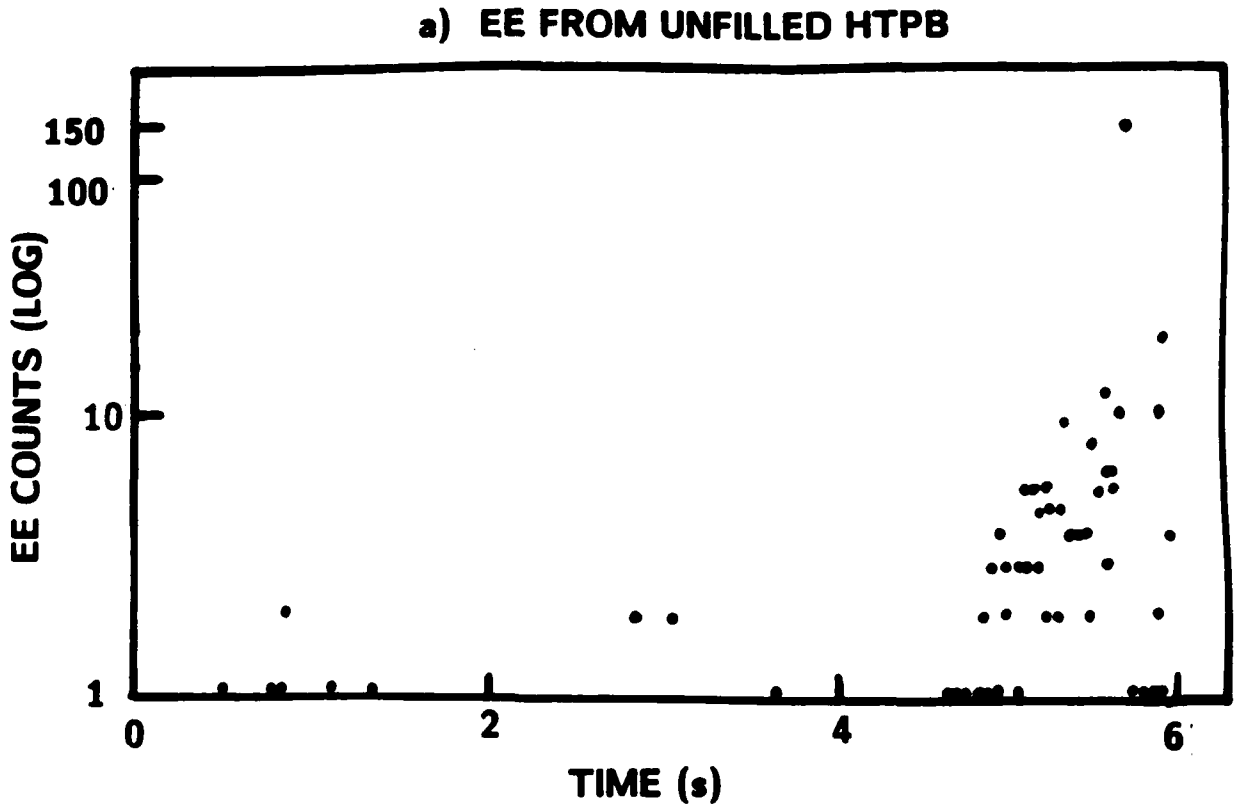
a) EE FROM UNFILLED HTPB
150
100
10
1
EE COUNTS (LOG)
0
2
4
6
TIME (s)

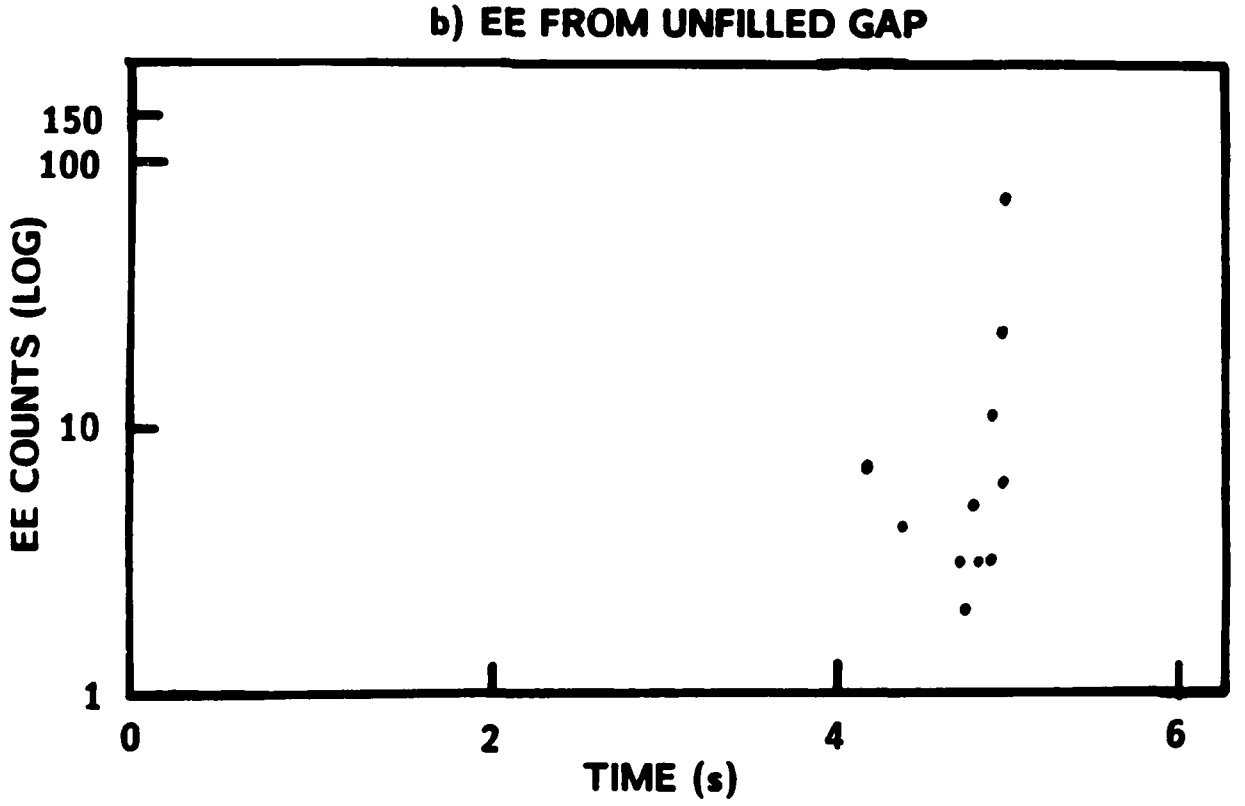
b) EE FROM UNFILLED GAP
150
100
10
1
EE COUNTS (LOG)
0
2
4
6
TIME (s)

Fig. 5

EE FROM PEELING BINDER FROM
RDX SINGLE CRYSTAL

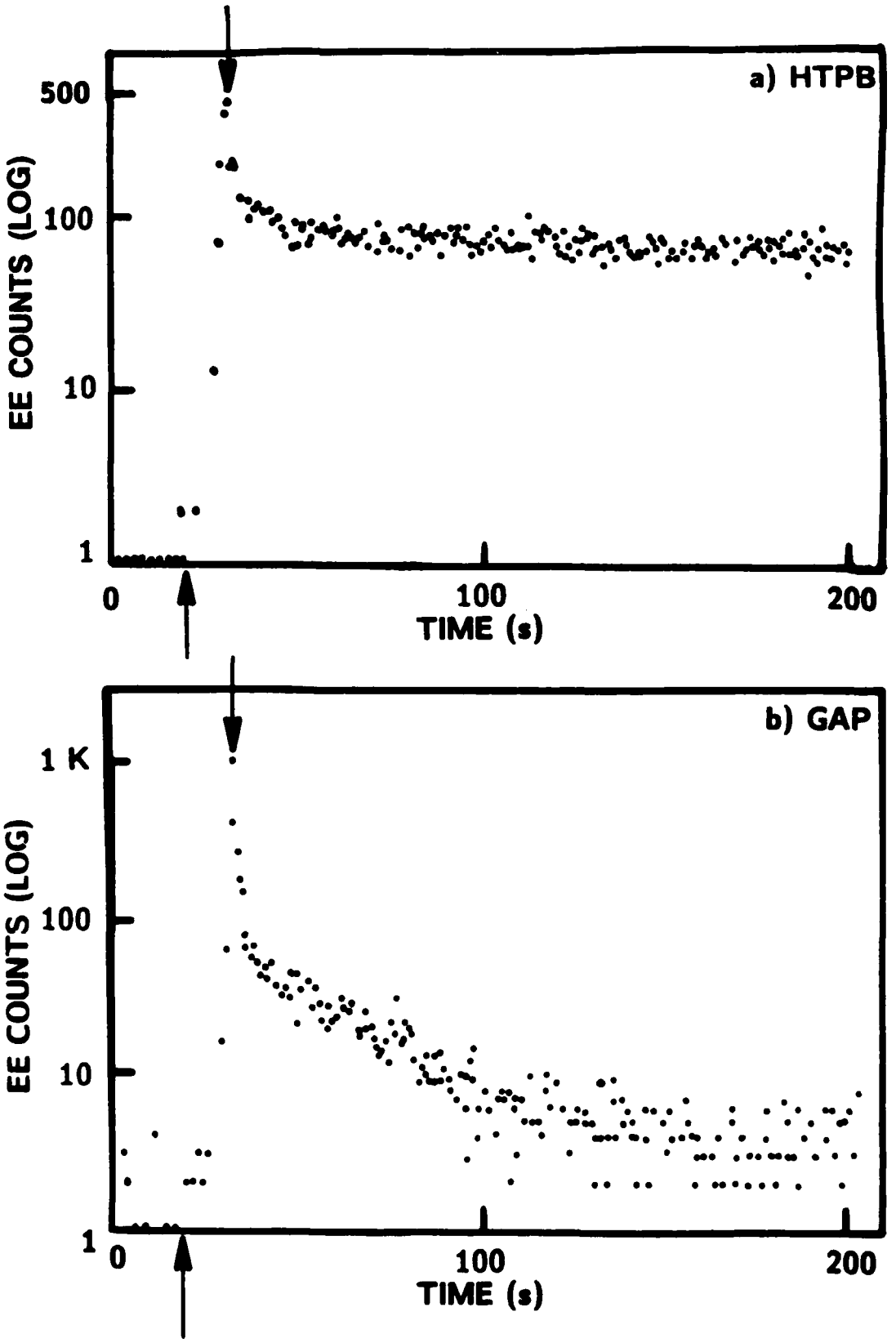

Fig. 6

HTPB PEEL FROM RDX SINGLE CRYSTAL

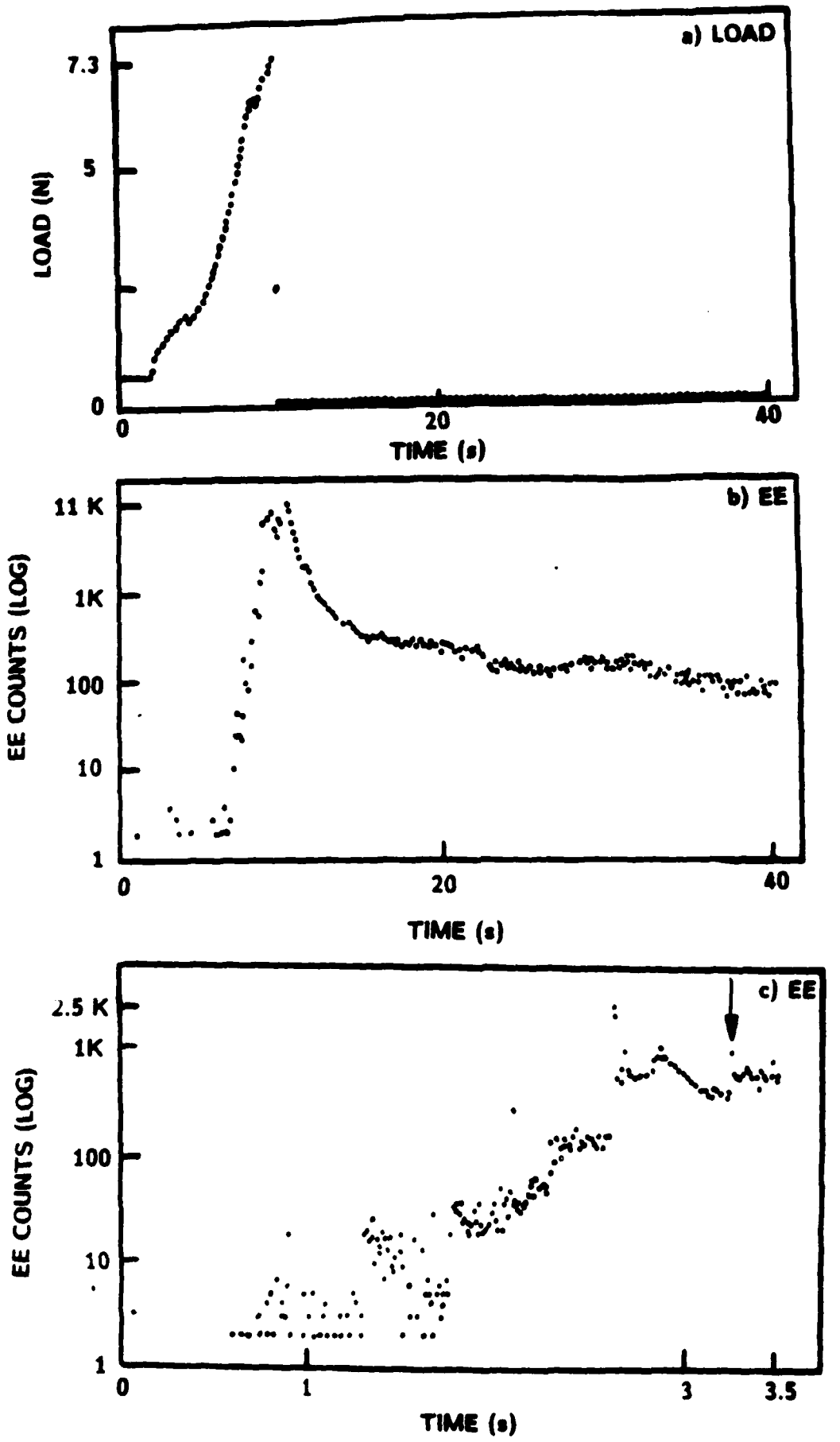

Fig. 7

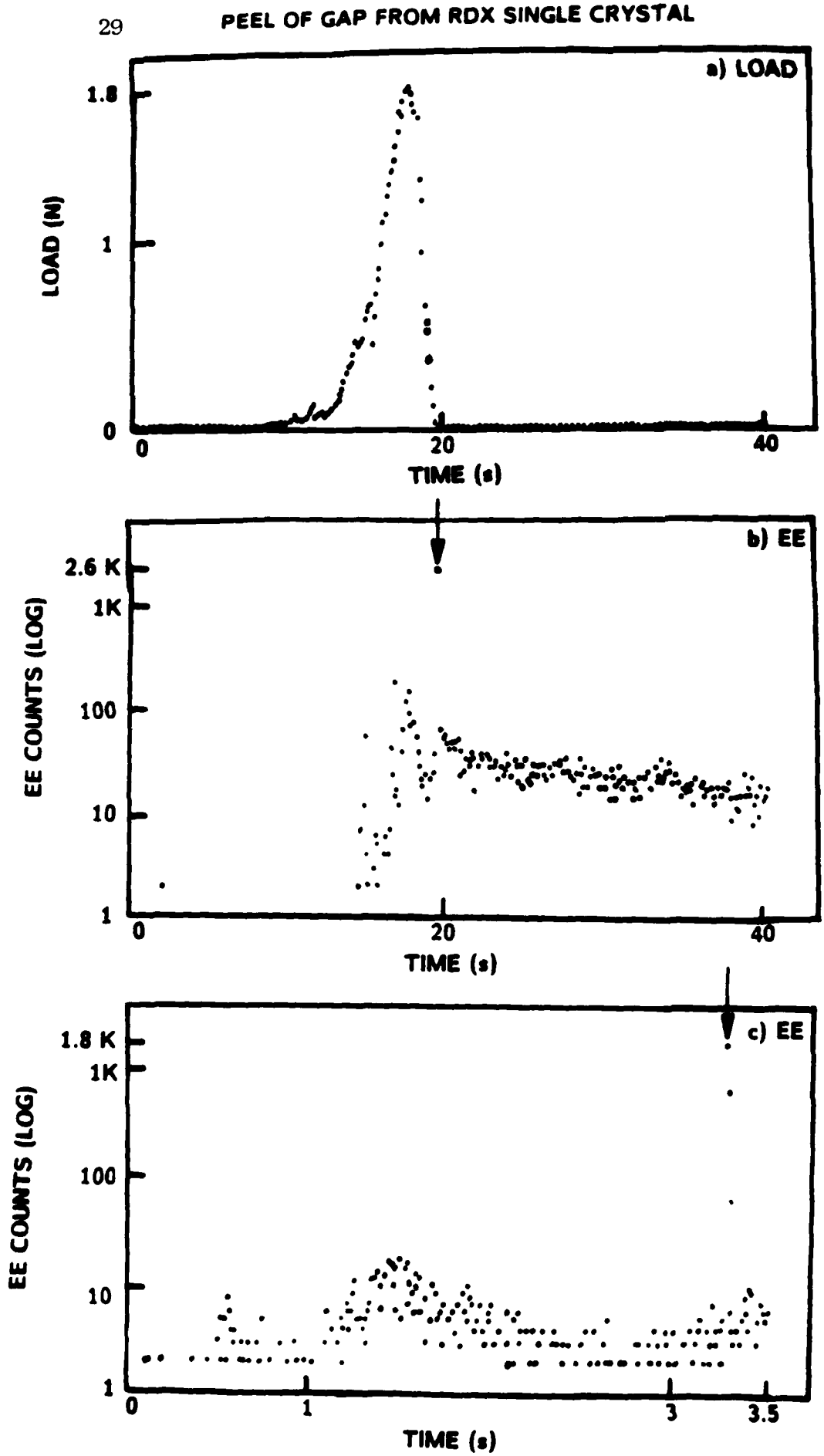
PEEL OF GAP FROM RDX SINGLE CRYSTAL
a) LOAD
LOAD (N)
1.8
1
0
0
20
40
TIME (s)
b) EE
EE COUNTS (LOG)
2.6 K
1K
100
10
1
0
20
40
TIME (s)
c) EE
EE COUNTS (LOG)
1.8 K
1K
100
10
1
0
1
3
3.5
TIME (s)

Fig. 8

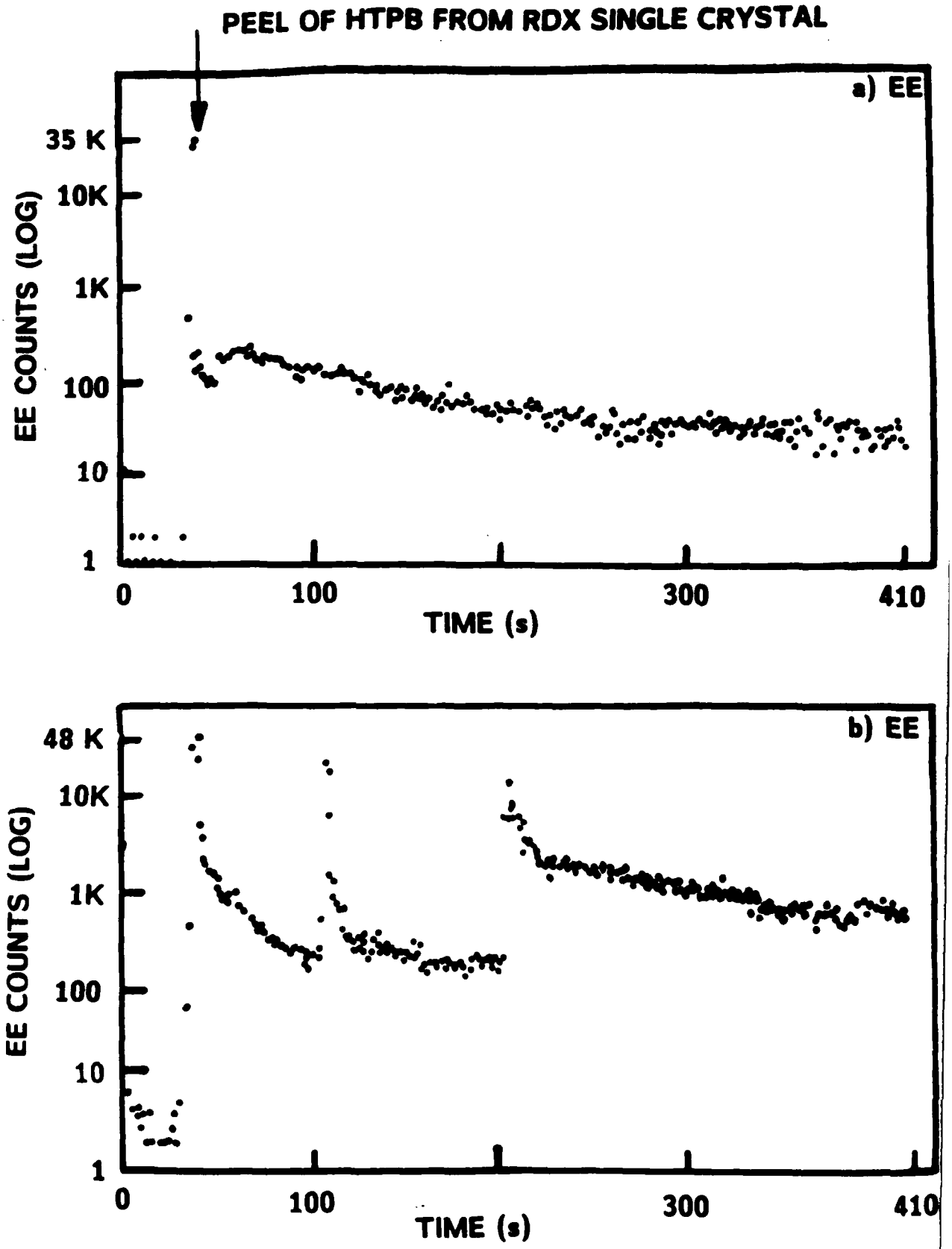
PEEL OF HTPB FROM RDX SINGLE CRYSTAL
a) EE
35 K
10K
1K
100
10
1
EE COUNTS (LOG)
0
100
300
410
TIME (s)
b) EE
48 K
10K
1K
100
10
1
EE COUNTS (LOG)
0
100
300
410
TIME (s)

Fig. 9

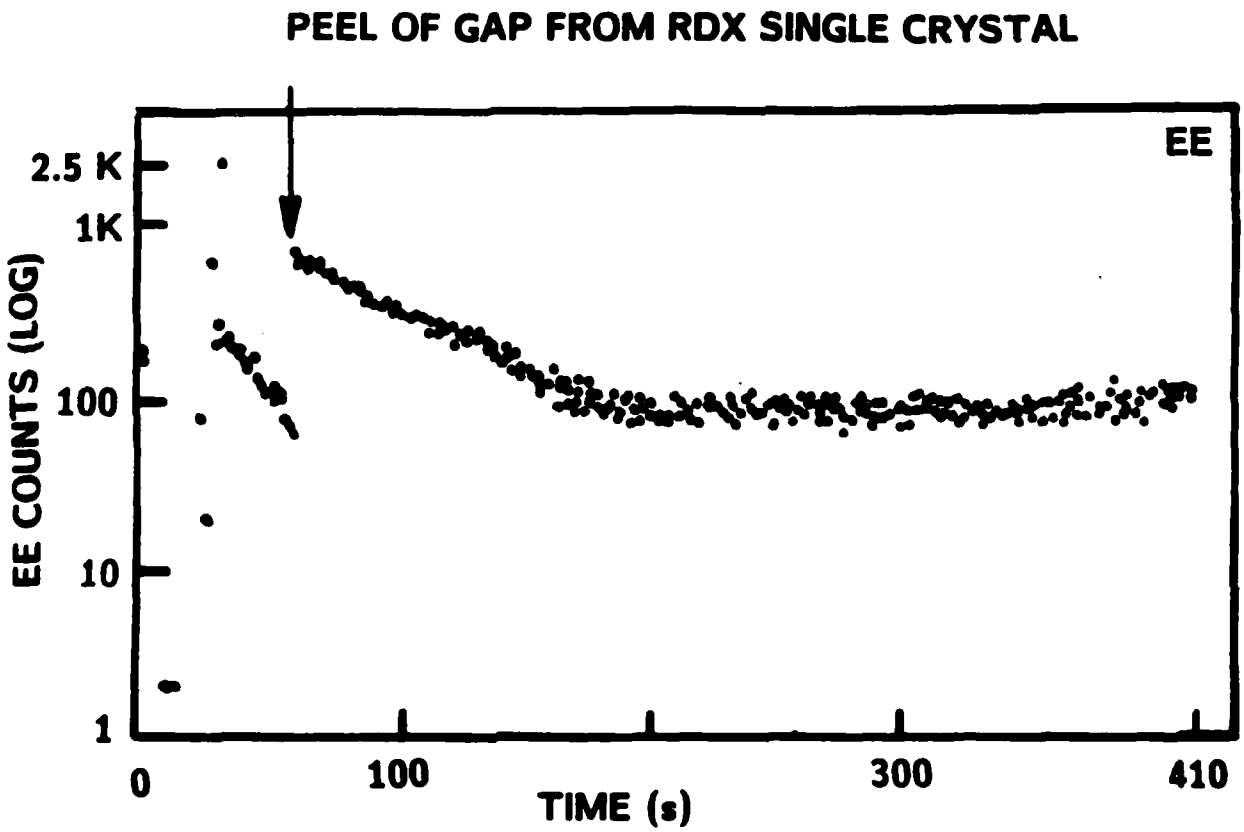
PEEL OF GAP FROM RDX SINGLE CRYSTAL
EE
2.5 K
1K
100
10
1
EE COUNTS (LOG)
0
100
300
410
TIME (s)

Fig. 10.

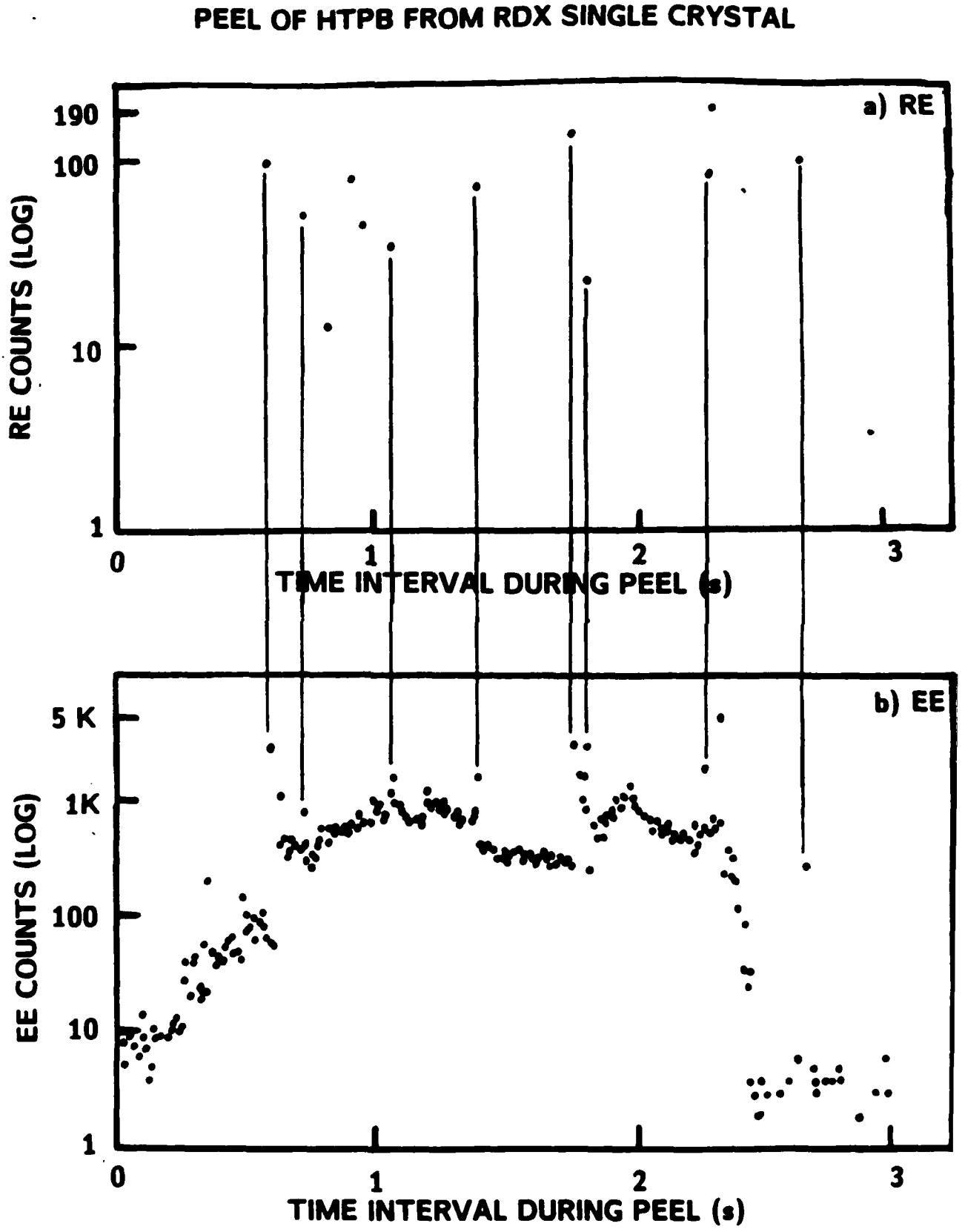
PEEL OF HTPB FROM RDX SINGLE CRYSTAL
a) RE
190
100
10
1
RE COUNTS (LOG)
0
1
2
3
TIME INTERVAL DURING PEEL (s)
b) EE
5 K
1K
100
10
1
EE COUNTS (LOG)
0
1
2
3
TIME INTERVAL DURING PEEL (s)

Fig. 11

IV. AUTOGRAPHS FROM PEELING PRESSURE SENSITIVE ADHESIVES: DIRECT RECORDING OF FRACTURE-INDUCED PHOTON EMISSION

J. T. Dickinson and E. E. Donaldson
Department of Physics
Washington State University
Pullman, WA 99164-2814

Katisha: **"Volcanoes have a splendour that is grim, And Earthquakes only terrify the dolts, But to him who's scientific, There is nothing that's terrific, In the falling of a flight of thunderbolts!"**

KoKo: **"Yes, In spite of all my meekness, If I have a little weakness, It's a passion for a flight of thunderbolts!...."**

Gilbert and Sullivan,
The Mikado.

ABSTRACT

It is well known that visible light is emitted during the peeling of adhesives from various substrates. The major source of light has been identified as small gaseous discharges that result from the intense charge separation accompanying detachment of dissimilar materials. In this paper, we describe an experimental technique which produces clear images of the photons created by peeling pressure sensitive adhesives directly from the surface of a film emulsion or from the surface of a glass fiber optic face plate in contact with the film. The resulting autographs of the emitted light show in considerable detail the spatial structure of the photon emission which in turn reveals the mechanical and electrical behavior of these materials during the peeling process.

KEYWORDS: Pressure Sensitive Adhesives, Peeling, Adhesive Failure, Fracture, Fracto-Emission, Triboluminescence, Electrical Charge Separation, Imaging, Autograph.

I. INTRODUCTION

Accompanying the deformation and fracture of materials, particles and radiation are emitted (collectively known as fracto-emission[1-16]). The types of particles that have been observed include electrons, ions, neutral species, photons (often referred to as triboluminescence), and long wavelength electromagnetic radiation (radiowaves). These emissions can often serve as sensitive probes of bond breaking, locus of fracture, crack velocity, and other properties of the fracture process. In previous work,[1-16] we have presented experimental studies of the photon emission (phE), electron emission (EE), positive ion emission (PIE), and the neutral emission (atoms and molecules --NE) accompanying fracture. This includes studies of composites, metal/inorganic interfaces, and the peeling of pressure sensitive adhesives from several substrates, in various gases, and in vacuum.

When an adhesive is peeled in air and other gases,[16] the time variations of the phE detected with a fast photomultiplier tube could be characterized as having two components:
a) very fast bursts (peak width on the order of 50 ns or less), followed by
b) characteristic non-first order decay lasting as long as a few tenths of seconds.
The bursts of light were found to be in coincidence with bursts of long wavelength electromagnetic radiation. These observations supported the view that as small regions of the adhesive detach from the substrate, patches of electrical charge are created which lead to gaseous breakdown (micro - "thunderbolts") in and near the crack tip. This light is very likely similar in wavelength to a weak discharge in air which is dominated by molecular nitrogen emission lines. We have attributed the slower-decaying component to a phosphorescence-like emission from the adhesive and/or substrate which is excited *by the discharge*, i.e., the resultant particle bombardment of the surface(s), created by the discharge and accelerated by the charged surfaces. In polymers, the relaxation from such stimuli is multicomponent in nature, consisting of fluorescence decay (the decay of excited electronic states created at t=0) and photons from the recombination of charge carriers, defects, and/or free radicals. The latter is rate limited by

diffusion of "reactants" (the mobile species frequently being electrons) and is therefore a thermally activated process.[17]

In this paper, we present a novel method of examining the characteristics of these light emissions. Early attempts using a camera equipped with fast film and a large aperture lens were not successful due to insufficient light intensity. However, by placing the adhesive joint in close proximity to the film while the adhesive was undergoing failure we were able to obtain images. In an early experiment we peeled tapes from a glass slide in contact with the film. Although the resulting images were poorly resolved due to the spreading of the light through the thickness of the glass, this experiment demonstrated that photons from peeling (as opposed to electrons, x-rays, or chemical reactions) did indeed produce images on photographic film. As we shall show, extremely clear images were obtained by peeling adhesives directly from the surface of the film emulsion or from a fiber optic face plate in contact with the film. Furthermore, we also show that details of the adhesive bonding and the peeling mechanics greatly influence the resulting images.

II. EXPERIMENTAL

In these experiments, two types of pressure sensitive adhesives were used: 3M Scotch Brand Magic Tape [No. 810] and 3M Brand Filament Tape [No. 893]. We refer to these tapes as Magic Tape and Filament Tape, respectively. Magic Tape consists of a cellulose acetate backing which carries a back release coating having a critical surface tension for wetting of approximately 21 dynes/cm. The adhesive is a long-side-chain alkyl acrylate. Filament Tape has an adhesive of natural rubber combined with varying amounts of a tackifying agent which is a hydrocarbon resin, apparently terpene based. More tackifier is used on the face of the adhesive and less in the saturating layer binding the glass filaments to the backing. In Filament Tape, the polyester tape backing has been treated with a release coating having a critical surface tension for wetting of approximately 21 dyne/cm.

In the work presented here, Polaroid films were used exclusively; the following films were used to record the images:

Film Emulsion Type (Polaroid)	ISO (ASA)	Coating
146	200	Uncoated
47	3000	Gelatin
107C	3000	Gelatin
612	20000	Proprietary

These films are all available in flat or roll format and were loaded in the appropriate Polaroid camera back which made the emulsion side of the film surface conveniently available for experimenting. A dark slide protected the film when room light was on. Experiments were conducted in a darkroom with typical times of exposure to the "background" light being a minute or two. No evidence of fogging from background light was observed.

Experiments were carried out by pressing the tape down by hand on the chosen substrate and then stripping by hand, usually in a 90° peel geometry. Approximate peel speeds were estimated by timing the duration of the peel and measuring the distance peeled from the image itself. Of course, instantaneous peel speeds varied considerably. After each experiment was completed, the Polaroid films were developed in a standard fashion, producing a "print" in a few seconds. Materials placed between the adhesive and the film emulsion were useful in demonstrating the nature of the emitted light. To determine if residue of the adhesive left on the surface of the film following peeling might prevent subsequent normal development, we exposed the film to light before *or* after peeling. These films showed normal sensitivity in the

region where the tape was attached and removed proving that the images were not altered by a possible thin contamination layer.

III. RESULTS AND DISCUSSION

The results to be presented in this section involve presentation of the resulting images from various substrates and peeling configurations. In general, in the figures shown, the peeling was from left to right and (unless otherwise stated) in 90° peel geometry.

Glass Slide as Substrate. As mentioned previously, the peeling of various tapes from glass slides held in contact with the Polaroid film was investigated. Figures 1 and 2 show the resulting images from Magic Tape and Filament Tape peeled from the glass slide at approximately 15 cm/s, using Type 107C Film and Type 612 Film. The images are somewhat blurred because the glass slide allows the light to spread. Although this results in images with poor resolution, the glass assured us that only *visible light* reached the film, excluding charged particles, reactive chemical species, and ultraviolet light. Since peeling tape directly from the film produced images of a similar nature, it implies that these clearer images [autographs] are indeed due to photon emission. Note that the image intensities in fact correlate as expected with the ISO numbers. Similar patterns could be created using other transparent substrates (e.g., PMMA). Note that the outline of the slide can be seen clearly from the light scattered along the edges into the film by internal reflection.

Film Emulsions as Substrates. Placing the adhesive in direct contact with the film emulsion and peeling it off within a few seconds of application produced autographs of the highest resolution. In Fig. 3, we see typical patterns from the peeling of both Filament and Magic Tapes from Type 146 Polaroid Projection Film, where the peel was from left to right in a 90° geometry. The peel was accelerated during the peeling from a speed of ~ 1mm/s to ~ 5 cm/s. Both adhesives show striations or stripes in the emission pattern for both fast and slow

peels. This is a consequence of the stick-slip behavior characteristic of peeling with an elastic backing material. Presumably the brightest regions occur during the "slip", i.e., during the fastest detachment. The darker regions are not totally dark, particularly in the case of Magic Tape (Fig. 3a). The sharpest features seen for both tapes must occur quite close to the emulsion surface. The larger, more diffuse features most likely occur at slightly greater distances from the film. However, it was shown earlier[16] that when Filament Tape was peeled off of its own backing, some light was emitted even during the minima in intensity (the stick-slip peeling behavior shows up also as intensity variations in time). We also note that preliminary measurements of the charge density remaining on substrates *after* peeling show similar spacings in the charged patches (approximately 1.0 mm in "wavelength" for similar peel velocities).

Also, consistent with previous results,[16] the numerous bright spots seen in Fig. 3b (Filament Tape) correspond to the very fast and intense bursts that we showed were due to the more intense microdischarge events accompanying peeling. In the case of Filament Tape, we see from the images that the intensity and number of these stronger arcs increase with peel speed. When these intense spots are examined under magnification, there is considerable structure suggesting breakdown paths parallel to the film surface. Also, it should be noted that the number density of these bright bursts at fast peel speeds is roughly 1 arc/mm^2 which is consistent with the number of radiowave bursts detected during comparable peeling.[16]

Smaller, individual arcs are also observable for Magic Tape/Type 146 Film and are most evident at slower peel speeds. At higher speeds, large numbers of these arcs merge to form a nearly continuous line across the width of the tape image. In the original photographs viewed with magnification, it is also evident that the regions of lower intensity emission are in fact the result of many low intensity discharge events.

The spacing of the striations is governed by the geometry of peeling, by the viscoelastic properties of the adhesive, and the elastic properties of both the tape backing and the film substrate. One can effectively modify the stiffness of the tape backing by applying one or two layers of electrical tape to the back of the adhesive tape being tested prior to peeling. In Fig.4,

we show the resulting image for modified Magic Tape. The striations now have a wave length of 2 mm as compared to 1 mm for peeling unbacked Magic Tape at about the same speed. Note also the reduction in intensity and larger width of each striation due to changes in the mechanics of peeling.

We also tested the effect of peel geometry on emission patterns. In Fig. 5 the peeling of Magic Tape from type 47 film was started at approximately 180° (parallel to the film),then the peel angle was changed to about 90° at approximately the same peel speed. The striations are considerably closer together for the 90° peel angle with fewer high intensity "thunderbolts". The latter may well be due to the distribution and density of charge favoring higher intensity discharges in the case of the 180° peel.

When a different film is used as a substrate, there are considerable differences in the resulting patterns. In spite of a factor of 10 increase in ISO, the peeling of tape from Type 47 and Type 107C Films does not produce as bright an image as from Type 146 Film, in contrast to the observations in Figures 1 and 2. We show the records for Magic Tape peeled at three different peeling speeds from Type 107C Film in Fig. 6, which results in visible but less intense images. This means that considerably less light per unit area was produced during the peeling. The likely explanation for the reduced emission is differences in the substrate surfaces which result in less contact charging [i.e., in the case of Type 107C Film], thus producing less electrostatic discharge activity upon peeling. This demonstrates the important role played by the interface in creating the conditions which produce these emissions.

At higher speeds, Fig. 6c, one sees aligned and imbedded in the less intense vertical striations of light, the appearance of a number of very bright discharges, occasionally several per strip. The very dark circles are due to bubbles inadvertently formed when applying the tape. Flaws in the adhesive produce very similar features. Frequently, extremely sharp, enhanced images of the tape edges are produced. The mechanics of peeling the tape is known to produce a positive pressure rise along these edges as the crack tip approaches. This momentarily improves the contact between the adhesive and substrate which appears to assist

the resulting emission, visible in the bottom of Fig. 6c. As we show below, if we purposely produce high pressure regions during the attachment of the adhesive to the emulsion surface, higher intensity emission is observed.

Fig. 7 shows similar results for three peel speeds of the Filament Tape peeled from the surface of Type 107C Film. Again, note the diminished images relative to Type 146 Film. As the peel speed increases, the striations become less noticeable and the individual discharges, although fewer, are considerably stronger.

Fig. 8 shows one of the more intricate patterns of surface arcs observed. During the initial slow part of the peel, there is considerable evidence of longitudinal streamers. When the peel speed was increased, several large star-shaped arcs occurred and subsequently many longitudinal surface arcs are found adjacent to the lines of intense emission. Because these arcs are very clear (particularly in the original photograph) it means that they occurred on the surface of the film emulsion. Note that at the higher speeds (to the right), the total light emission actually diminished.

Fig. 9 shows slow peeling from the surface of a much faster film, Polaroid Type 612 Film, which is a high contrast film used for recording traces on a cathode ray tube (oscilloscope). With this film there tends to be no gray scale in terms of brightness; nevertheless, considerable detail is still observable. Obviously, the higher ISO (20,000) greatly increases the sensitivity and could be useful for interfaces that are less emissive. The dark regions are due to creases in the tape where there was no adhesive in contact with the film.

Effect of Application Pressure. As mentioned above, contact pressure can influence the intensity of the emission. Fig. 10 illustrates such a situation, where during attachment greater pressure was used on the bottom half to produce a better bond between the Magic Tape and Type 107C Film. The region where the highest pressure was applied yields more emission.

Tape as a Substrate. To vary the type of failure (cohesive vs adhesive), we first attached a layer of Scotch Double Stick Tape to the film emulsion and used this as a platform for attaching various substrates with little loss of resolution due to the thin tape backing. Once a test was

performed, this platform lifted from the film without additional photon emission by wetting the adhesive with methanol applied by a cotton swab adjacent to the peel zone. The methanol appears to fill the capillary crack, and either provides a conducting path which suppresses micro-arcs or simply destroys the adhesive bond. Following removal of this platform layer, the film could be developed in the ordinary fashion.

In photomultiplier experiments as well as electron and positive ion emission experiments (performed in vacuum), we have found that the emission intensity from adhesive failure is considerably more intense than from cohesive failure.[11-14] For illustration, we arranged the peeling of surfaces of Magic Tape so that the block letters *W S U* peeled in an adhesive fashion (adhesive from backing) and surrounding the letters, only adhesive-from-adhesive was peeled. Where the adhesive was peeled from the backing, much less force was required than the cohesive failure of the adhesive. The top of Fig. 11 shows the actual sample (reattached) used. The resulting image (light passing through various tape layers to the film) is shown on the bottom of Fig. 11; the light came from the adhesive-from-backing separation, i.e, from the regions where adhesive failure occurred. The cohesive failure of polymers *can* produce photon emission,[15] although it is typically orders of magnitude lower in intensity and in this case was not visible on the developed film.

Release Agents. We noted frequently that where the adhesive side of the tape had been touched by a finger, we could see the finger print in the image, where the print was *dark* relative to the normal light emission. The oils from the fingers were possibly serving as a release agent (or a conducting path - thus suppressing the discharges). Fig. 12 shows a fingerprint (EED's) deliberately put on the adhesive tape prior to attaching to Type 146 Film. A careful examination of some of the other figures may reveal inadvertent fingerprints on the edges or ends of the images (a sure way to identify stolen data).

Similarly, we marked on the adhesive side of the tape (*or* on the film surface) with a felt tip pen, allowed the ink to dry, then applied the tape to Type 107C film and peeled. The ink layer produced a peel strength about 1/5 that of untreated Magic Tape. In Fig. 13 we show the

reconstructed sample on top (viewed from the adhesive side), and the resulting photon emission from peeling (bottom). Clearly, wherever there was ink the light emission was negligible compared to the surrounding, normal peel. Thus, such release surface modifications can greatly influence the resulting emission. We point out that similar results were obtained when the ink was applied to the film emulsion.

Metal Present at Interface. The production of charge separation during the peeling should lead to strong electric fields. If a conductor is placed in the region between the film substrate and the adhesive, then as the peel front approaches the metal, sufficient charge can be induced on the metal to cause breakdown from the metal edges to the surrounding dielectric (the nearby film surface). In effect, sharp edges of the conductor can act as a charge density "concentrator". The image shown in Fig. 14a was made by placing several pieces of alumin foil on the adhesive of Magic Tape. This tape was then pressed on the surface of Type 107C Film with finger pressure (reconstructed sample shown on top). Subsequent peeling (>10 cm/s) of the tape resulted in the usual emission where adhesive failure was occurring (bottom of Fig. 14a). Surrounding the foil there is a dark area which is due to bridg ng of the tape between the film and the foil, thus producing a moat of no contact. Along the trailing edge of the aluminum foil, we observe that there are clear images due to sharp discharges occurring along the trailing edge of the aluminum foil, occasionally along the sides of the foil, and never along the leading edge. These patterns suggest that as the peel line advances, the charge created on the tape (which is lifting the back of the aluminum foil) induces the same *SIGN* charge on the opposite edges of the conducting foil. When sufficient charge is induced so that the breakdown voltage of air is reached , the "sparks" occur.

To show that it is not necessary to completely peel the tape past the region where breakdown occurs, we used a triangular piece of foil, with the sharp tip which concentrates induced charge pointing away from the advancing peel (reconstructed sample shown in bottom of Fig. 14b. The resulting breakdown at the tip of the metal where the peel was stopped 7 mm

from the tip is seen in the top of Fig. 14b. The remaining portion of the attached tape was lifted off of the film without producing additional light emission by wetting the adhesive with methanol. The tip being in intimate contact with the film produces very sharp images from microdischarges in the high charge density portion of the tip. Microscopic asperities along the cut edges are the likely sources of the individual arcs observed. With the use of an electrometer, we found that a negative charge $|Q| > 10^{-8}$ C is induced on the foil as the crack tip advances along the edges of the conductor, which is quite sufficient for producing breakdown in a number of gaseous environments, including Pullman air.

Fiber Optics Face Plate as Substrate. With the use of a fiber optic face plate, one can transmit light from a substrate above the film, e.g., the top surface of the glass plate itself. The face plate was circular 4 cm in diameter, 4.4 mm thick, and consisted of 6 um diameter fibers. The transmission of the face plate was only a few percent so we used the sensitive Type 612 Film. Figure 15 shows the images produced by peeling magic tape from the top surface of the face plate. The resulting images are similar to Fig. 6 except that with this rigid substrate the striations of stick slip failure are not as prevalent and are really strong only at the highest peel speeds. The microarcs are very distinctly seen with high resolution. The advantage of using a fiber plate is that thin films can be deposited on it and any substrate that transmits light can be studied. These include thin films of polymers and perhaps even metals. Furthermore, the fiber bundle could easily be coupled with an image intensifier, then to film, thereby obtaining even more sensitivity.

IV. CONCLUSION

Spatial images in the form of autographs of the photon emission accompanying the peeling of pressure sensitive adhesives from various substrates have been produced. The best images were created either by peeling tapes directly from Polaroid emulsion surfaces or from the top surface of a glass fiber optics face plate. Several features were consistent with other measurements:

e.g., a) striations which correspond to periodic variations in time of the phE intensities, b) corresponding variations in charge density on similar insulating substrates, and c) the number density of large discharges from Filament Tape as seen in these images agreed in magnitude with the observed frequency of the large radiowave bursts accompanying peeling. Also, the increase in emission intensity with peeling speed and the appearance of large individual bursts of light at higher speeds was observed in the photomultiplier experiments.[3] The observations of the influence of the mechanics of peeling (stick-slip, edge effects, role of release agents) may be of interest in studying details of the peeling process. The use of a fiber optics plate removes the need to use the emulsion as a substrate to create clear, distinct images and allows the introduction of a variety of substrates for further study. Finally, we mention that we have detected in composite structures photon emission coming from *inside* glass fiber-epoxy specimens[18] and have shown that it is due to interfacial failure between the fiber and the matrix. With the use of image intensifiers it may be possible to create images of this type of emission and pinpoint the location of yet another type of adhesive failure. Also, color slide films are available (e.g., Fuji Film, Type DX-400) which can be pushed to ISO 1600 by special developing techniques. This sensitivity was found sufficient to produce faint but distinct blue images of both 3M tapes studied here when peeled from the film emulsion.

V. ACKNOWLEDGMENTS

We wish to thank Russ Corey, a WSU undergraduate physics student who made a number of the film images. This work was supported by McDonnell Douglas Independent Development Fund, the Washington Technology Center, and the Office of Naval Research under Contract N00014-80-C-0213, NR 659-803.

REFERENCES

1. J. T. Dickinson, E. E. Donaldson, and M. K. Park, "The Emission of Electrons and Positive Ions from Fracture of Materials," J. Mat. Sci 16, 2897-2908 (1981).

2. J. T. Dickinson, L. C. Jensen, and A. Jahan-Latibari, "Fracto-Emission from Filled and Unfilled Elastomers," Rubber Chemistry and Technology 56, 927-941 (1983).

3. J. T. Dickinson, "Fracto-Emission Accompanying Adhesive Failure," in *Adhesive Chemistry-Developments and Trends*; Edited by L. H. Lee, Plenum, New York, (1985).

4. J. T. Dickinson, A. Jahan-Latibari, and L. C. Jensen, "Electron Emission and Acoustic Emission from the Fracture of Graphite/Epoxy Composites," J. Mat. Sci. 19, 1510 (1984).

5. J. T. Dickinson, L. C. Jensen, and S. K. Bhattacharya, "Fracto-Emission from the Failure of Metal-Epoxy Interfaces", J. Vac. Sci. Technol. A3, 1398 (1985).

6. J. T. Dickinson, L. B. Brix, and L. C. Jensen, "Electron and Positive Ion Emission Accompanying Fracture of Wint-o-Green Lifesavers and Single-Crystal Sucrose," J. Phys. Chem. 88, 1698-1701 (1984).

7. J. T. Dickinson, L. C. Jensen, M. R. McKay, and F. Freund, "The Emission of Atoms and Molecules Accompanying Fracture of Single Crystal MgO," J. Vac. Sci. Technol., A4 1648 (1986).

8. J. T. Dickinson, M. R. McKay, and L. C. Jensen, "Neutral Molecule Emission From Fracture of Crystalline MgO," J. Vac. Sci. Technol., to be published.

9. S. C. Langford, J. T. Dickinson, and L. C. Jensen, "Simultaneous Measurements of the Electron and Photon Emission Accompanying Fracture of Single Crystal MgO", submitted to J. Appl. Phys.

10. J. T. Dickinson and L. C. Jensen, "Fracto-Emission from Lead Zirconate-Titanate," J. Am. Ceramics Soc. 68, 235 (1986).

11. J. T. Dickinson and L. C. Jensen, "Crack Velocity Dependence of Electron Emission During Fracture of Filled Elastomers," J. Poly. Sci.: Poly. Phys. Ed., 20, 1925-1932 (1982).

12. J. T. Dickinson, M. K. Park, E. E. Donaldson, and L. C. Jensen, "Fracto-Emission Accompanying Adhesive Failure," J. Vac. Sci. Technol. 22, 436-439 (1982).

13. L. A. K'Singam, J. T. Dickinson, and L. C. Jensen, "Fracto-Emission from Failure of Metal/Glass Interfaces", J. Am. Ceramics Soc. 68, 510 (1985).

14. J. T. Dickinson, L. C. Jensen, and A. Jahan-Latibari, "Fracto-Emission: The Role of Charge Separation," J. Vac. Sci. Technol. A4, 1112-1116 (1984).

15. J. T. Dickinson, and L. C. Jensen, "Fracto-Emission from Filled and Unfilled Polybutadiene," J. Poly. Sci.: Poly. Phys. Ed. 23, 873 (1985).

16. E. E. Donaldson, J. T. Dickinson, and X. A. Shen, "Time and Size Correlations of Photon and Radiowave Bursts from Peeling Pressure Sensitive Adhesives in Air", J. Adhesion 19, 267 (1986).

17. R. Chen and Y. Kirsh, *Analysis of Thermally Stimulated Processes*, Pergamon, Oxford, 1981.

18. A. S. Castro, R. Corey, J. T. Dickinson, R.V. Subramanian, and Y. Eckstein, "Correlation of Photon and Acoustic Emission with Failure Events in Model Composites," submitted to Composites Science and Technology.

FIGURE CAPTIONS

Fig. 1. Images from peeling a) 3M Magic Tape and b) 3M Filament Tape (below) from glass slides placed directly upon the emulsion of Polaroid Type 107C Film, where peeling started at ~1mm/sec and was accelerated. Here and in all other cases, the tape was peeled from left to right. Unless otherwise stated, the peels were in a 90° geometry.

Fig. 2 Images from peeling a) 3M Magic Tape and b) 3M Filament Tape from glass slides placed directly upon the emulsion of Polaroid Type 612 film.

Fig. 3. a) Magic Tape and b) Filament Tape peeled from the negative emulsion of Polaroid Type 146 Film. For scale we note that the tapes are 19 mm wide. In this case the peel speed was accelerated during peeling beginning at ~ 1 mm/sec and proceeding to ~ 5 cm/sec.

Fig. 4 Magic Tape stiffened by two layers of electrical tape then peeled from Type 107C Film.

Fig. 5 Effect of peel geometry. First 180° then 90° peel angle, Magic Tape and Type 47 Film.

Fig. 6. Magic Tape peeled from Type 107C Film at speeds a) 1 mm/s, b) 1 cm/sec, and c) 30 cm/s.

Fig. 7. Filament Tape peeled from Type 107C Film at speeds a) 1 mm/s, b) 1 cm/sec, and c) 30 cm/s.

Fig. 8 An example of complex discharge activity during peeling. Magic Tape peeled from Type 47 Film at an increasing speed.

Fig. 9. Filament Tape peeled from Type 612 Polaroid Film.

Fig. 10. The consequence of increased pressure during attachment of the adhesive to the film emulsion (Type 107C Film).

Fig. 11. Cohesive-adhesive failure. A sandwich of Magic Tape was separated while it was held in close contact with the Type 107C Film by Double Stick Tape. The letters *W S U* were regions where the Magic Tape peeled from its backing, surrounded by adhesive-from-adhesive peeling.

Fig. 12. A fingerprint (the *dark* pattern) produced by imprinting the adhesive side of Magic Tape before attaching to Type 146 Film. The oil from the finger serves as a release agent.

Fig. 13. A release coating of ink from a felt tip pen was applied to the adhesive surface before the joint was made (Staedtler Lumocolor pen was used). The ink decreased the adhesion by a factor of five and greatly suppressed the light emission. The reconstructed sample is shown on the top.

Fig. 14. The consequence of peeling in the presence of aluminum foil between the adhesive and the film. a) Various strips of aluminum foil placed across the width

of the tape; b) a pointed piece of foil oriented "downstream" from the advancing peel line. The charge induced on the metal is the cause of the breakdown at the metal edges. The corresponding reconstructed samples are shown at the top and bottom, respectively.

Fig. 15. Magic Tape peeled from the top surface of a glass fiber optic face plate which was held in close contact with the surface of Type 612 Film.

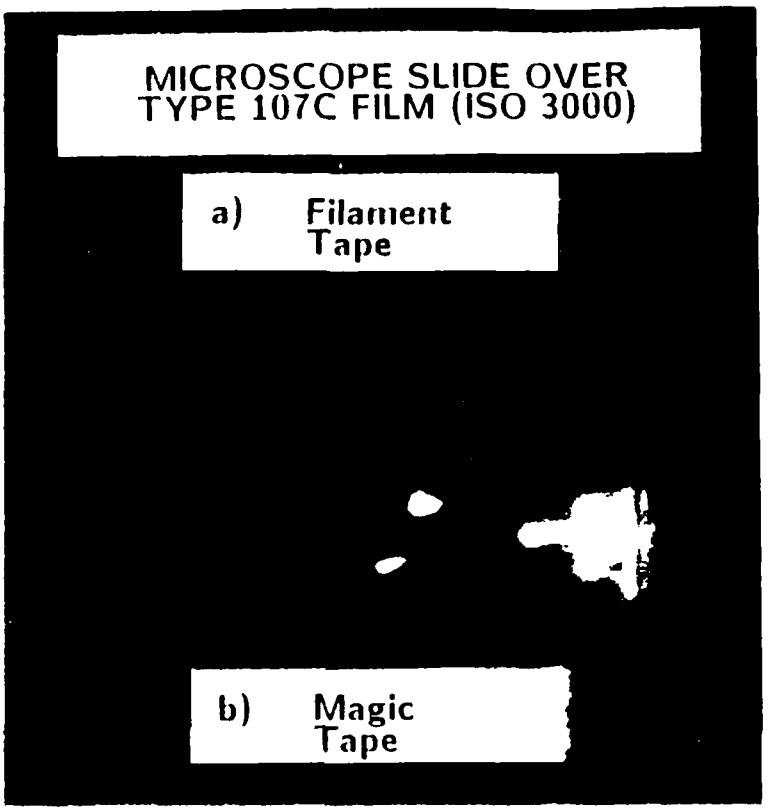
MICROSCOPE SLIDE OVER
TYPE 107C FILM (ISO 3000)
a) Filament Tape
b) Magic Tape

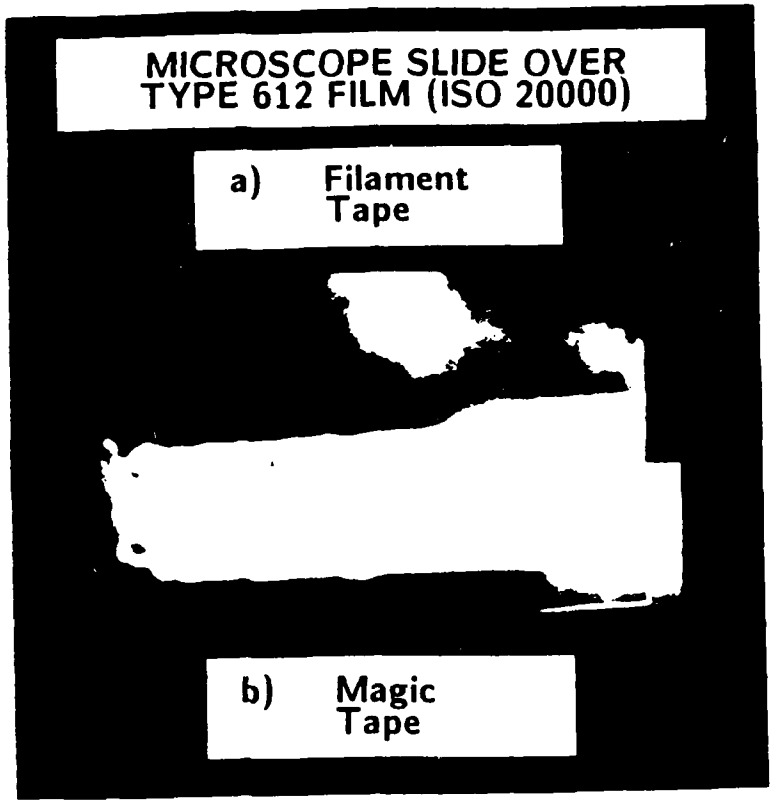
MICROSCOPE SLIDE OVER
TYPE 612 FILM (ISO 20000)
a) Filament
Tape
b) Magic
Tape

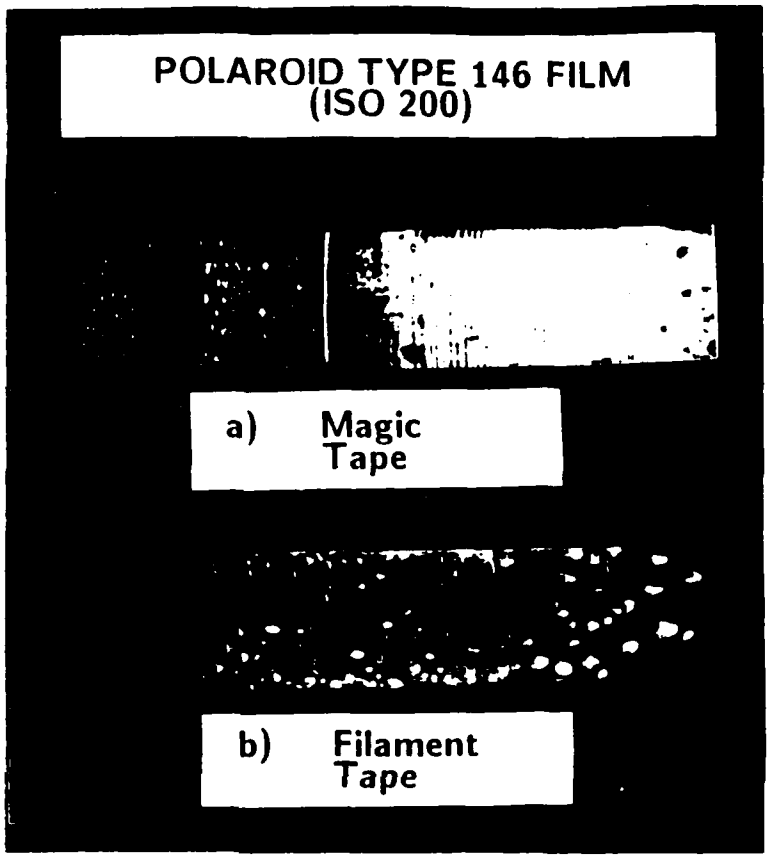
POLAROID TYPE 146 FILM
(ISO 200)
a) Magic Tape
b) Filament Tape

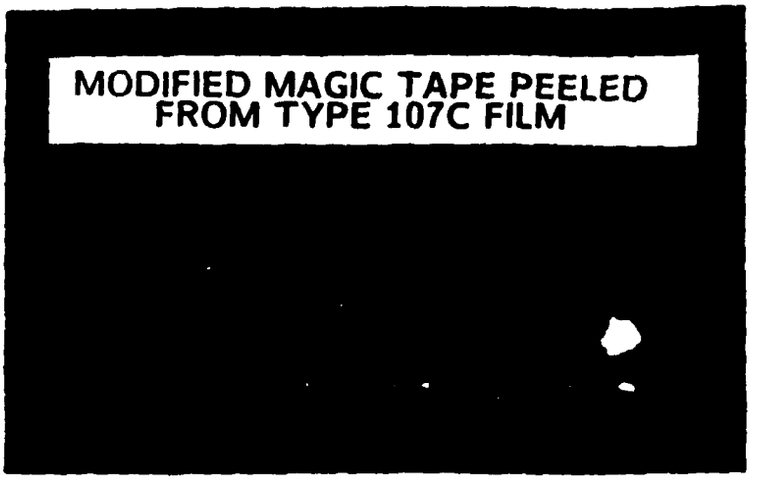
MODIFIED MAGIC TAPE PEELED
FROM TYPE 107C FILM

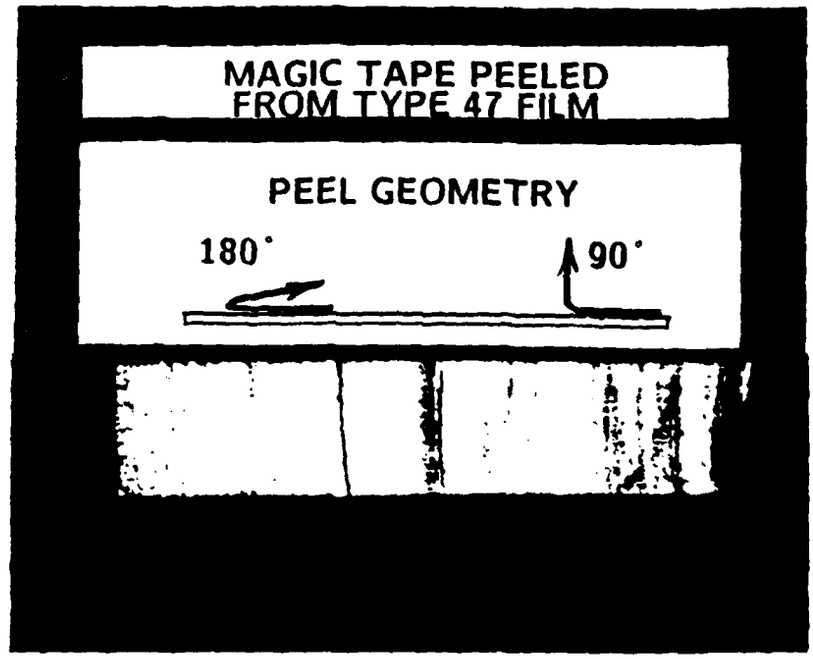
MAGIC TAPE PEELED
FROM TYPE 47 FILM
PEEL GEOMETRY
180°
90°

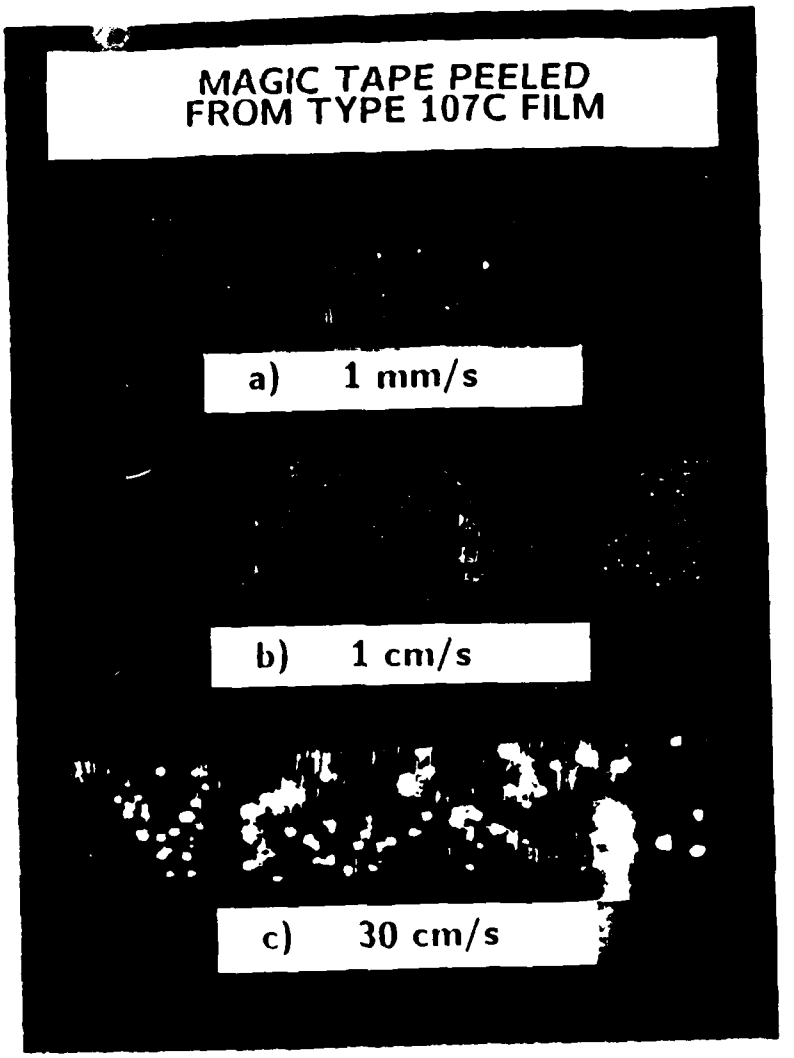
MAGIC TAPE PEELED
FROM TYPE 107C FILM
a) 1 mm/s
b) 1 cm/s
c) 30 cm/s

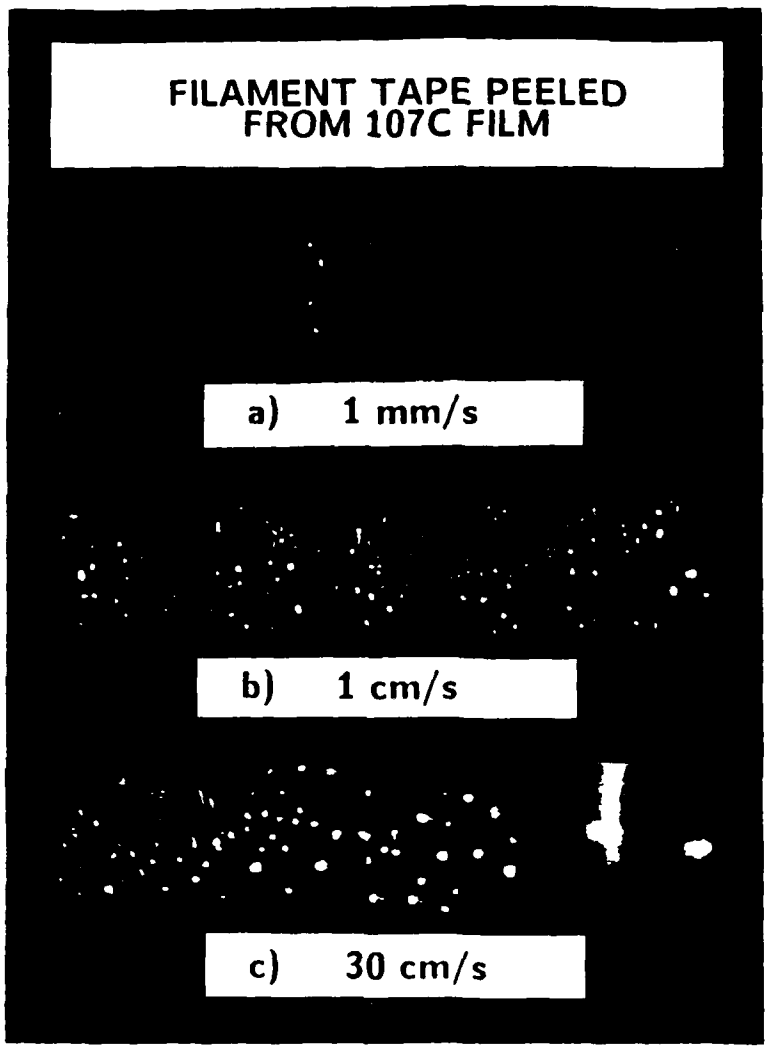
FILAMENT TAPE PEELED
FROM 107C FILM
a) 1 mm/s
b) 1 cm/s
c) 30 cm/s

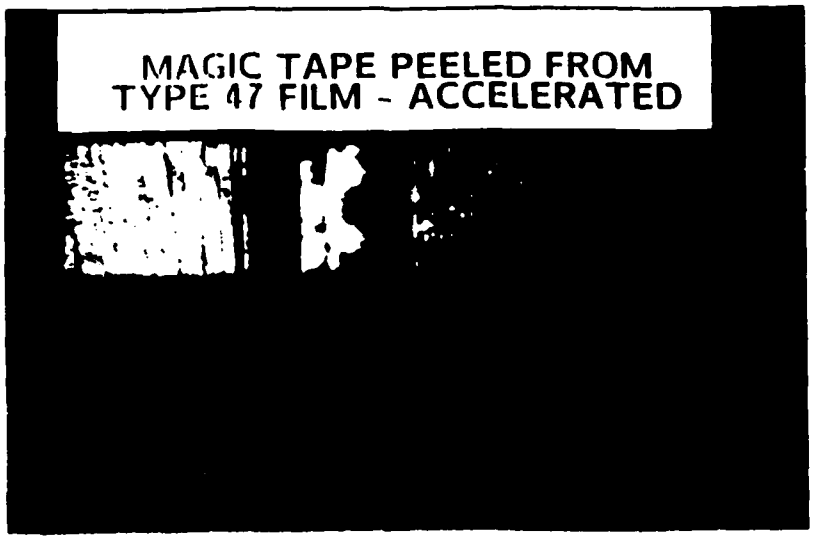
MAGIC TAPE PEELED FROM
TYPE 47 FILM - ACCELERATED

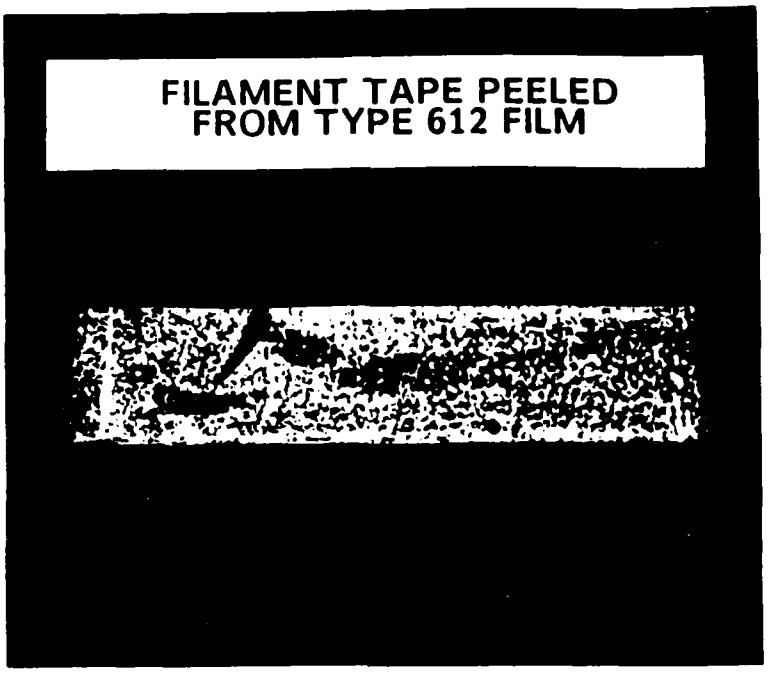
FILAMENT TAPE PEELED
FROM TYPE 612 FILM

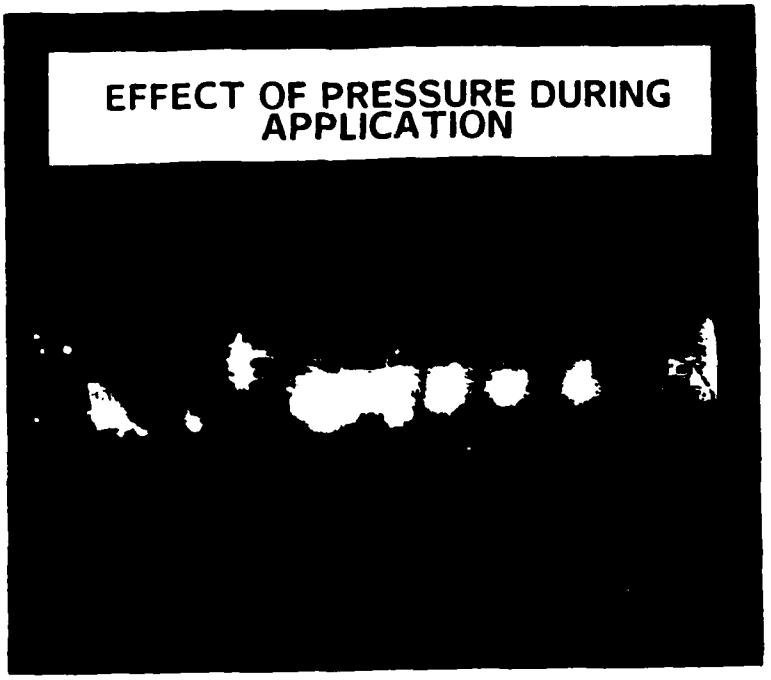
EFFECT OF PRESSURE DURING APPLICATION

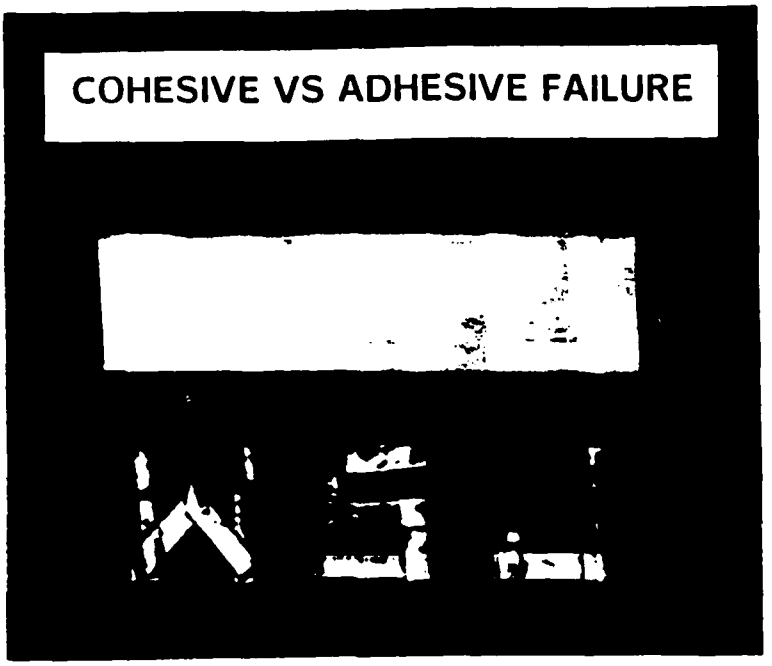
COHESIVE VS ADHESIVE FAILURE

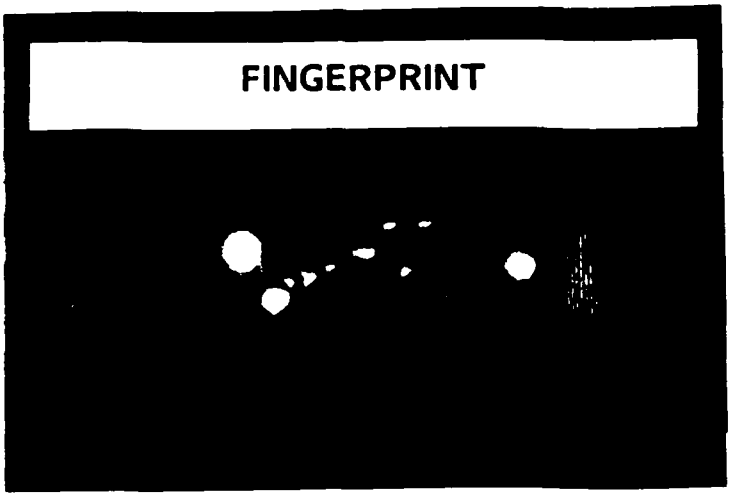
FINGERPRINT

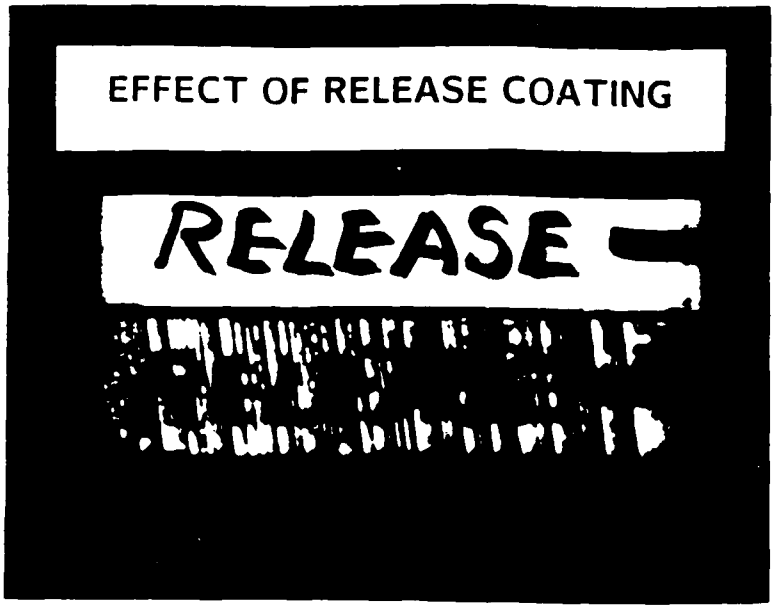
EFFECT OF RELEASE COATING
RELEASE

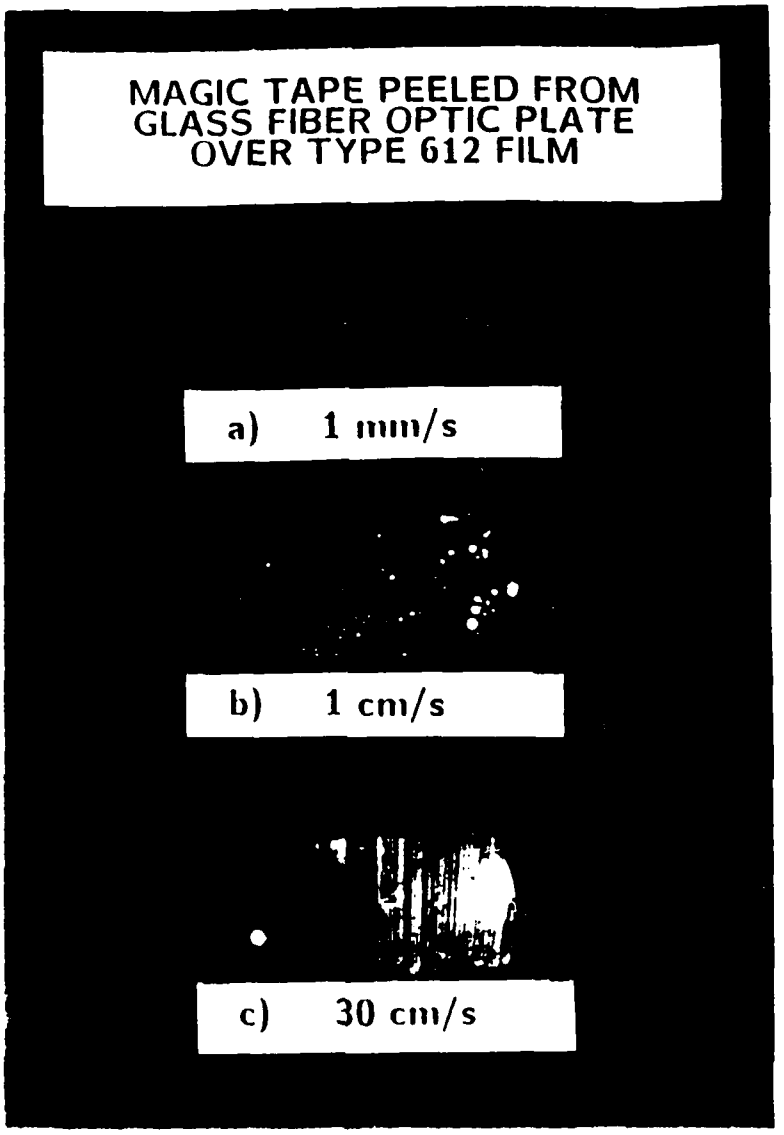
MAGIC TAPE PEELED FROM
GLASS FIBER OPTIC PLATE
OVER TYPE 612 FILM
a) 1 mm/s
b) 1 cm/s
c) 30 cm/s

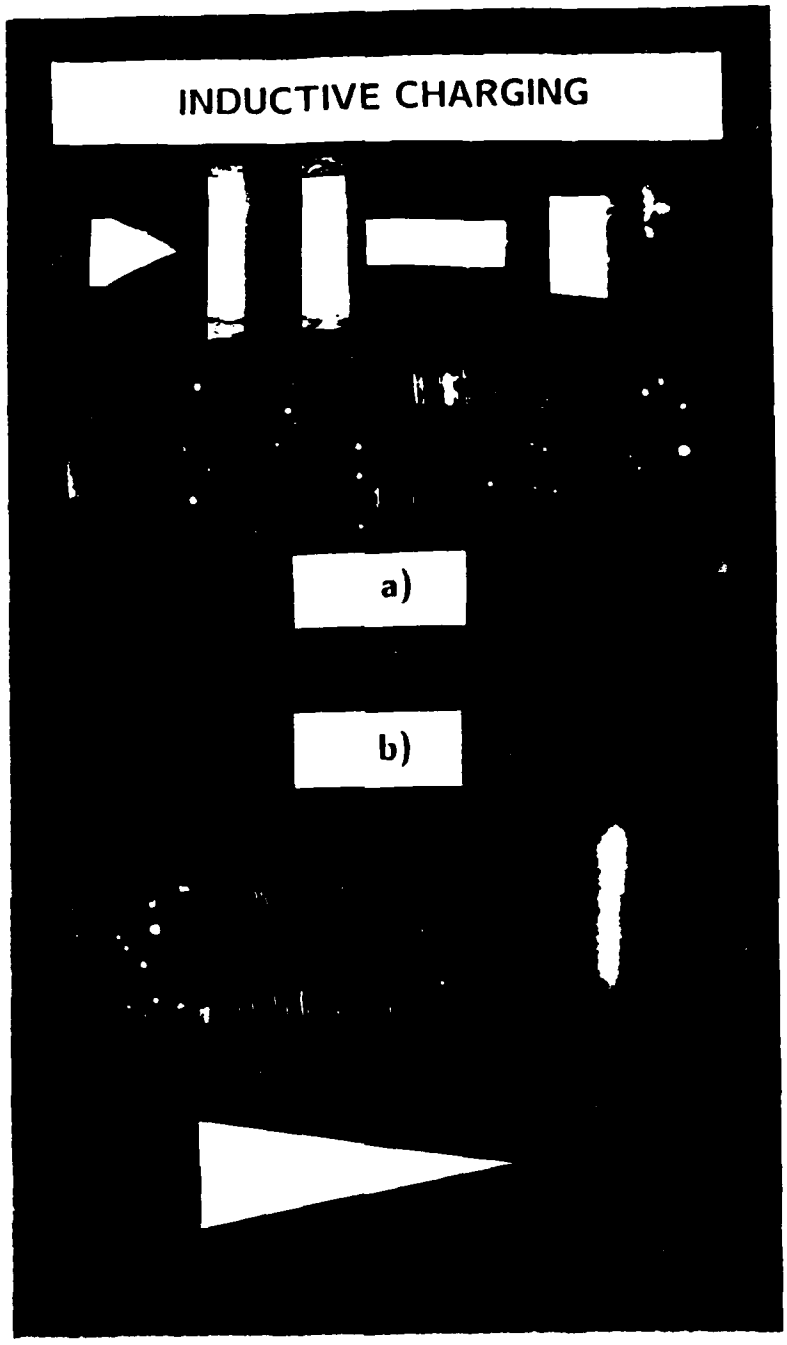
INDUCTIVE CHARGING
a)
b)

V. Neutral Molecule Emission From the Fracture of Crystalline MgO

J. T. Dickinson, L. C. Jensen, and M. R. McKay
Department of Physics
Washington State University
Pullman, WA 99164-2814

ABSTRACT

We present further measurements of the neutral molecule emission accompanying the fracture of single crystal MgO. Comparison is made of the intensities and species of this emission for basically two types of MgO: optically clear and so-called "cloudy" MgO. The latter material contains voids and precipitates of micron and sub-micron dimensions. In addition to time resolved mass selected measurements of the released neutral species we also examine the fractrography of the fracture surfaces and infrared spectroscopy of the bulk material. These measurements strongly support a correlation between O_2, CO, H_2O, and CH_4 emission intensities and the presence of dissolved H_2O, microscopic voids, and precipitates in the MgO. Segregation of gases in zones near precipitates may be the major source of O_2 emission.

I. INTRODUCTION

We have been investigating emission processes during deformation and fracture of materials [1-5 and references therein]. The types of emission observed include the release of electrons, ions, neutral atoms and molecules, and photons (so-called triboluminescence as well as long wavelength electromagnetic radiation) and are referred to collectively as fracto-emission (FE). In a previous paper[1], we presented initial results on the neutral emission (atoms and molecules) accompanying the fracture of single crystal MgO. We reported observing the emission of O_2, H_2O, CO, CO_2, H_2, CH_4, atomic Mg, as well as higher mass hydrocarbons from the fracture of MgO. We also noted[1] that variations in the oxygen related emissions were observed.

Further study of different types of MgO has revealed that even larger variations in the intensities of a number of these species were observed, depending on the source of single crystal MgO. The major feature that correlated with the emission intensities was the opacity of the crystals. An important part of this paper addresses the observed differences in gaseous emission induced by fracture between these different types of MgO. It should be noted that the opacity of MgO is strongly linked to the presence of voids, and precipitates that are formed during the manufacturing of the crystals, which in turn is dependent on the presence of dissolved H_2O. As we shall see, the origin of these fracture-induced neutral emission species is a very complicated problem.

We point out that these measurements have considerable importance concerning the nature, mobility, and chemical reactivity of low Z element impurities in ceramic materials. There are also geological implications in relation to abiogenic sources of gases found in rocks and in the atmosphere. In addition, these studies relate directly to the details of fracture and failure mechanisms in ceramics, which is an ever present part of ceramics research. Recent interesting results of Mg atom emission from fracture, whose intensity is independent on the type of MgO, as well as the detection of O_2 emission

prior to failure due to microcracking will be presented in later papers due to space limitations.

II. EXPERIMENTAL

All measurements were carried out at a background pressure =< 1 x 10^{-8} Torr in a system pumped simultaneously with a cryopump and magnetically suspended turbomolecular pump. Because most signals were of a duration of less than 0.1 s, there was no need for concern of adsorption of background gases on the fracture surfaces producing changes in desorption. Great care was taken to eliminate any artifacts of signals due to motion or rubbing of metal parts. The coincidence (to within a few microseconds) of the onset of emission with the fracture event was the most reliable indicator of gas from the specimen.

Since beginning these studies, four types of single crystal MgO have been studied which may be characterized by their appearance, as shown in Table I. All of these crystals were synthetically grown by arc fusion and have cation purities ranging from 99.9 to 99.99%. Our first report[1] of the neutral emission from MgO was data taken with Spicer1 single crystals. Additional studies were begun using a new block of MgO (Spicer2) which was obviously of higher transparency. Specimens from Spicer2 showed considerable reduction in the emission of O_2. On the other hand, experiments using a third set of crystals, SR Cloudy, showed considerably more intense emission of a number of the masses, in particular the O_2 emission. The uncut SR Cloudy MgO crystals were quite opaque and milky white in appearance, except for a region near the surface of the material (or near a grain boundary in the original block of material) that was transparent. The cloudiness was not uniformly dense, with veins of more intense light scattering. From the clear regions of the SR crystals, we were able to cut a few single crystals of what we call SR Clear. The few mass peaks measured from SR Clear showed

results similar to the Spicer crystals. Samples of Spicer2, SR Cloudy, and SR Clear single crystal MgO were cut from several cm^3 blocks using a diamond saw. Some were polished using 0.25 um diamond paste. The dimensions of the individual samples were typically 12 x 5 x 1 mm. All samples were cleaned ultrasonically in acetone, dried, then mounted in a three-point bending apparatus. Recently, a multiple sample holder was installed where up to 30 samples could be "injected" one at a time (like razor blades) into the breaking mechanism by translation from outside the vacuum system. The span of the three point bend was 2.5 mm and the breaking force was applied in the center with a "pusher" with either a 0.75 mm or 1.5 mm radius of curvature. The "pusher" advanced against the sample at 0.1 cm/second. From the fractography of the fracture surfaces it could be seen that the specimens tended to initiate cracks at the edges of the crystals opposite to the pusher, grow down the front face of the crystal (facing the mass spectrometer ionizer), then grow inward, with the most rapid crack growth in the later part of the fracture. Various force and acoustic transducers were used to determine the time of failure.

The neutral emission from the sample was monitored with a UTI 100C quadrupole mass spectrometer and a Bayard-Alpert gauge (BAG); these detectors were positioned 1.2 cm and 20 cm from the sample, respectively. The BAG was out of line-of-sight of the sample so that only non-condensable species (e.g., O_2, CO, CO_2) were detected. To minimize ripple of the collected ion current, the BAG filament was powered by a separate DC power supply. The quadrupole was normally tuned to a single mass peak due to the transient nature of the gas release. The electrometer outputs from the quadrupole and the ion gauge were digitized at 80-100 us/channel with a LeCroy Data Acquisition System. The time response of the mass spectrometer electronics was 20 us; the ion gauge electronics response time was 40 ms. Emission peaks are all shown with the background signals subtracted out.

III. RESULTS

Table II presents the average intensities for the mass peaks measured for the various types of MgO used. The most intense parent molecules are indicated. The entries marked with * or nm represent those which were either undiscernible from the background noise or "not measured", respectively. We note that the O_2 and H_2O emission from Spicer2 is greatly reduced. In contrast, the molecular emission from a third source of high purity MgO, SR Cloudy, increased dramatically, with the O_2 emission several orders of magnitude more intense than Spicer2. We will discuss the SR Clear results in a later section.

As further characterization of the differences in emission intensities between Spicer2 and SR cloudy, we compare typical total pressure changes p accompanying the fracture of these two materials in Fig. 1. Due to the location of the ion gauge, these signals represent only the non-condensable components of the neutral emission. In general the peak shapes of p for the two MgO types are the same; however, the magnitudes of the pressure changes are quite different, with the intensity of p for SR Cloudy MgO usually an order of magnitude or more greater than the intensity of p for the Spicer2 MgO. Assuming the major component of this emission to be O_2, these signals correspond to roughly one monolayer of non-condensable gases desorbed from SR Cloudy MgO fracture surfaces, and about 0.05 monolayers from Spicer2 MgO.

Fig. 2 shows the output signals of the quadrupole mass spectrometer at mass 32 (O_2) from SR Cloudy and Spicer2 MgO (both taken at an electrometer setting of 10^{-6} A full scale). The arrow indicates the time of fracture for the two specimens. The SR Cloudy peak, which is approximately 1000 times higher than Spicer2 emission, is extremely intense. In contrast, some Spicer2 specimens yielded no detectable mass 32. The time dependence of the mass 32 signal from the SR Cloudy crystals typically requires 400 us to reach its peak value, which is longer than the response time of the electrometer. If

one examines numerically the partial pressure of a gas in a pumped vacuum system as predicted by the so called "Redhead equation"[6] one finds that the rise in pressure follows the source function, N(t), independent of S/V, where S is the system pumping speed and V is the system volume. [We ignore the time for any instantaneous change in N(t) to reach randomization inside the chamber; this is estimated to be on the order of 10 us]. Thus, the observed O_2 rise is considered to be limited by the actual O_2 release process rather than an artifact of the vacuum system and spectrometer.

For finite S/V, the decay of the partial pressure can, of course, be considerably longer than the actual decrease in N(t). Using measured values of S/V, we find that the first part of the mass 32 decay (approximately the first 2 ms) could be due to finite S/V. The longer feature (which actually extends several hundred ms) is either due to adsorption/desorption on chamber surfaces or, more likely, a small amount of desorption continuing from the specimen after fracture.

Fig. 3 shows a comparison of the mass 18 peak (H_2O) for SR Cloudy and Spicer2 MgO, where the signal from the Cloudy specimens rises 30-50 times the background mass 18 level; the data shown was taken on the 10^{-7} A scale. Sequences of emission curves taken at mass 18 and mass 17 show good agreement in amplitude with the cracking fraction of H_2O. The change in pressure for Spicer2 specimens was hardly detectable.

Mass 2 emission peaks from the SR Cloudy and Spicer2 MgO are shown in Fig. 4. The amplitudes and time dependence for these two types of MgO specimens are essentially the same (relatively small), with slightly larger signals from the fracture of SR Cloudy. Most of the Mass 2 signal is attributed to H_2, with small contribution coming from cracking fractions of H_2O and hydrocarbons.

Masses 15, 28, and 44 from SR Cloudy are shown in Fig. 5; we have assigned these peaks to the parent molecules CH_4, CO, and CO_2. Mass 16 was predominantly due to the O_2 and CO cracking fractions. The CO peak is seen to be almost as intense as the

O_2 emission. (Thus, the total pressure change curve for SR Cloudy in Fig. 1 is almost all due to O_2 and CO). A related study of gas emission from fracture under compression (crushing) has shown the emissions at these masses to be extremely small from Spicer2.

In searching for explanations for these extraordinary differences in the neutral emission intensities, particularly comparing Spicer2 and SR Cloudy, it is necessary to consider the role of impurities and heterogeneities in the crystals. To provide additional information, we have carried out measurements of the infrared spectra in the vicinity of the OH stretch frequencies for Spicer2 and SR MgO. Fig. 6a show the spectra of SR Cloudy and Spicer2, respectively. Essentially no lines are seen in the Spicer2 spectrum. The rising background in the SR Cloudy curve is due to scattering of the IR by the microscopic voids and precipitates present in the SR Cloudy MgO. Fig. 6b shows the expanded spectrum of SR Cloudy MgO in the range 3200-3900 cm^{-1}. The peaks indicated are at 3296, 3312, and 3701 cm^{-1}, with a smaller peak at 3555 cm^{-1}. The peaks at 3296 and 3312 cm^{-1} indicate the presence of OH stretching in a half compensated defect site (i.e., of the form $OH^-[++]O^{2-}$, where [++] refers to a Mg^{2+} vacancy) in slightly different environments.[7] These defects are equivalent to a V_{OH} center. Peaks at 3555 cm^{-1} would be indicative of OH stretching in a fully compensated defect site (i.e., of the form $OH^-[++]OH^-$). The peak at 3701 cm^{-1} is due to a $Mg(OH)_2$ (brucite) phase.[8]

Using the relation A=e*p*c, where A is the absorptance, p is the path length, c is the concentration, and a molar extinction coefficient e of 81 l/mole-cm,[9] the OH concentrations can be calculated. In half compensated defect sites the OH concentration is on the order of 10^{18} cm^3, and for fully compensated defect sites it is approximately 10^{17} cm^3.

Fig. 6c shows the IR spectrum for a sample cut from the aforementioned transparent region of the SR block, i.e., SR Clear. This spectrum also shows peaks (down by a

factor of 5) at 3296 cm^{-1} and 3312 cm^{-1}, again indicating the presence of OH stretching in half compensated defect sites. There is also a peak at 3555 cm^{-1}, indicative of OH stretching in fully compensated defect sites. The approximate OH concentrations in the SR Clear material are on the order of $10^{17}/cm^3$ for both half and fully compensated defect sites. In contrast to the SR cloudy spectrum of Fig. 6c, however, there is no peak at 3701 cm^{-1}, indicating the lack of $Mg(OH)_2$.

When samples of SR Clear were fractured and mass 32 and the other oxygen containing peaks (44, 28, 18, and 17) measured, the emission was found to be considerably smaller than SR Cloudy (see Table II), quite similar to the Spicer2 MgO. In addition, the total pressure change accompanying these measurements was similar to the Spicer2 MgO.

It is important to emphasize that there are no absorption peaks at any of the above wavenumbers for the Spicer2 MgO; i.e. the concentrations of OH-compensated defect sites and $Mg(OH)_2$ in Spicer2 MgO are below the detection limit of the spectrometer. These results are in agreement with a study done by Briggs[10] correlating opacity and IR spectra.

We have not performed IR spectroscopy on the Spicer1 specimens. However, when compared visually side by side with Spicer2 crystals, there is clearly a difference in that the Spicer1 crystals show limited but detectable opacity in normal lighting and among different Spicer1 crystals, there was a discernible range of opacity. This suggests that Spicer1 is MgO that would be intermediate and variable in its content of OH^-, $Mg(OH)_2$, and associated macroscopic defects (voids and/or precipitates).

The fractography of the SR Cloudy (strong O_2 emitter) shows that there are very few voids on the exposed fracture surface. Fig. 7a shows an SEM photograph of voids in SR Cloudy; these features could be found only by close inspection of the fracture surface. As shown here, they are often seen in clusters of a single large void, accompanied by a few smaller voids. Occasionally, smaller voids are found in isolation. A rough estimate

of the surface density of the larger voids is $10/cm^2$ and 10^4 small voids/cm^2. The accepted growth mechanism involves dissolved H_2O which is incorporated into the crystal during high temperature growth. OH^- frequently associates with Mg^{2+} vacancies to produce V_{OH} centers. V_{OH} centers and oxygen vacancies combine to produce divacancies, which in turn agglomerate to create tiny voids, believed to be filled with hydrogen.[10-12] These voids have been found to be typically 0.1-10 um in diameter,[10,12] and are often associated with subgrain boundaries and tangled dislocation networks. As mentioned previously, the cloudiness in the SR MgO samples has been attributed to these microscopic voids due to light scattering.

It is also possible that precipitates are also contributing significantly to the SR Cloudy opacity; a significant number of precipitates are observed, as seen in Fig. 7b, showing a region of the SR Cloudy surface filled with precipitates. These have surprisingly uniform sizes (TM 0.1 um) and often occur along what appears to be subgrain boundaries. An estimate of the average surface density of visible precipitates on the fracture surface is $10^6/cm^2$. Similar SEM photographs on Spicer2 crystals show void (surface) densities on the order of $10^2/cm^2$ and precipitate (surface) densities on the order of $10^3/cm^2$, considerably lower than for SR Cloudy. These precipitates are of the correct size to yield Mie scattering, which is what we observe with HeNe laser light. We have not determined directly the composition of these precipitates but suspect that they are $Mg(OH)_2$, consistent with the IR spectrum above. Briggs[13] has shown direct evidence of brucite precipitates in MgO and verified that their crystal structure was ordered with respect to the MgO lattice.

IV. DISCUSSION

In summary, then, the SR Cloudy MgO (which yields intense O_2, CO, and H_2O emission) has associated with it higher void, precipitate (probably $Mg(OH)_2$), and bulk

OH^- concentrations. The latter is accompanied with O^- defects (e.g., V_I defects: an O^- associated with a cation vacancy), which could serve as a source of oxygen atoms. It is compelling to link the mechanism of the emission of oxygen containing gases to these entities rather than any inherent bond breaking mechanism. In other words, "pure" MgO (to which Spicer2 is an approximation) yields very little O_2, CO, and H_2D emission; bond scissions occurring during fracture of Mg--O ionic bonds in material with low defect concentrations under our loading conditions do not alone lead to the formation of significant quantities of O_2(g).

At this point we can only speculate to the origin of these gaseous species and the role the above entities play (e.g., the precipitates, their interface with the MgO, and/or the surrounding MgO (laden with O and H containing defects) as the source of oxygen containing gases. Assuming that the precipitates are indeed the hydroxide, it has been well established[9,14] that the decomposition path for $Mg(OH)_2$ is as follows: $Mg(OH)_2$ --> $MgO + H_2O$; thus, one would expect that the only product that could involve the precipitate alone would be H_2O.

The O_2 (which is by far the most intense emission peak from SR Cloudy) is not likely coming from the voids. Unless there are far larger numbers of voids below our SEM resolution, the total volume of the voids is just too small. Rather, the O_2 may in fact be present as a gas trapped at the precipitate interfaces and subgrain boundaries associated with these precipitates. This precipitate zone would serve as a reservoir which suddenly becomes exposed to the vacuum at the time of fracture, releasing the O_2. [Studies of MgO bicrystals have shown that fracture can nucleate at or near grain boundaries, where dislocations formed during deformation pile up due to a pinning effect[15]. The precipitates at subgrain boundaries would make these regions preferred fracture sites in single crystal MgO.] We have fractured samples of identical size of polycrystalline brucite, a mineral obtained from Stevens County, Washington, and looked for O_2 emission; the resulting mass 32 signal was about 10% of what we observed from

Since these macroscopic defects are always associated with high OH^- concentrations, which in turn leads to defects of the type V_{OH}, V_I, and hydrogen-Mg vacancy defects, we cannot rule out a O_2 and H_2O emission mechanism that involves the solid state chemistry of these defects and impurities, as previously described.[1] However, we note that SR Clear, with high concentrations of OH^- showed minimal O_2 and H_2O emission, suggesting that this is not the dominant mechanism. Secondly, the bulk concentration of the OH^- related defects is on the order of 100 ppm, which makes it very difficult to support the idea that fracture is triggering solid state/surface reactions (on the millisecond time scale) which could produce the molecular emission of monolayer quantities that we observe. This is why we have stressed the role of the macroscopic defects and associated zones that would serve as reservoirs of the observed gases.

In contrast, the atomic magnesium emission intensity[1], only briefly mentioned here, is independent of the type of MgO fractured, and may indeed be a result of free atoms created by bond breaking. This work shall be discussed further in a publication in preparation.

V. ACKNOWLEDGMENTS

This work was supported by the Ceramics and Electronics Materials Division of the National Science Foundation under Grants DMR 8210406 and DMR 8601281 and the Office of Naval Research Contract No. N00014-80-C-0213, NR 659-803. We wish to thank Dr. Kerry Hipps, Dr. Phil Rosenberg, and Steve Langford, Washington State University, for their assistance in this work. We also wish to thank Dr. Friedemann Freund, U. of Koln, for several stimulating discussions and for providing the SR Cloudy samples.

SR Cloudy. SEM examination of the brucite fracture surface with SEM showed the failure to be mixed intra- and inter-granular. The mineral showed roughly 95% brucite with magnesite impurities. The fact that mass 32 emission was observed suggests that fracture along macroscopic grain boundaries in $Mg(OH)_2$ can result in O_2 release.

Similarly, the CO and CO_2 which are also relatively intense from SR Cloudy vs SR Clear and Spicer crystals, appears to be similar to the intense O_2 emission. MgO is known to contain concentrations of bulk carbon due to the dissolution of CO_2. Studies by Freund, et. al.[16] have shown this type of MgO contains on the order of 50-800 wt. ppm, and has been attributed to dissolved CO_2. We propose that the CO and CO_2 we observe are also present and trapped in these precipitate zones and are released at fracture.

Given the cavity growth mechanism described above, one would expect that the very small H2 signals are from H_2 gas trapped in the voids which would be released immediately upon fracture. Briggs[13] calculated that the cavity pressure should be on the order of 300 atm, which means that to obtain a partial pressure rise at mass 2 which we observe, one would only need 30 small voids. Since we observe on the order of 10^3 small voids per fracture surface in SR Cloudy, the H_2 pressure inside the voids would have to be more like 10^{-2} atm. This indicates that most of the H_2 created during void growth has moved out of the voids. The fact that we see essentially no difference in the H_2 signals for the different types of MgO with a wide range of void densities may in fact mean that the H_2 we observe is distributed throughout the bulk of the crystal. A mechanism for this has been suggested by Freund et al.[17]

A small part of the "missing" H_2 could have reacted with bulk carbon, presumably on the walls of the cavities where it would be trapped due to the size of the molecule. Fracture simply opens the voids, releasing the methane. The very small amount of heavier hydrocarbons that we see probably coming from the same location, namely the voids.

Table I. Types of MgO single crystals used in Ref. 1 and this study.

Identifier	Source of Crystal	Appearance	Emission of O_2 related species
Spicer1 used in ref. 1.	W. & C. Spicer Ltd., Cheltenham, England	relatively clear; occasional patches of cloudiness	variable, often intense.
Spicer2	" "	extremely clear; free of visible scattering centers	generally weak
SR Cloudy	Super Refractories, Cheltenham, England	very cloudy	extremely intense
SR Clear	" "	relatively clear	generally weak

Table II. Comparison of neutral molecule emission mass peaks from the fracture of various types of single crystal MgO.

Crystal Type	Mass Peak								
	2 H_2	12 CO_x	15 CH_4	16 O_2	18 H_2O	24 Mg	28 CO	32 O_2	44 CO_2
Spicer1	30	1	0.5	10	5	1	10	100	1
Spicer2	30	1	*	nm	10	1	nm	0.2	nm
SR Cloudy	30	nm	50	3000	800	1	10000	20000	25
SR Clear	30	1	2	3	4	1	6	0.2	1

REFERENCES

1. J. T. Dickinson, L. C. Jensen, and M. R. McKay, J. Vac. Sci. Technol. A4, 1648 (1986).
2. J. T. Dickinson, W. D. Williams, and L. C. Jensen, J. Am. Ceramics Soc. 68 235 (1985).
3. L. A. K'Singam, J. T. Dickinson, and L. C. Jensen, J. Am. Ceramics Soc. 68 510 (1985).
4. J. T. Dickinson and L. C. Jensen, J. Poly. Sci.: Poly. Phys. Ed. 23, 873 (1985).
5. J. T. Dickinson, L. C. Jensen, and A. Jahan-Latibari, J. Vac. Sci. Technol. A2, 1112 (1984).
6. P. A. Redhead, Vacuum 12, 203 (1976).
7. M. S. Corisco, R. Gonzalez, and C. Ballesteros, Phil. Mag. A 52, 699 (1985).
8. R. A. Buchanan, H. H. Caspers, and J. Murphy, Applied Optics 2, 1147 (1963).
9. W. K. Thompson, Trans. Faraday Soc. 61, 2635 (1965).
10. A. Briggs, J. Mat. Sci. 10, 729 (1975).
11. B. Henderson and J. E. Wertz, Defects in the Alkaline Earth Oxides, Taylor and Francis, London (1977).
12. A. Briggs and D. H. Bowen, Natl. Bur. Standards Spec. Publ. 296, 103 (1968).
13. A. Briggs, J. Mat. Sci. Lett. 12, 637 (1977).
14. J. Green, J. Mat. Sci. 18, 637 (1983).
15. Y. Moriyoshi, W. D. Kingery, and J. B. VanderSande, J. Mat. Sci. 12, 1062 (1977) and references therein.
16. H. Wengeler, R. Knobel, H. Kathrein, F. Freund, G. Demortier, and G. Wolff, J. Phys. Chem. Solids 43, 59 (1982).
17. F. Freund and H. Wengeler, J. Phys. Chem. Solids 43 129 (1982).

FIGURE CAPTIONS

Fig. 1. Total Pressure change accompanying the fracture of SR Cloudy and Spicer2 single crystal MgO.

Fig. 2. Mass 32 emission from the fracture of a) SR Cloudy MgO and b) Spicer2 MgO. The total gas emitted differs by over a factor of 1000.

Fig. 3. Mass 18 (H_2O) emission from the fracture of SR Cloudy and Spicer2 MgO, shown on the same scale.

Fig. 4. Mass 2 (H_2) emission from Spicer2 and SR Cloudy MgO, shown on the same plot. Spicer1 and SR Clear H_2 emission were essentially identical to these peaks.

Fig. 5. Mass 15, 28, and 44 emission from SR Cloudy MgO.

Fig. 6. Infrared absorption spectra for SR Cloudy, Spicer2, and SR Clear MgO.

Fig. 7. SEM photographs of fracture surfaces of SR Cloudy MgO showing a) voids and b) precipitates (and a few small voids). The precipitates greatly influenced the crack path.

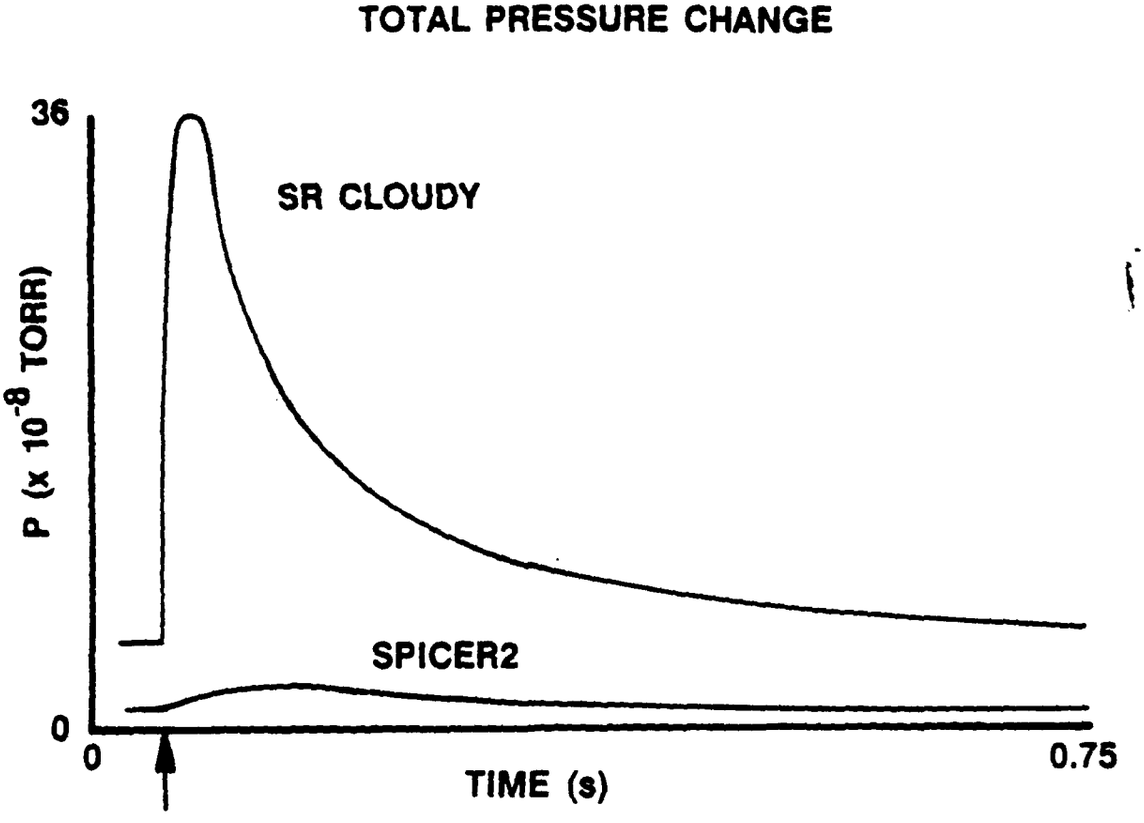
TOTAL PRESSURE CHANGE
36
SR CLOUDY
P (x 10-8 TORR)
SPICER2
0
0
0.75
TIME (s)

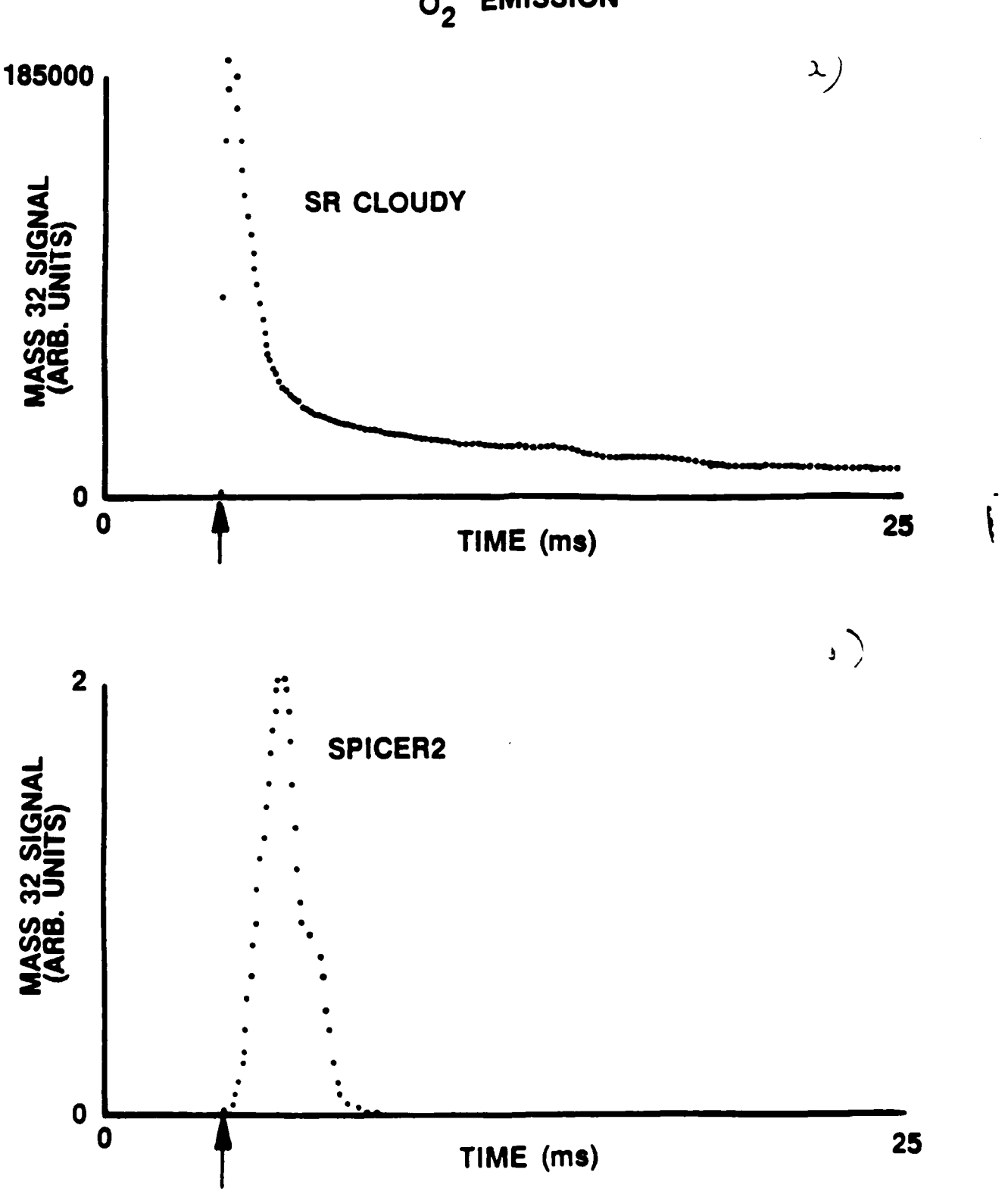
O_2 EMISSION
185000
MASS 32 SIGNAL (ARB. UNITS)
SR CLOUDY
0
0
TIME (ms)
25
2
MASS 32 SIGNAL (ARB. UNITS)
SPICER2
0
0
TIME (ms)
25

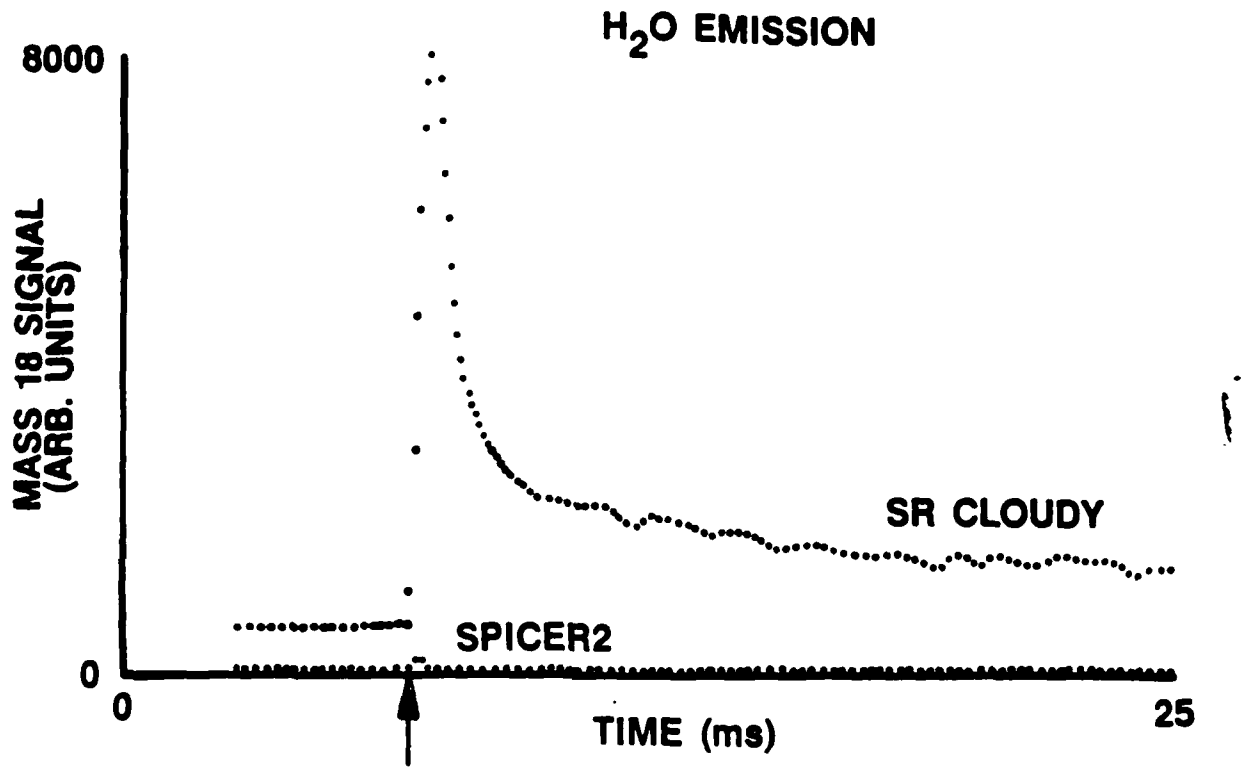
H_2O EMISSION
8000
MASS 18 SIGNAL (ARB. UNITS)
0
0
SR CLOUDY
SPICER2
TIME (ms)
25

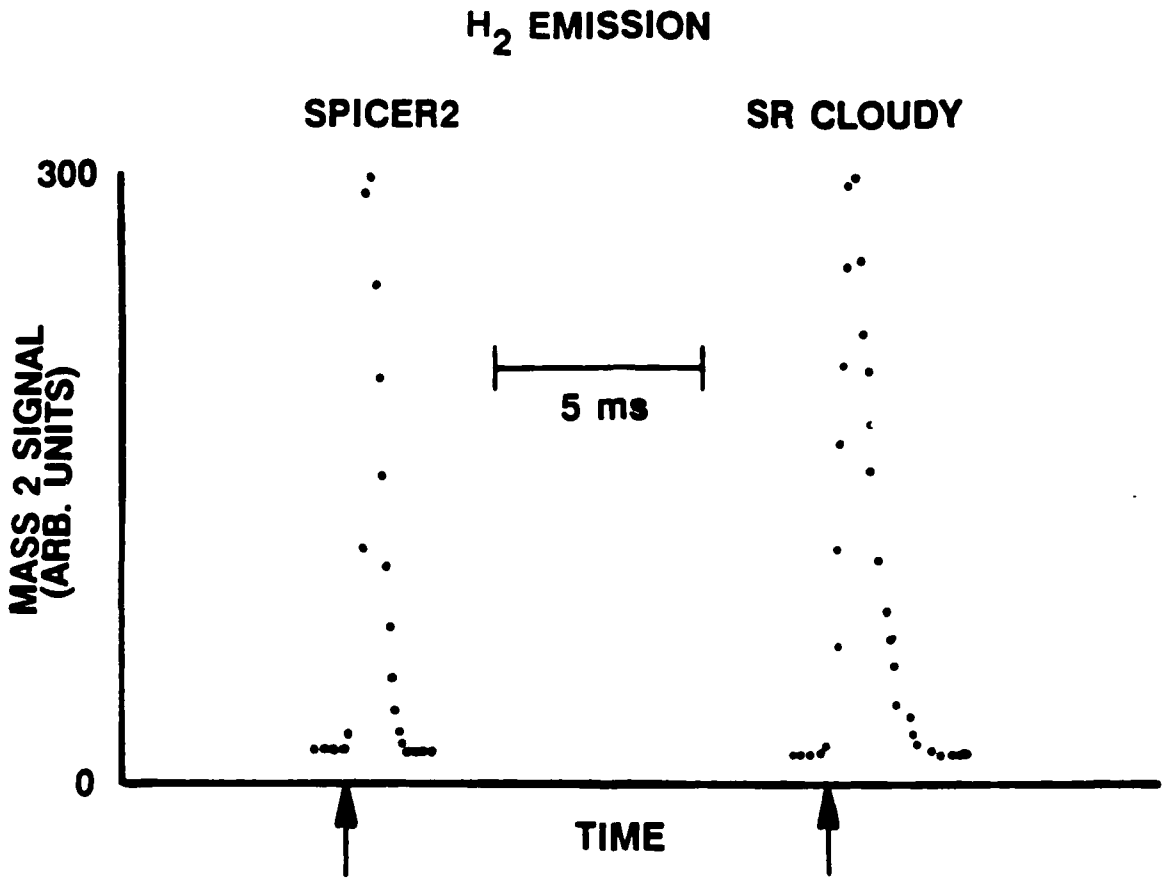
H_2 EMISSION
SPICER2
SR CLOUDY
300
0
MASS 2 SIGNAL (ARB. UNITS)
5 ms
TIME

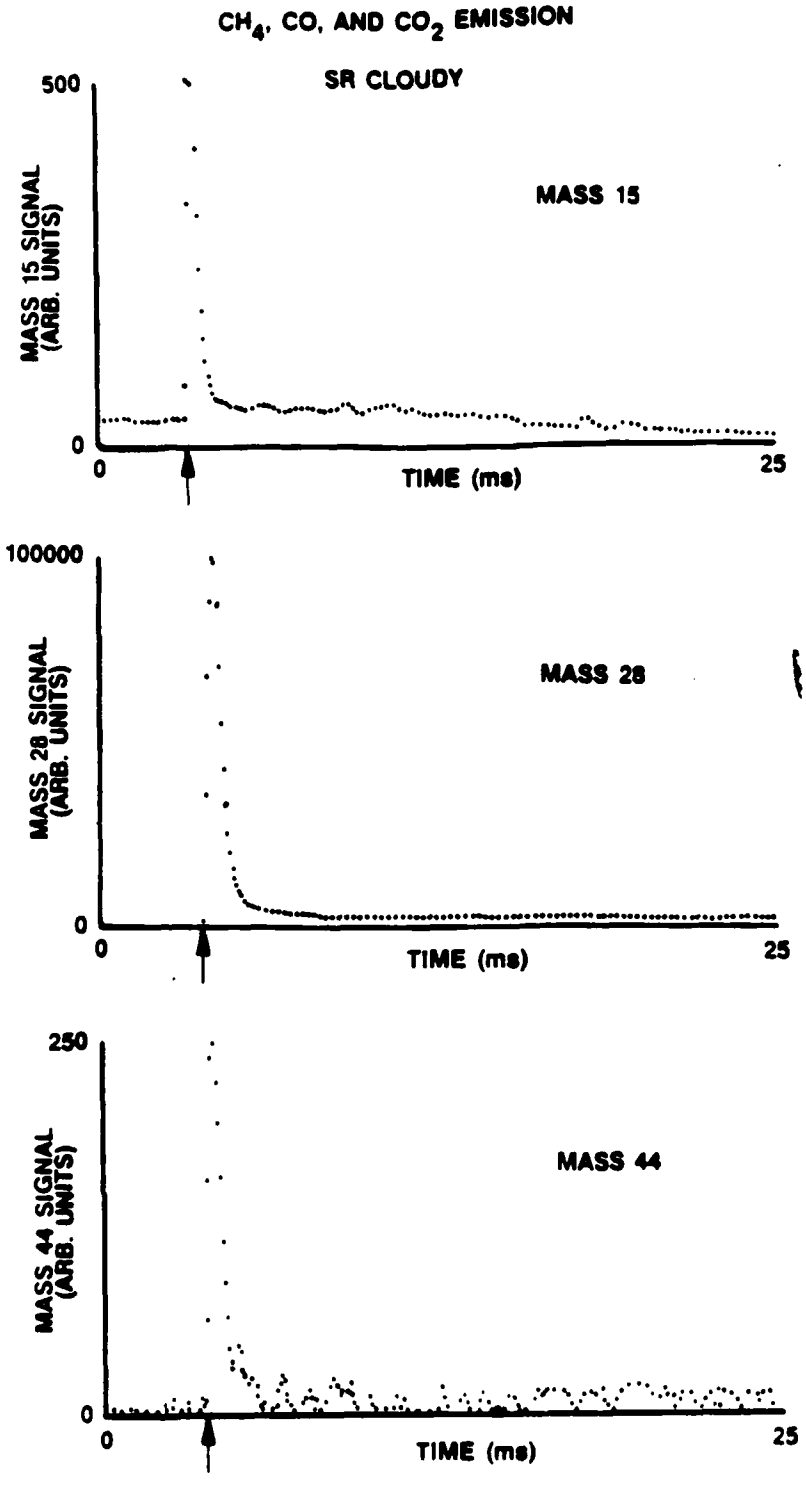
CH_4, CO, AND CO_2 EMISSION
SR CLOUDY
500
MASS 15 SIGNAL (ARB. UNITS)
MASS 15
0
0
TIME (ms)
25
100000
MASS 28 SIGNAL (ARB. UNITS)
MASS 28
0
0
TIME (ms)
25
250
MASS 44 SIGNAL (ARB. UNITS)
MASS 44
0
0
TIME (ms)
25

5

IR SPECTRA- MgO

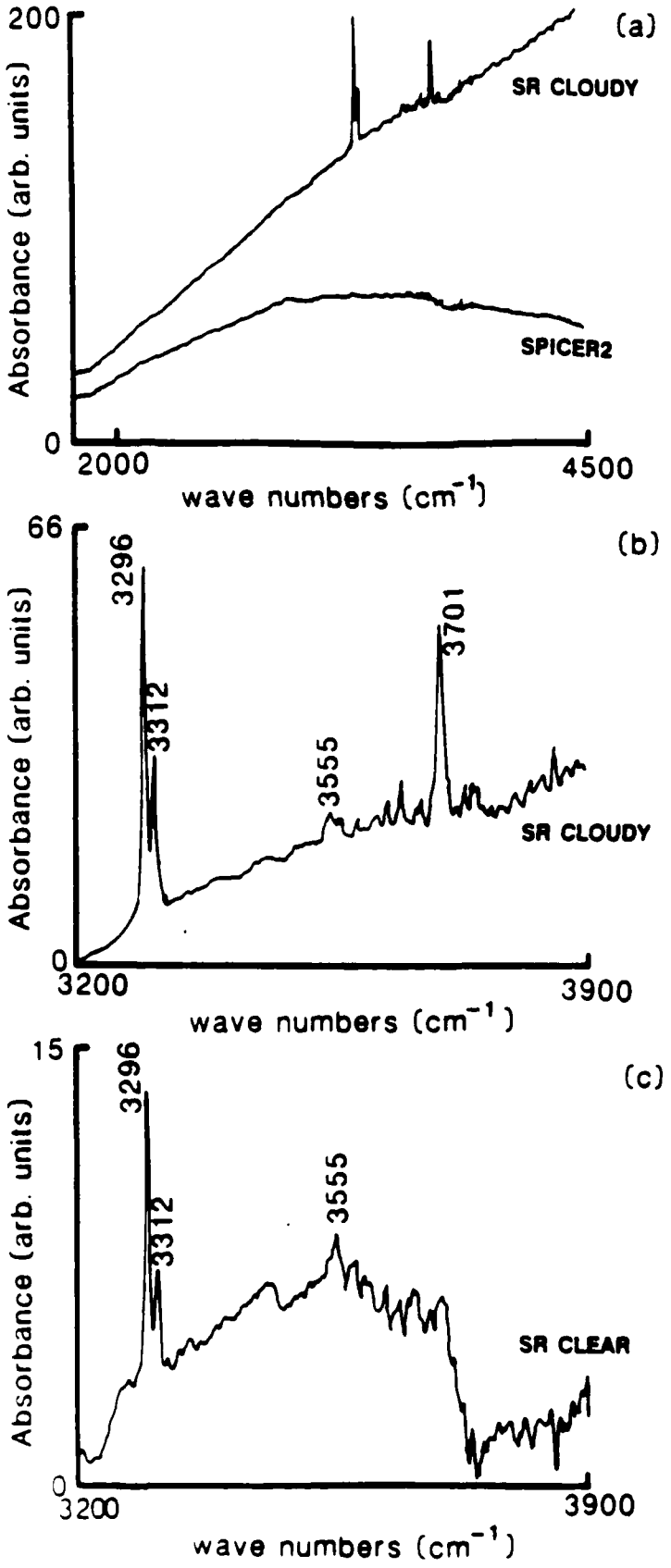

SR CLOUDY

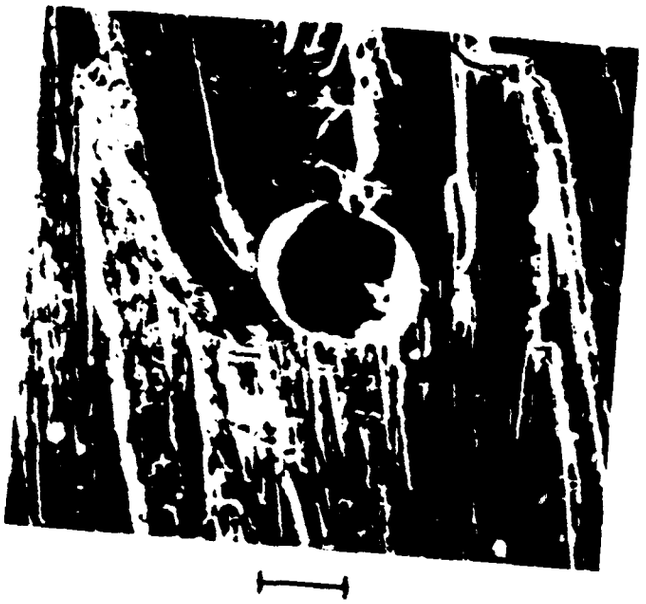

a)

10 µm

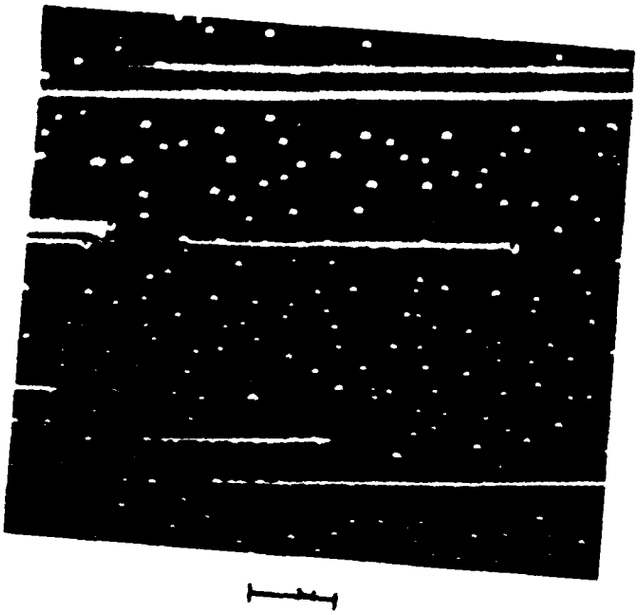

b)

5 µm

VI. Fracto-Emission From Polymers, Crystals, and Interfaces

J. Thomas Dickinson
Department of Physics
Washington State University
Pullman, WA 99164-2814

Abstract

When materials are deformed and broken, surfaces are formed which may have charge concentrations as well as defects and displaced atoms. The consequences of such departures from non-equilibrium can lead to the emission of particles (electrons, ions, and neutral species) as well as photons (triboluminescence). Collectively, we refer to these emissions as fracto-emission. We present measurements of various components of emission from a variety of materials and show that a number of features of the emission involve the transport of charge.

Introduction

Fracto-Emission (FE) is the emission of particles and photons during and after fracture of materials. The types of particles that have been observed include electrons (EE), positive ions (PIE), neutral species in both the ground state (NE) and in excited states (NE*), and visible photons (phE)--often called triboluminescence. This emission can often serve as a sensitive probe of crack growth and may prove to be a useful tool for investigating molecular and microscopic events accompanying formation of cracks and details of failure modes in a variety of materials. There is also interest in these effects in terms of their relations to electrostatic consequences of bond breaking (e.g., noise generated in sensitive circuits under stress), the detection of fracture inside the earth's crust, and the transport of atoms and gases in geological systems.

Past studies of FE have included work on adhesive failure,[1-9] the fracture of oxide coatings on metals[10-15], organic crystals[16-19], and inorganic crystals.[20-27] A number of studies on inorganic single crystals have concentrated on the emission of electrons from the cleavage of alkali halides in vacuum. The general features of EE from cleavage or fracture in vacuum are the following:

(a) To a first approximation, the emission begins and is most intense <u>during</u> the cleavage or fracture.[28]

(b) The kinetic energy of the electrons appears to be very high, with energies extending out to keV, perhaps even several hundred keV.[24]

(c) EE continues <u>after</u> fracture, suggesting that the fracture surfaces are in an activated state which relaxes, at least in part, via a non-radiative process.[29-31] The "time

constants" of this "after-emission", which vary from ms to several seconds, are very strongly dependent on the fractured material and can depend on the type of loading and strain rate causing the fracture.[19]

(d) In the few cases where thermal stimulation of the fracture surface has been performed[26,30], EE glow curves similar to those obtained from stimulation of the materials with x-rays or energetic electrons were observed. In the case of alkali halides, the temperature of the crystals at fracture had to be above a minimum temperature in order to produce such EE glow curves. The peaks, when they were observed, could be correlated with the activation of known defect chemistry (e.g., V_K and V_F - center annihilation).[26]

The origin of electron emission from fracture has frequently been attributed to: a) field emission due to electric fields produced by charge separation, or b) various non-adiabatic processes (e.g. stress induced electron transfer)[26] which are believed to create the necessary excitations that lead to subsequent electron emission from the solid.

We have proposed a simpler model for systems involving charge separation during fracture. We have tested various aspects of this model on a number of materials.[17-19, 29,30,32] The basic features of this model as they relate to the fracture of materials in vacuum are the following:

(a) During crack propagation, charge separation occurs on the freshly created fracture surfaces.

(b) During crack propagation, neutral species are emitted into the crack tip region, producing a region of elevated pressure.

(c) A microdischarge thus occurs during fracture yielding charged particles (generally electrons and positive ions) as well as photons (phE) and long wavelength electromagnetic radiation (RE for radiowave emission).

(d) The fracture surfaces are bombarded by the discharge products during fracture. It is this bombardment which provides the stimulation of the fracture surfaces and yields the after-emission from the fracture surfaces.

(e) The static charge on the fracture surfaces leads to acceleration of the emitted electrons modifying their energy distributions. A large portion of the EE is pulled back into the surface causing a self bombardment to occur. This results in the emission of ions[2,15,33,34] (PIE) and excited neutrals[34] (NED*U) via an electron stimulated desorption (ESD) process.[35]

Different types of photon emission have been observed. As we shall show, phE can occur prior to fracture in a number of systems. In some cases, this light is due to microfracture events that precede failure. In single crystal inorganics there is evidence that moving dislocations generate recombination of defects which yields light. Following fracture, some materials "glow" with characteristic decaying signals, much like phosphorescence. We shall show an example of this behavior below.

In this paper, we therefore examine the fracto-emission from some representative materials and geometries and examine some of the relations to the above mentioned models.

Experimental

Details of our experimental arrangements can be found in references.[2-8, 10-19, 21-23] The majority of the experiments shown here were performed in vacuum, ranging from 10^{-7} to $10s^{-9}$ torr. During straining of the samples, either in tension or 3 point bend, one - three types of emission were monitored (e.g., electrons, positive ions, photons, neutrals, and/or low frequency electromagnetic radiation). The detectors used for charged particle detection were Galileo Electro-optics Corporation Channeltron Electron Multipliers (CEM) which produce fast (10 ns) pulses with high detection efficiency for both electrons and positive ions. Background noise counts typically ranged from 1 to 10 counts/s. The detectors were positioned within a centimeter of the sample with proper bias voltage on the front cone to attract the charged particles of interest.[2] It should be noted that in studies on organic polymers we have shown that the principle particles detected for plus and minus bias on the CEM front cone were electrons and positive ions, respectively.

Photon detectors (e.g., Thorn-EMI 99^{24}QB) are placed inside the vacuum system or, when used in air, are contained in a cooled housing which greatly reduces the background noise level (to approx. 10 counts/s).

The low frequency electromagnetic waves (RE--for radiowave emission) are detected with coil antennas placed a few mm from the sample. Such an antenna couples to a changing B field. It should be emphasized that this arrangement detects the near-field electromagnetic "emission" because of the close proximity of the coils to the source. A simultaneous burst of visible photons coincident with the observed RE burst reinforces the interpretation that these signals are caused by a microdischarge.

Neutral particles (not discussed here) are detected with a quadrupole mass spectrometer, generally tuned to a single mass peak. The neutrals are ionized by electron impact at an energy of 70 eV.

Results and Discussion

Fig. 1 shows the striking difference (several orders of magnitude) in intensity and duration of the electron emission that result from fracture of an epoxy [bisphenol-A/epichlorohydrin resin - Epon 828] with and without a filler material consisting of small (7 um) alumina particles. (Note that most of the data presented here is plotted on a log intensity scale.) For the unfilled material, the major cause of emission is attributed to the bond breaking occurring during fracture which produces free radicals on and near the fracture surface (similar to the mechanical production of free radicals studied by DeVries[36] in other polymers. Subsequent recombination reactions (e.g., radicals + electrons) provide discrete transitions which yield photons (radiative) and electrons (Auger-like transitions). The filled material fits the category of a system which yields intense charge separation; thus, the enhanced emission.

Supporting the idea that the slow decay following fracture seen for the filled epoxy is a thermally activated process, we show in Fig. 2 the consequences of heating the surface approximately 50 C in a few seconds immediately following fracture (at the arrow) with a heating strip attached to the sample. The response to this increase in temperature is essentially a "glow curve", similar to what is obtained from materials following exposure to radiation.

Although the unfilled material results in intensities several orders of magnitude smaller, we have found that during fracture, we obtain very easily measured and interesting curves. Fig. 3a shows the resulting photon emission during fracture of the unfilled TGDDM/DDS, acquired at 100 ns/channel. Simultaneously, shown in Fig. 3b,

is the signal indicating when the grid wires deposited on the side of the sample were broken. Thus, the duration of the crack tip motion was approximately 20 us. We first note that the onset of phE agrees well with the beginning of crack motion and that the major phE intensities are observed during crack motion. The tail observed in the phE after fracture is actually of longer duration than indicated here. In order to prevent saturation of the photomultiplier during fracture it was necessary to reduce the gain considerably, thereby losing sensitivity. During relatively constant average crack velocity (approximately 400 m/s), the photon emission is rapidly fluctuating. We have analyzed the statistics of these signals in light of (no pun intended) the expected fluctuations from a photomultiplier and found that all of the larger fluctuations were well outside of the predicted noise. Thus, these fluctuations are non-stochastic, similar to flicker noise. This suggests that the phE fluctuations may result from rapid variations in the bond breaking rate as the crack advances, perhaps due to fibral fracture and/or crack branching.

Another feature of these measurements concerns comparisons of phE and EE intensities from a number of samples with the corresponding fractographs. We observe a very strong correlation between increasing emission intensity and the degree of roughness or "hackling". The molecular motion and bond alterations associated with the localized deformations as the crack moves and branches may prove to be important factors leading to variations in both instantaneous and total emission intensities. [illegible] shows data for essentially two identical samples of tetraglycidyl 4,4 diaminodiphenylmethane (TGDDM) cured with diaminodiphenyl [illegible] specimens taken at the same detector sensitivity and the [illegible] the fracture surfaces. Because of loading conditions [illegible] different: the top, weak emission corresponding [illegible] vs the much more intense phE emission [illegible].

In the case of fiber reinforced epoxy, a poor bond between the fibers and the matrix can lead to pre-failure emission. Approximately 100 E-glass fibers (10 um in dia.) were embedded in Epon 828/Jessamine Hardner (which produces a clear, flexible epoxy) and strained in tension. In this study[37] we have found that internal failure of fibers and subsequent debonding yields the photon emission shown in Fig. 5a. The arrow indicates the time of ultimate failure of the specimen (i.e., when the entire specimen breaks). Because of the clarity of the epoxy, the photons created during debonding easily escape and can be detected. These experiments were performed in the atmosphere since there is no need to protect the photomultiplier from a gaseous environment. When epoxy compatible sizing coats the fibers, which greatly enhances the adhesion between the fibers and the epoxy matrix, there is very little phE before failure, even though fiber fracture has occurred. To further test this observation, we embedded a Boron-Carbon single filament (100 um in dia.) into the same matrix. When a release agent (Silicone oil) was applied to the fiber before embedding it in the resin, the debonding was easily observed under a microscope. On an identical sample, we saw the photon emission shown in Fig. 5b, where again, the arrow indicates where the epoxy sample fractured. In terms of probing the failure mechanisms of composites, this is an important result.

In Fig. 6, we show the EE, RE, and phE accompanying the failure of an aluminum-epoxy interface where the Al surface preparation was a simple degreasing. To the eye the failure was strictly interfacial. Similar to the results shown for a wide range of materials, during fracture, intense FE was observed, followed by decaying EE and phE. These three signals are in complete agreement with predictions from the model described above. If we arrange the metal/epoxy interface so that we can apply an external electric field across it, we expect to raise the charge density at the interface and perhaps enhance the resulting emission. Fig. 7 shows the comparison of the "field-on" vs "field-off" condition, where with the applied field we see almost two orders of

magnitude increase in the EE intensity. Corresponding increases in the phE and RE amplitudes were also recorded.

Another system of interest involves metal/insulator interfaces. Such systems are important in the electronic industry as well as formation of metal/glass and metal/ceramic joints. We chose to examine the fracto-emission accompanying the detachment of gold films from glass substrates. Fig. 8a shows the experimental arrangement, where the detectors are arranged for EE and phE. Fig. 8b is typical EE and phE from a fast peel of the metal from the glass. Interestingly, the intense, long lasting emission associated with interfacial failure built up over a time period of days, indicating that the interface undergoes changes (physical and/or chemical) which substantially influence the charge separation.

In Fig. 9 we show the simultaneous measurements of the EE and phE during the loading and fracture (at the vertical arrows) of single crystal MgO. Prior to fracture, very soon after the onset of loading the crystal in 3 point bend, we observe the build up of phE. Some samples showed a significant increase in the pre-emission immediately before fracture. This luminescence due to deformation of the crystal is attributed to excitonic transitions occurring at vacancy clusters formed during deformation. The defects responsible for these emissions are strongly localized in the regions of dislocations, slip bands, and related structures which become mobile during loading, thereby exciting these defects. Thus, this pre-failure phE serves as a probe of dislocation motion in a relatively brittle material.

At failure, the crack moves rapidly through the crystal and generates the very intense phE and EE seen at the arrow, followed by the slow decay. The two curves, when normalized at a single point, have identical kinetics. We have fit these curves with a simple trap model, used frequently in thermoluminescence work, described by Chen and Kirsch38. We find an activation energy for the mobile species (most likely an electron) of approximately 0.4 eV, corresponding to the fit shown in Fig. 10. The likely

recombination center is a surface F^+ center. Again, EE and phE are parallel processes. This model provides us with a number of experimental tests (e.g., sensitivity to quenching gases, thermal stimulation after fracture, and the expected spectrum of the phE) which we are currently pursuing.

Conclusions

In general, the use of EE and possibly other FE signals such as photon emission, neutral emission, and even radio-frequency electromagnetic radiation accompanying the deformation and fracture of composites will allow more details of failure mechanisms and fracture phenomena to be obtained. FE potentially can assist in the interpretation of other probes such as acoustic emission, and also provide an independent probe of the micro-events occurring prior to failure. For example, we have shown that FE is sensitive to the locus of fracture in a composite material. Our goal is to continue to study the mechanisms and applications of FE to the study of early stages of fracture and failure modes in a variety of materials.

Acknowledgments

This work was supported by the Ceramics and Electronics Materials Division of the National Science Foundation, DMR 8210406, the Office of Naval Research Contract No. NOOO14-8O-C-O213, NR659-803, McDonnell Douglas Independent Research and Development Program, and the Washington Technology Center. We wish to thank our Washington State University colleagues E. E. Donaldson and R. V. Subramanian for helpful discussions. We also thank S. Langford, S. Bhattacharya, R. Corey, and A. Castro for their assistance in this work.

References

1. B. V. Derjaguin, N. A. Krotova, and V. P. Smilga, Adhesion of Solids: (English Translation), Consultants Bureau, New York, (1978).
2. J. T. Dickinson, E. E. Donaldson, and M. K. Park, "The Emission of Electrons and Positive Ions from Fracture of Materials," J.Mat. Sci, 1166, 2897-2908 (1981).
3. J. T. Dickinson, M. K. Park, E. E. Donaldson, and L. C. Jensen, "Fracto-Emission Accompanying Adhesive Failure," J.Vac. Sci. Technol., 2222, 436-439 (1982).
4. J. T. Dickinson, L. C. Jensen, and A. Jahan-Latibari, "Fracto-Emission from Filled and Unfilled Elastomers," Rubber Chemistry and Technology, 5566, 927-941 (1983).
5. J. T. Dickinson, "Fracto-Emission Accompanying Adhesive Failure," in Adhesive Chemistry-Developments and Trends: Edited by L. H. Lee, Plenum, New York, in press.
6. J. T. Dickinson, A. Jahan-Latibari, and L. C. Jensen, "Electron Emission and Acoustic Emission from the Fracture of Graphite/Epoxy Composites," J. Mat. Sci., 1199, 1510 (1984).
7. J. T. Dickinson, L. C. Jensen, and S. K. Bhattacharya, "Fracto-Emission from the Failure of Metal-Epoxy Interfaces", J. Vac. Sci. Technol. AA33, 1398 (1985).
8. L. A. K'Singam, J. T. Dickinson, and L. C. Jensen, "Fracto-Emission from Failure of Metal/Glass Interfaces", J. Am. Ceramics Soc., 6688, 510 (1985).
9. B. Sujak and A. Gieroszynski, "Exoelectron Emission in Vacuum in the Absence of Light During Plastic Deformation of Aluminum Thickly Coated with Oxide," Acta Phys. Polon., 2288, 311-327 (1965).
10. J. T. Dickinson, P. F. Braunlich, L. A. Larson, and A. Marceau, "Characteristic Emission of Negatively Charged Particles During Tensile Deformation of Oxide-Covered Aluminum Alloys," Appl. Surf. Sci., 11, 515-537 (1978).
11. D. C. Doering, T. Oda, J. T. Dickinson, and P. F. Braunlich, "Characterization of Anodic Oxide Coatings on Aluminum by Tribostimulated Exoemission," Appl. Surf. Sci., 33, 196-210 (1979).
12. L. A. Larson, J. T. Dickinson, P. F. Braunlich, D. B. Snyder, "Emission of Neutral Particles from Anodized Aluminum Surfaces During Tensile Deformation," J. Vac. Sci. Technol., 1166, 590-593 (1979).
13. J. T. Dickinson, D. B. Snyder, and E. E. Donaldson, "Electron and Acoustic Emission Accompanying Oxide Coating Fracture," Thin Solid Films, 7722, 223-228 (1980).
14. J. T. Dickinson, D. B. Snyder, and E. E. Donaldson, "Acoustic Emission and Electron Emission During Deformation of Anodized Aluminum" J. Vac. Sci. Technol., 1177, 429-432 (1980).
15. J. T. Dickinson, E. E. Donaldson, and D. B. Snyder, "Emission of Electrons and Positive Ions upon Fracture of Oxide Films," J. Vac. Sci. Technol., 1188, 238-242 (1981).
16. M. H. Miles and J. T. Dickinson, "Fracto-Emission from Pentaerythritol Tetranitrate and Cyclotetramethylene Tetranitramine," Appl. Phys. Lett., 4411, 924-926 (1982).
17. J. T. Dickinson, M. H. Miles, W. L. Wilson, and R. G. Rosemeier, "Fracto-Emission from Cyclotrimethylene Trinitramine (RDX) Explosive Single Crystals," J. Appl. Phys., 5555, 3994-3998 (1984).
18. J. T. Dickinson, L. B. Brix, and L. C. Jensen, "Electron and Positive Ion Emission Accompanying Fracture of Wint-o-Green Lifesavers and Single-Crystal Sucrose," J. Phys. Chem., 8888, 1698-1701 (1984).
19. M. H. Miles, J. T. Dickinson, and L. C. Jensen, "Fracto-Emission from Single Crystal Pentaerythirtol," J. Appl. Phys., 5577 5048 (1985).
20. B. V. Derjaguin, N. A. Krotova, and V. V. Karesev, "Electrical Phenomena in the Disruption Mechanism of some Solids," Doklady Akad. Nauk SSSR, 110099, 728-730 (1956).

21. J. T. Dickinson, L. C. Jensen, M. R. McKay, and F. Freund, "The Emission of Atoms and Molecules Accompanying Fracture of Single Crystal MgO," J. Vac. Sci. Technol., AA44 1648 (1986).
22. J. T. Dickinson, M. R. McKay, and L. C. Jensen, "Neutral Molecule Emission From Fracture of Crystalline MgO," J. Vac. Sci. Technol., to be published.
23. S. C. Langford, J. T. Dickinson, and L. C. Jensen, "Simultaneous Measurements of the Electron and Photon Emission Accompanying Fracture of Single Crystal MgO", to be submitted to J. Appl. Phys.
24. J. Wollbrandt, E. Linke, and K. Meyer, "Emission of High Energy Electrons During Mechanical Treatment of Alkali Halides," phys. stat. sol. (a), 2277, K53-K55 (1975).
25. J. Wollbrandt, V. Bruckner, E. Linke, "Investigations of Mechanically Induced Excited States on Cleavage Planes of Ionic Crystals I.," phys. stat. sol (a), 7777, 545-552 (1983).
26. J. Wollbrandt, V. Bruckner, E. Linke, "Investigations of Mechanically Induced Excited States on Cleavage Planes in Ionic Crystals II.," phys. stat. sol (a), 7788, 163-168 (1983).
27. J. T. Dickinson and L. C. Jensen, "Fracto-Emission from Lead Zirconate-Titanate," J. Am. Ceramics Soc. 6688, 235 (1986).
28. J. T. Dickinson and L. C. Jensen, "Crack Velocity Dependence of Electron Emission During Fracture of Filled Elastomers," J. Poly. Sci.: Poly. Phys. Ed., 2200, 1925-1932 (1982).
29. J. T. Dickinson, L. C. Jensen, and A. Jahan-Latibari, "Fracto-Emission: The Role of Charge Separation," J. Vac. Sci. Technol., 22AA, 1112-1116 (1984).
30. J. T. Dickinson, and L. C. Jensen, "Fracto-Emission from Filled and Unfilled Polybutadiene," J. Poly. Sci.: Poly. Phys. Ed., 2233, 873 (1985).
31. V. Bichevin and H. Kaambre, "A Possible Manifestation of Auger Processes in Thermostimulated Electron Emission," phys. stat. sol. (a), 44, K235-K238 (1971).
32. J. T. Dickinson, L. C. Jensen, and A. Jahan-Latabari, "Fracto-Emission from Single Fibers of Kevlar," J. Mat. Sci., to be published.
33. J. T. Dickinson, L. C. Jensen, and M. K. Park, "Mass-to-Charge Ratio and Kinetic Energy of Positive Ion Emission Accompanying Fracture of a Filled Elastomer," Appl. Phys. Lett., 4411, 827-829 (1982).
34. J. T. Dickinson, L. C. Jensen, and M. K. Park, "Time Correlation of Electron and Positive Ion Emission Accompanying and Following Fracture of a Filled Elastomer," Appl. Phys. Lett., 4411, 443-445 (1982).
35. M. L. Knotek, "Electron- and Photon-Stimulated Desorption," AIP Conf. Proc., NNoo.. 9944, 772-786 (1982).
36. K. L. DeVries, "Free Radical Processes in Mechano-Chemical Degradation of Plastics and Rubbers," J. Applied Polymer Sci.: Applied Polymer Symposium 3355, B. Ranby and J. F. Rabek, ed., John Wiley & Sons, (1979).
37. A. S. Castro, R. Corey, J. T. Dickinson, R.V. Subramanian, and Y. Eckstein, "Correlation of Photon and Acoustic Emission with Failure Events in Model Composites," submitted to Composites Science and Technology.
38. R. Chen and Y. Kirsch, Analysis of Thermally Stimulated Processes, (Pergamon Press, Oxford, 1981), p 18.
39. J. I. Zink, "Squeezing Light out of Crystals: Triboluminescence," Naturwissenschaften, 6688, 507-512 (1981).
40. A. J. Walton, "Triboluminescence," Adv. Phys., 2266, 887-948 (1977).

Figure Captions

Fig. 1. EE plotted for both filled and unfilled (7 um alumina particles) Epon 828 epoxy. Several orders of magnitude difference in intensities are observed; the larger and longer lasting emissions occur when interfaces fail.

Fig. 2. The response of the EE from particulate filled Epon 828 epoxy to thermal stimulation following fracture. The bottom arrow indicates when the temperature increase began. This supports the concept of a thermally stimulated process.

Fig. 3. a) The phE during fracture of unfilled Epon 828 Epoxy. The data was acquired at 100 ns/channel. b) A voltage vs time curve indicating when small grid wires deposited on the side of the sample were broken, indicating the position of the crack tip vs time.

Fig. 4. The photon emission accompanying fracture of TGDDM/DDS epoxy for two samples with different emission intensities and fractography. Highly hackled surfaces seen in b) corresponded to higher phE.

Fig. 5. a) The photon emission for a glass fiber/epoxy composite where the fibers debond inside the epoxy matrix, yielding visible photons detected with a photomultiplier. The arrow indicates where the entire sample failed. b) The same type of data from debonding occurring in a single fiber specimen. Again, the arrow indicates when the entire sample fractured.

Fig. 6. Simultaneous emission of electrons (EE), photons (phE), and long wavelength radiation (RE) from the failure of an Al/epoxy interface.

Fig. 7. The decaying "tails" of the electron emission accompanying failure of Al/epoxy interfaces for 0 and 1500 V applied across the dielectric. The enhanced charge separation causes an increase in the emission.

Fig. 8. a) Diagram of experimental arrangement for detecting charged particle and photon emission from failure of metal/glass interfaces; CEM = electron multiplier. b) The EE and phE from a rapid detachment of approximately 1 cm^2 of a gold film from a glass surface. The detachment occurred at the arrow.

Fig. 9. The photon and electron emission measured simultaneously during the deformation and fracture of single crystal MgO. The arrow indicates when fracture occurred. Note the photon emission prior to failure.

Fig. 10. A fit to the photon emission decay curve from the fracture of MgO. The equations used are those for a simple trap - recombination model.

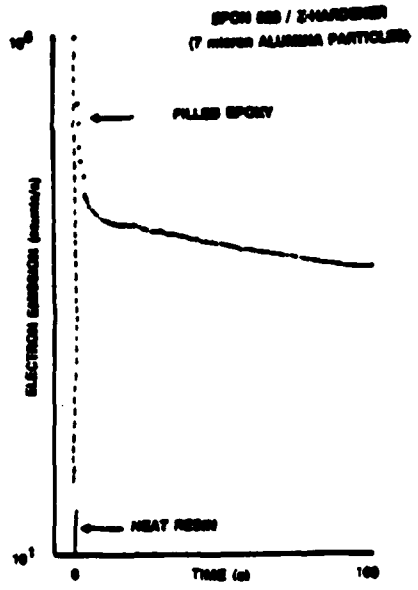

Fig. 1.

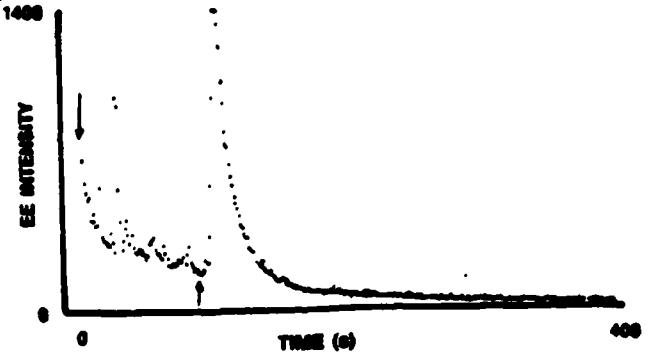

Fig. 2.

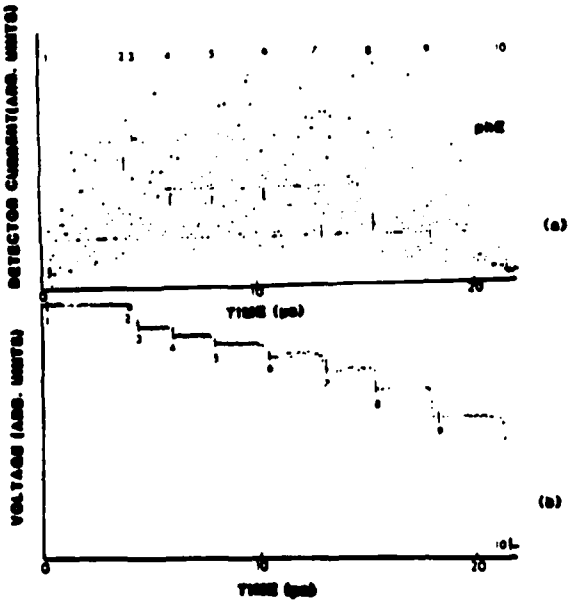

Fig. 3.

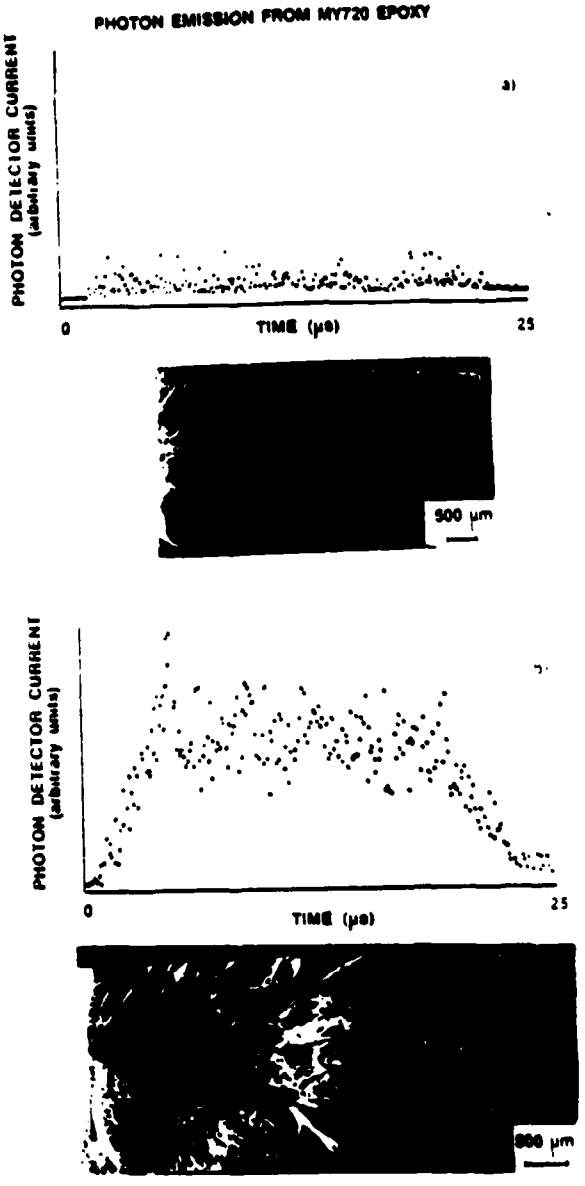

Fig. 4

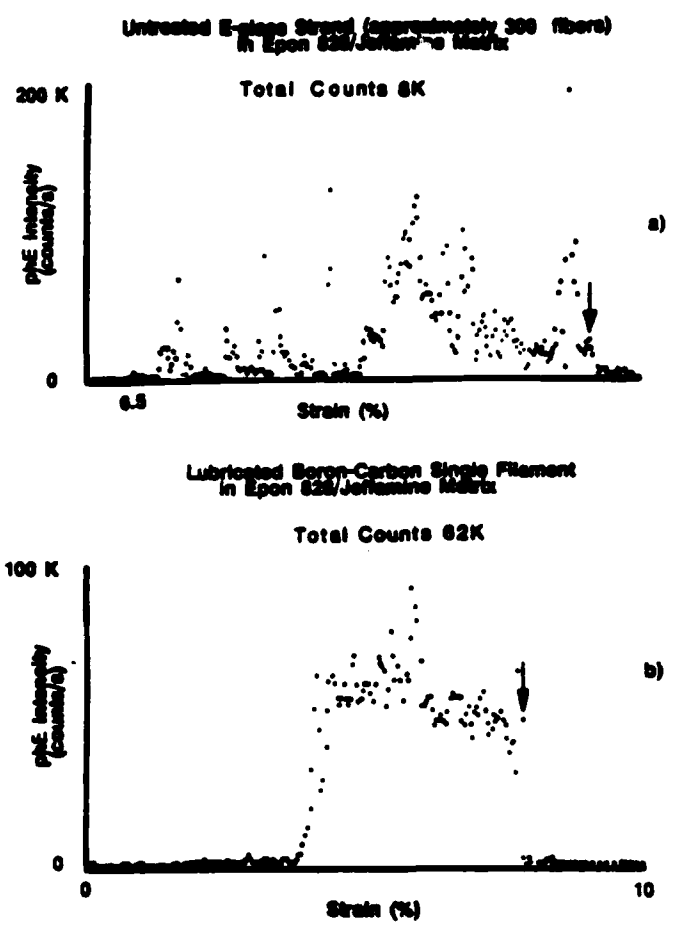

Fig. 5.

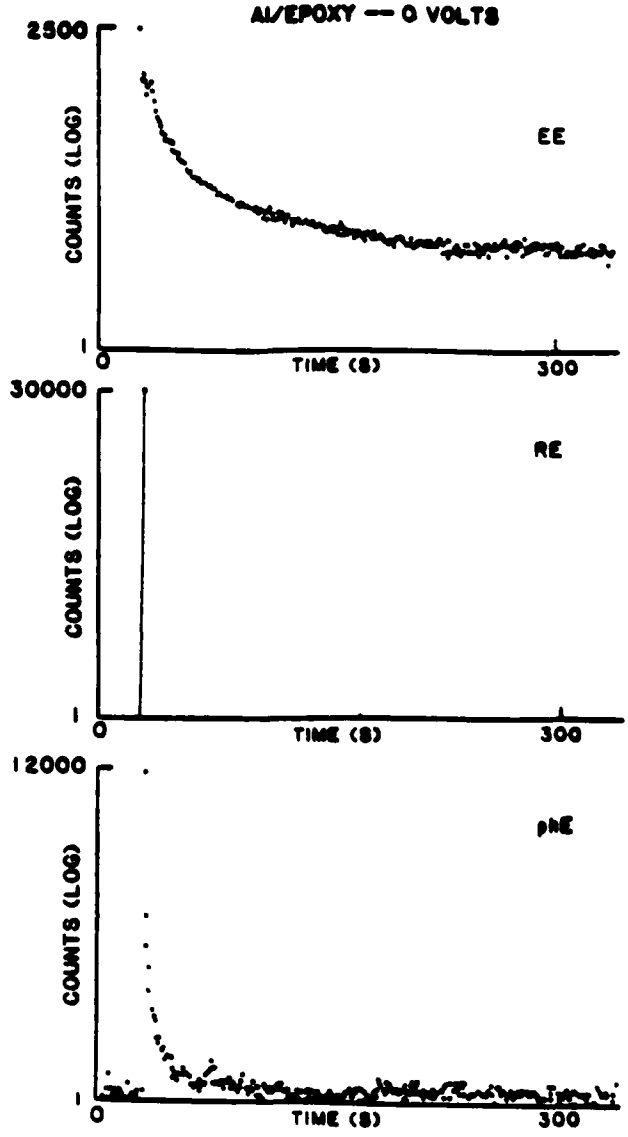

Fig. 6.

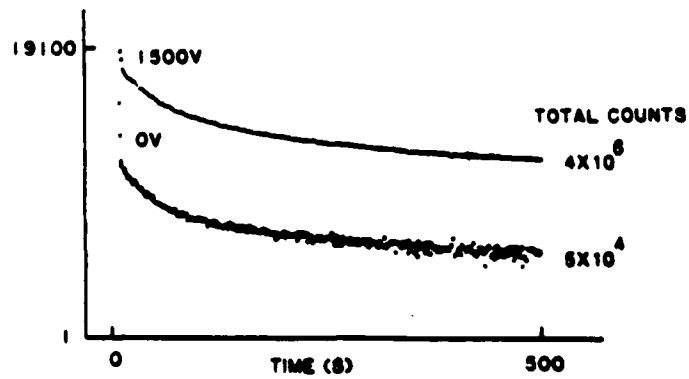

Fig. 7.

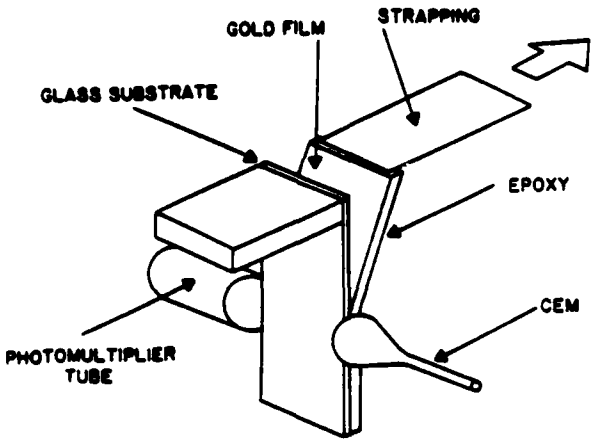

Au/GLASS - 6 WEEKS

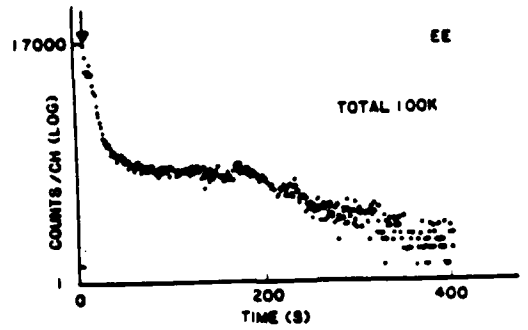

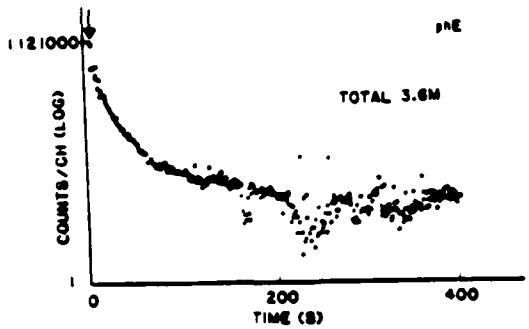

Fig. 8

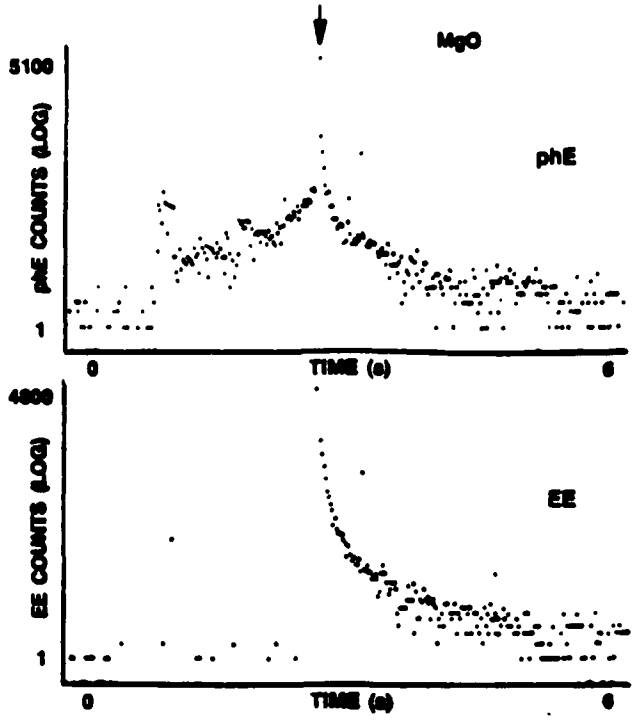

Fig. 9.

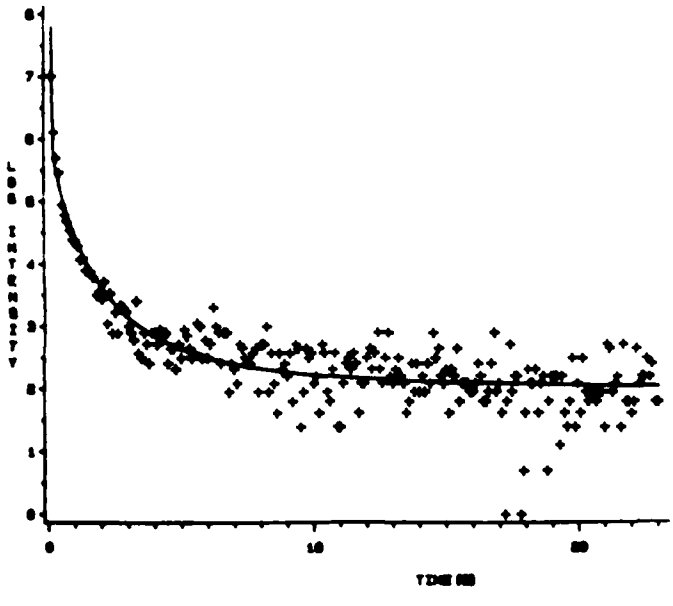

Fig. 10.

VII. CRACK INITIATION AND CRACK GROWTH IN POLYMERS INDUCED BY ELECTRON BOMBARDMENT

J. T. Dickinson, K. Tonyali, M. L. Klakken, and L. C. Jensen
Department of Physics
Washington State University
Pullman, WA 99164-2814

ABSTRACT

The response to electron bombardment of highly stressed Kapton-H™, Teflon™ (PTFE), and linear high density polyethylene (LHDPE) is investigated. Evidence is presented for electron induced crack initiation and crack growth. Calculations show that the electron exposures used in these experiments are sufficiently small that thermal heating of the zone near the crack tip does not dominate. Video recording of the shape of the crack before and during bombardment is presented as well as SEM analysis of the bombarded regions of the specimens. Instabilities in the form of microcracks appear to be the dominant consequence of electron bombardment of stressed materials. The role of highly localized electronic excitations of stressed molecular bonds is also discussed.

I. INTRODUCTION

High energy electrons bombarding a polymer interact with the polymer via inelastic collisions causing energy deposition in the material. These inelastic collisions may cause vibrational excitations of the molecules, ionization, and broken bonds. The chemical effects resulting from these interactions which tend to "strengthen" the material may include additional polymerization, crosslinking and branching of the polymer. Likewise, the chemical effects that tend to "weaken" the material may include bond scissions, molecular dissociation (via electronic excitations), electron stimulated desorption of ions and neutral species (again, via electronic excitations), as well as thermal degradation and gas evolution (due to a temperature rise in the material being bombarded). All of these events can have mechanical consequences if the material is subjected to deformation.

In earlier work[1-4] and in this paper the consequences of simultaneously subjecting materials to stress and electron bombardment is studied. The primary motivation for such an experiment is to examine the consequences of fracture in a high energy environment. Examples that are of interest may include stressed materials exposed to radiation, advanced machining and cutting techniques, preparation of surfaces for adhesive bonds, combustion of rocket propellents, and materials exposed to plasma environments. Secondly, the use of electron beam excitation of the crack tip may further our understanding of the physics of fracture and may eventually lead to selective and controlled bond breaking and/or activated stress-dependent chemistry. Third, we suggest that we are seeing a unique form of electronic excitation, where localization is enhanced by the presence of stress on the molecular bonds. Finally, a long term goal is to eventually perform various electron spectroscopies, e.g. electron energy loss spectroscopy, on stressed molecules to provide useful information about the state of these molecules. In this paper we concentrate on the mechanical response of polymers experiencing stress plus electron beam irradiation on the following materials: Kapton-H^{TM}, Teflon^{TM} (PTFE), and linear high density polyethylene (LHDPE).

II. EXPERIMENTAL

The Kapton-H samples, supplied by E. I. Dupont de Nemours and Co., are a pure polyimide derived from the combination of 4,4'diaminodiphenyl ether and pyromellitic dianhydride. Our samples had typical dimensions of 75 um x 10 mm x 30 mm with a 3 mm notch cut in the side nearest the electron gun.

The Teflon (PTFE, polytetraflouroethylene) samples were obtained from commercial rolls of Scotch 48, Thread Sealant and Lubricant) produced by 3M. These samples typically had the dimensions of 80 um x 12 mm x 30 mm, again with a 3 mm notch placed in the side nearest the electron beam source.

The polyethylene samples were from commercial sheets of linear high density polyethylene (U. S. Industrial Chemicals LR 20175); the density was 0.95 g/cm^3 and a characteristic melt index of 0.1. The samples had the typical dimensions of 40 um x 10 mm x 30 mm and for the notched samples, a 3 mm long notch.

Rectangular test specimens of the polymers were mounted in a vacuum system equipped for straining materials in tension. The system has been described previously[1-4]. The normal sample orientations were a) electrons focused into the notch (edge-on bombardment), and b) electrons incident on the side of the sample (side-on bombardment). The materials chosen were deformed to yield an open, U-shaped crack, allowing convenient electron beam bombardment in the region of high stress, either in the notch itself or on the side.

The samples were subjected to a constant strain rate of 0.6 %/s. A load cell (Sensotec, Model 11) was used to monitor the force applied to the sample. Most of the tests were carried out at a pressure of 10^{-5} Pa. A Varian Glancing Incidence Auger Electron gun with a 2-3 mm spot size was mounted so that the electron beam of 10-200 uA at kinetic energies of 1.5-3.0 keV would strike the sample at or near the focal point. In all experiments the time that the beam was actually on the sample was

minimized to avoid the build-up of surface charge which would tend to reduce the current density bombarding the polymer surface.

An electrometer connected to a metal collector mounted behind the sample was used to measure the electron current to the sample or blocked off by the sample. If the sample was partially or completely blocking the electron beam, the time at which the electron beam came on, off, or penetrated through the sample could be determined quite accurately.

The appropriate signals from the various transducers were all simultaneously digitized with 0.01 s time resolution using a LeCroy Data Acquisition System and stored on disk for later analysis.

For some of the thin sheet specimens, a video camera was mounted such that a video recording of the crack and its propagation while under electron bombardment could be obtained. For these experiments, the applied load and current density were also recorded by the same techniques as described before. The time correlation between the measured load and current and the videc recording was accomplished by using a strobe light mounted to produce a flash directly towards the camera at the approximate instant that the electron beam was applied. The error in the synchronization of the video images and the motion of the electron beam are estimated to be 0.1 s.

III. RESULTS

We have carried out studies of edge-on, notch bombardment of thin sheets of Kapton-H, PTFE, and LHDPE. Kapton-H, being the most radiation resistant of these materials, was found to require relatively higher electron currents and stress to produce measurable responses. When the notched specimens were stressed to the point of slow crack growth, the application of a 2.5 KeV, 300 uA beam into the notch would result in an instantaneous response of crack acceleration and failure of the sample. Fig. 1a shows the typical load versus time curve for a Kapton-H specimen strained close to the maximum stress without exposure to the electron beam. By means of simultaneous video recording, one can correlate points on this curve with the specimen response. Three crack growth regions are observed, as indicated. In region I, crack formation is occurring, somewhat like a tearing

process, in the area of maximum load. When the load begins to decrease, region II, stable crack propagation is occurring. Finally, the load drops rapidly, in region III, corresponding to fast rupture of the specimen.

Fig. 1b represents the response of the Kapton-H sample when the 300 uA electron beam is applied to the sample notch just as the stable crack growth region (region II) has been reached; the arrow indicates the time when the beam just starts coming onto the sample. The point of maximum current density on the sample is in the center of the ON-OFF arrows. The drop in force is accelerated by the application of the electron beam. The video recording of the specimen shows that the crack velocity increased substantially, leading to final rupture. When the electron beam is applied to the specimen notch before stable crack growth is reached (i.e., in region I), the response is not as catastrophic, as seen in the load versus time curve shown in Fig. 1c. Initially with the application of the electron beam the crack velocity increases slightly but then stops soon after the electron beam moves off the specimen. At this point, the sample load levels off followed by rapid sample failure occurring much later.

Fig. 2 shows the load vs time curves for edge-on (notch) bombardment (Fig. 2a) and side-on bombardment (Fig. 2b) for a beam energy of 1.5 KeV and a current of 150 uA. As seen, the application of the electron beam on the side of the specimen is more effective in causing fracture. In Fig. 2b the stress drop at application of the electron beam (side-on) is very large compared to that of Fig. 2a (edge-on), corresponding to a larger extension of the crack. Note that both specimens were hit before the maximum force was attained, which discouraged catastrophic failure from being induced by bombardment.

Analysis of the fracture surfaces of Kapton-H under optical and scanning electron microscopes indicated extensive microcrack formation. Fig. 3 shows the extensive microcracking created on the side surface of Kapton-H exposed to electrons. These cracks are presumably also being produced in the crack-tip, leading to high stress concentration. When such cracks coalesce, the main crack then propagates. Such an array of cracks is a set of instabilities (small compared to the area exposed to the

beam) and suggests that the microstructure of the material responding to the applied stress is playing an important role in the formation of such microcracks under the beam.

The beam power level (current x energy in volts) required to start crack propagation in Teflon (PTFE) is an order of magnitude less than the power required to start crack propagation in Kapton-H. A 50 uA, 1500 eV electron beam was sufficient to cause crack growth in notched, side-on specimens of PTFE at stresses below the onset of mechanical crack growth (the critical stress). The same electron beam conditions, applied edge-on, produced no noticeable effect on similar PTFE samples. As shown in Fig. 4a, coincident with the beam application, the load drops constantly and the crack is observed to propagate at a constant speed. As is the case for most of the materials studied, the direction of crack growth could be controlled by the position of the electron beam. SEM photographs of the strained material without exposure to electrons (Fig. 4b) show that a drawing process occurs which leads to strands or fibrillated material whose length runs in the direction of elongation. The bombarded surface and fracture surface are seen in Fig. 4c. It appears as though the electron beam is cleanly severing the fibrils. Away from the region of highest stress, partial cutting of the fibrils yields the microcracks shown. The fracture surface consists of domains of fibrils, cleanly cut, forming a smooth fracture surface. The corrugated fracture surface, when viewed under varying magnification, appears to be almost "fractal" in nature.

Fig. 5 shows the response in the load versus time on a notched side-on linear high density polyethylene (LHDPE) specimen under 50 uA, 1500 eV electron beam. Again, the electron beam induces the crack to advance at stresses below the critical value. As is the case with other specimens, hitting the LHDPE specimens on the side rather than at the edge was more effective in causing failure. The fractography indicates that again microcrack formation is the main mechanism for failure of LHDPE samples under the electron beam. Fig. 5b shows an SEM of the strained LHDPE surface in the region ahead of the notch. Fig. 5c shows the same region that has been bombarded at a low current (10 uA) which exhibits microcracks normal to the tensile direction. Fig. 5d shows the fracture surface of an electron beam failed LHDPE specimen (50 uA, 1500 eV) where the crack tip was exposed, showing formation of the type of surface previously observed[1] during electron beam

induced fracture in other polymers. We have attributed this structure to a combination of crosslinking and bond breaking occurring under the beam.

Video recording of the crack propagation in PTFE and LHDPE was made simultaneously with measurements of the applied load and current. Fig. 6 shows the load vs time curves and corresponding video frames obtained for PTFE and LHDPE. The electron beam is centered in the notch of both samples with a diameter of approximately 2/3 the notch width. As reported previously, for both samples the load drops and the crack propagates when the beam was swept across the sample notch. The shape of both crack tips are sharper than before the beam, supporting our statement that thermal effects are not dominant. Each time the beam was applied, the crack shape would be seen to sharpen. When the beam was removed, the crack would stop and begin opening up. Because PTFE tends to fail by chain slippage, the formation of a relatively sharp crack indicates that chains are being broken by the electron beam.

Unbombarded LHDPE samples, on the other hand, fail by a crazing or thinning process. The regions of high stress concentration near the crack tip craze and draw out. In the LHDPE photographs, on the left hand side of Fig. 6, the bright spots correspond to the area of the sample where the thinning process is occurring. The electron induced process is concentrated in a region that is much smaller than the diameter of the electron beam, within this thinned region. This indicates that stress is a critical factor in the probability that an electron induced chain scission yields an irreversibly broken bond.

IV. DISCUSSION

The basic characteristics of electron beam induced fracture which we can state at this point are the following:

1) The polymers must be elongated beyond a certain stress state to observe crack growth under bombardment. In the case of Kapton-H, a very radiation resistant material, reasonable incident current densities required an initially slowly moving crack to observe a rapid response under the electron beam. For PTFE and LHDPE, the electron beam could easily induce crack growth below the critical stress concentration.

2) The current densities necessary to obtain noticeable crack growth below critical stress levels were on the order of 10-100 uA/cm^2.

3) The higher the stress, the more evident the response to the electron beam.

4) The calculated heating effect of the electron beam on this time scale, based on a development given by Jaeger,[4] is on the order of 10-30 C, which is too small to stimulate crack growth.[1,3]

5) In the case of PTFE, the failure mechanism is completely changed from a slipping type process to chain scissions due to electron beam interactions.

6) Fracture surface studies show that Kapton-H, LHDPE, and PTFE fail due to electron beam induced microcracking. This involves a multitude of instabilities created by the combination of stress and radiation. We suspect that the microstructure of the stressed materials is the cause of creating these localized damage zones.

These results support the idea that the phenomenon of electron beam induced fracture which we observe here is not dominated by thermal effects, but instead appears to be a direct consequence of electronic interactions; i.e., direct scissions of load bearing molecular chains by inelastic electron collisions. These scissions result in an increase in load of neighboring chains, which can cause them to fail, also. We hypothesize that when a radiation-sensitive material is under stress, fewer bonds can reform, thus greatly encouraging irreversible bond scissions. We also suggest that there may be an enhanced localization of excitations from electron collisions which promotes this irreversible bond breaking.

The mechanism for failure appears to be microcrack formation, which requires the influence of the beam to be very localized. Once the microcracks form, the resulting high stress concentration quickly leads to crack formation in the material. Below critical stresses and crack lengths, when the electron beam is removed, the crack arrests, which implies that the dynamics of creating the array of damage zones is necessary to keep the crack moving. If the stress distribution in the specimen is sufficiently intense, the induced crack growth can lead to total failure.

We have shown that three polymers, namely, Kapton-H, LHDPE, and PTFE, show microcracking under the electron beam. We propose that permanent scissions of the chains under stress occurred because the separation of the newly created chain ends would be greatly encouraged, thereby partially suppressing reattachment and favoring crack growth. This is consistent with the observations that a minimum stress is required for the effect of the electron beam to be clearly noticeable and that

electron beam fracture appears to be a "cool" process, perhaps similar to ablative photodecomposition.[6,7]

The prospect of performing controlled direct rupture of bonds under stress with external radiation sources appears promising and should lead to improved understanding of fracture in elastomers and polymeric materials. This work is being extended to other radiation sources such as uv photons and fast atom bombardment as well as other types of materials. The clear indications of crack initiation that we are finding are of considerable importance with regard to the lifetime of stressed polymers in a radiation environment.

V. ACKNOWLEDGMENTS

The authors would like to thank Clarence Wolf from McDonnell Douglas Research Laboratories for useful discussions and for providing the Kapton-H samples. This work was supported by McDonnell Douglas Independent Research and Development Program, the Office of Naval Research, Contract N00014-80-C-0213, NR 659-803, and the Washington Technology Center. One of us (M.L.K.) wishes to thank the NASA-Johnson Space Center for Graduate Student Fellowship support.

VI. REFERENCES

1. J. T. Dickinson, M. L. Klakken, M. H. Miles, and L. C. Jensen, J. Polymer Sci.: Poly. Phys. Ed. 23, 2273 (1985).

2. J. T. Dickinson, L. C. Jensen, M. L. Klakken, J. Vac. Sci. and Technol. A4, 1501 (1986).

3. R. Michael, S. Frank, D. Stulik, and J. T. Dickinson, Proceedings of 13th International Symposium on "Effects of Radiation on Materials", ASTM E-10, Seattle, WA, June, 1986.

4. J. Thomas Dickinson, M. L. Klakken, and L. C. Jensen, Proceedings of the 18th SAMPE International Technical Conference, SAMPE Publications, Corvina, CA (1986), pp. 983-992.

5. J. C. Jaeger, Australian Journal of Scientific Research 5, 1 (1952).

6. R. Srinivasan and V. Mayne-Banton, Appl. Phys. Lett. 41, 576 (1982).

7. B. J. Garrison and R. Srinivasan, J. Vac. Sci. and Technol. 3A 746 (1985).

FIGURE CAPTIONS

Fig. 1. Force vs time curves for notched Kapton-H near the region of fracture. a) no electron bombardment, showing the approach to maximum stress (region I), stable crack growth (region II), and crack acceleration to catastrophic failure (region III). Response to the application of a 2500 eV, 300 uA electron beam: b) when the beam is applied in region II, or c) in region I.

Fig. 2. The load vs time curves for a) edge-on (notch) bombardment, and b) side-on bombardment of Kapton-H for a beam energy of 1.5 KeV and a current of 150 uA.

Fig. 3. SEM photographs of surfaces of Kapton-H that have seen a) both high stress and electron beam bombardment, and b) stress alone.

Fig. 4. a) The mechanical response of a PTFE specimen exposed side-on to an electron beam. The arrow indicates the time when the beam just begins to come onto the sample. b) An SEM photograph of the fibrillation that occurs upon elongation without bombardment. c) The resulting microcracking and fracture surface created under side-on electron beam bombardment.

Fig. 5. a) The mechanical response of a LHDPE specimen exposed side-on to an electron beam. SEM photographs of the surface, are taken in the region indicated by the rectangles. b) No electron bombardment, c) side surface with 10 uA beam, d) fracture surface created by 50 uA, 1500 eV beam.

Fig. 6. Series of video images showing the propagation of the notch due to the application of the electron beam for two types of edge-on samples. Also shown are the corresponding plots of the load versus time. Left: LHDPE; Right: PTFE.

VIII. Changes in Surface Morphology and Microcrack Initiation in Polymers under Simultaneous Exposure to Stress and Fast Atom Bombardment

R. Michael, S. Frank, D. Stulik
Department of Chemistry

and

J. T. Dickinson
Department of Physics

Washington State University
Pullman, WA 99164

ABSTRACT

We present studies of the changes in surface morphology due to simultaneous exposure of polymers to stress and fast atom bombardment. The polymers examined were Teflon^R, Kapton^R, Nylon^R, and Kevlar-49^R. The incident particles were 6 keV xenon atoms. We show that in the presence of mechanical stress these polymers show topographical changes at particle doses considerably lower than similar changes produced on unstressed material. Applied stress also promotes the formation of surface microcracks which could greatly reduce the mechanical strength of the material.

^{R}Registered Trade-names of E. I. Dupont de Nemours and Co.

INTRODUCTION

Bombardment of material surfaces with energetic particles (electrons, ions, or neutral atoms) leads to emission of secondary particles (electrons, ions, atoms, and molecules) through various physical processes such as electron stimulated desorption and physical/chemical sputtering. The latter was first observed in 1852 when Grove published the first experimental evidence of sputter deposition of materials due to ion bombardment of a target [1]. Vast amounts of experimental data on sputtering of metals, alloys, and simple inorganic materials have been collected and the observed effects have attracted considerable theoretical effort to describe the process quantitatively [2]. In single element substrates and non-reactive incident particles, the dissipation of collision energy can only alter the physical structure of the material [3]. In the case of alloys and inorganic compounds, the observed changes can be considerably more complex, including preferential sputtering [4] and electronic excitations which can lead to loss of anions in ionic materials [5]. In the case of molecular solids, considerable changes in the chemistry of the bombarded surfaces can occur. Also, the chemical bonds and composition of the sample play major roles in the process of secondary particle emission and the resulting chemical changes due to bombardment [6].

Changes in surface morphology are also observed with increasing total particle bombarding dose on polymer surfaces. Our knowledge of the mechanisms of these changes is severely limited, including details of the physical and chemical structure

of the solid before exposure to bombardment. This limited description of the polymer surface is in part due to the tendency for such surfaces to be so readily damaged by radiation. Nevertheless, we feel that examining the overall changes in the material from exposure to various types of bombardment is of importance, particularly due to the technological interest in applications of polymers in increasingly severe environments.

Our previous studies [7,8] of the changes in the surface morphology in Teflon (polytetrafluroethyene) exposed to fast atom bombardment indicated that such changes differ substantially from what occurs on metal substrates [9]. The changes observed in Teflon start with tiny surface fissures which grow into small surface cracks, forming a dense crack network, which eventually forms filamentary structure and cone-like formations. It was also shown [8] that bombardment of Teflon in the presence of mechanical stress greatly increased the rate at which the surface morphology changed, including more rapid crack formation, when compared to the unstressed material.

In this paper, we examine these effects in Teflon as well as Kapton, Nylon, and Kevlar-49.

EXPERIMENTAL

The materials were all obtained from commercial sources. The Teflon and Kapton were in the form of thin sheets, 3 mm and 0.5 mm in thickness and Nylon and Kevlar-49 fibers were 120 um and 10 um in diameter, respectively. Fast Xe atoms with 6 keV kinetic

energy were produced using a saddle-field type Fast Atom Bombardment Gun (Ion Tech. Ltd.) and allowed to impinge on both stressed and unstressed polymer samples. The angle of incidence in most cases was 60 degrees with respect to the surface normal. During bombardment the pressure in the target chamber was 1.3×10^{-6} Torr. The samples were bombarded with various doses of Xe atoms ranging from 1×10^{16} to 3×10^{17} atoms/cm^2. Stressed samples were mounted next to unstressed samples of the same material. Stress was achieved by means of bending the thin sheets of the polymer in tight radii. In the case of the Nylon and Kevlar-49 fibers, these were bent over a stainless steel wire (1.2 mm in diameter). All specimens were partially covered with aluminum foil to block the incident atom beam so that the exposed regions could be readily compared with the original surfaces. After exposure to the fast atom beam the samples were coated with 300 A of gold and examined in an ETEC U-1 Scanning Electron Microscope.

RESULTS AND DISCUSSION

In Fig. 1a we show a SEM photograph of the sample holder with stressed and unstressed Teflon specimens. The bending deformation produces a surface in tension, although a certain amount of relaxation of the stress which was exposed to the fast atom beam. At low magnification differences in texture on the surface of these samples between exposed and unexposed regions

could already be seen. Closer examination of the bombarded area on the stressed specimen shows several rows of crack-like features in the surface with the major cracks oriented approximately normal to the direction of tension. The density of microcracking was observed to be much higher in regions where the beam was normal to the surface as opposed to glancing incidence.

No such structure can be seen in the area of the sample which was covered with aluminum foil which shows that the cracks are not simply due to mechanical deformation alone. A higher magnification view of the region outlined in the center of Fig. 1a is shown in Fig. 1b. Comparison of this structure with previous results obtained on unstressed Teflon samples [8,10] shows that such large cracks in the bombarded surface are atypical. Thus, we can conclude that the combination of stress and bombardment is responsible for the formation of these larger flaws.

The walls of the cracks have a columnar structure and in some parts of the crack, filamentary formation can be seen. The major cracks are very deep which suggests that stress resulted in opening and propagation of the crack from initial flaws created by bombardment.

Fig. 2 shows a comparison of the surface morphology developed on stressed and unstressed Kapton exposed to fast Xe atom bombardment. Kapton is known to be a heat and radiation resistant polymer material [11]. In comparison with Teflon, the development of visible surface effects on the Kapton for both the stressed and unstressed specimens required a substantial higher bombardment dose ($> 10^{16}$ atoms/cm^2). Likewise, in Kapton, the

stressed sample developed damage (shown in an advanced stage in Fig. 2b) at considerably lower doses than in the case of unstressed material. At the stress levels and fast atom beam doses used in these studies, we did not observe crack initiation.

Nylon fibers under stress and bombardment exhibit surface crack initiation, as shown in Fig. 3a. The part of the bombarded surface marked by the white square is shown at higher magnification in Fig. 3b. If we compare the structures shown here with the developed morphology in Teflon (Fig. 1b) we see that they have similar features, namely columnar structures with a tendency to separate into free-standing filaments, and similarly shaped microcracks. The doses required to achieve comparable damage are considerably larger in the case of Nylon compared to Teflon. If the dose used to create the damage in Nylon shown in Fig. 3 where applied to Teflon, it would create an advanced degree of cone formation on the Teflon surface [10]. Estimates of the sputtering yields of Nylon vs Teflon showed substantially lower values for Nylon. This suggests that the ability of the incident particle to break bonds and move atoms and molecules both <u>from</u> the surface and <u>on</u> the surface is a critical part of the damage mechanism.

Fig. 4a shows the surface morphology development on an unstressed Kevlar-49 fiber from fast Xe atom bombardment. Following a dose of 2.8×10^{16} atoms/cm^2, the relatively smooth fiber surface is transformed into a dramatic array of ridges which are oriented perpendicular to the direction of the incident particle beam which was also along the axis of the fiber. A stressed Kevlar-49 fiber (Fig. 4b) exposed to the same dose shows

a more advanced degree of development, where in some areas of the bombarded region there is a transition from ridges to columnar structures. The major axes of the columns are oriented parallel to the fiber axis and therefore parallel to the direction of incidence of the Xe atoms. We are currently determining if it is the fiber orientation or the direction of incidence that produces the orientation of these patterns. Kevlar is a highly structured material with strong orientation of crystalline regions [12], which may be the dominant cause of the structures we are seeing here.

CONCLUSIONS

We believe that the mechanisms for the creation of the wide variety of surface changes shown here involve physical sputtering (removal of molecular fragments) and movement of molecules on the surface. The details of these processes are obviously yet to be revealed. However, the substantial increase in the rate of formation of surface damage when the material is under stress as well as the appearance of surface microcracks indicates that the physical state of the near surface layer can play an important role. In other experiments [13-15], we are in fact studying the effects of focused radiation into stressed crack tips in polymers where the radiation induced bond breaking leads directly to crack propagation. Our immediate goal is to develop a more detailed quantitative and theoretical description of these effects of morphological changes, microcrack formation, and

bombardment induced crack propagation in polymers.

ACKNOWLEDGEMENTS

The authors wish to thank the WSU Electron Microscopy Center and Mr. Franklin Doolittle for generous use of the facilities. This work was supported in part by the McDonnell Douglas Independent Development Fund, the Office of Naval Research, Contract NOOO14-80-C-0213, NR 659-803, and the Washington Technology Center.

REFERENCES

1. W. R. Gove, Trans. R. Soc. London 142, 87 (1985).

2. R. Behrish, ed., Sputtering by Particle Bombardment, Vol. I-III, Springer-Verlag, Berlin, 1980-85.

3. E. C. Baranova, V. M. Gusev, Yu. V. Martynenko, C. V. Starinin, and I. B. Haibullin, Rad. Effects 18, 21 (1973).

4. J. M. E. Harper and R. J. Gambino, J. Vac. Sci. Technol. 16, 1901 (1979).

5. See articles in Desorption Induced by Electronic Transitions - DIET II, W. Brenig and D. Menzel, editors, Springer Verlag, Berlin, 1985.

6. R. G. Orth, H. T. Jonkman, D. Stulik, and J. Michl, Proc. 30th Ann. Conf. Mass Spectrom. Allied Topics, June, 1982, Honolulu, Am. Mass Spec. Soc., p. 212.

7. R. Michael and D. Stulik, Rad. Effect. Let.,87, 9 (1985).

8. R. Michael and D. Stulik, Nucl. Instrum. Methods, in print.

9. See articles in Ion Bombardment Modification of Surfaces, O. Auciello and R. Kelly, eds., Elsevier, Amsterdam, 1984.

10. R. Michael and D. Stulik, submitted to J. Vac. Sci. Technol.

11. See The Science and Technology of Polymer Films, Vol. II, O. J. Sweeting, ed., John Wiley, New York, 1971, chapter 16.

12. R. J. Morgan, C.O. Pruneda, and W. J. Steele, J. Polym Sci.: Polym. Phys. Ed. 21, 1757 (1983).

13. J. T. Dickinson, M. L. Klakken, M. H. Miles, and L. C. Jensen, J. Poly. Sci.: Poly. Phys. Ed. 23, 2273 (1985).

14. J. T. Dickinson, L. C. Jensen, and M. L. Klakken, J. Vac. Sci. Technol. A4, (1986).

15. J. T. Dickinson, K. Tonyali, M. L. Klakken, and L. C. Jensen, J. Vac. Sci. Technol., to be published.

FIGURE CAPTIONS

Figure 1. Crack Development in stressed Teflon.

a) Sample holder with stressed and unstressed Teflon samples.

b) Detail of surface morphology development on stressed sample (bombarding dose: 7.2×10^{16} Xe atoms/cm^2).

Figure 2. Surface morphology development on Kapton.

a) Unstressed sample (bombarding dose: 2.8×10^{17} Xe atoms/cm^2).

b) Stressed sample (bombarding dose: 2.0×10^{17} Xe atoms/cm^2). Arrows indicate the direction of applied stress.

Figure 3. Crack formation in Nylon fiber (bombarding dose: 2.8×10^{17} Xe atoms/cm^2).

a) Low magnification. Stress is perpendicular to major crack.

b) Detail of surface morphology development and crack initiation.

Figure 4. Surface morphology development on Kevlar fiber (bombarding dose 2.8×10^{17} Xe atoms/cm^2).

a) Unstressed fiber.

b) Stressed fiber (arrows indicate the direction of applied stress).

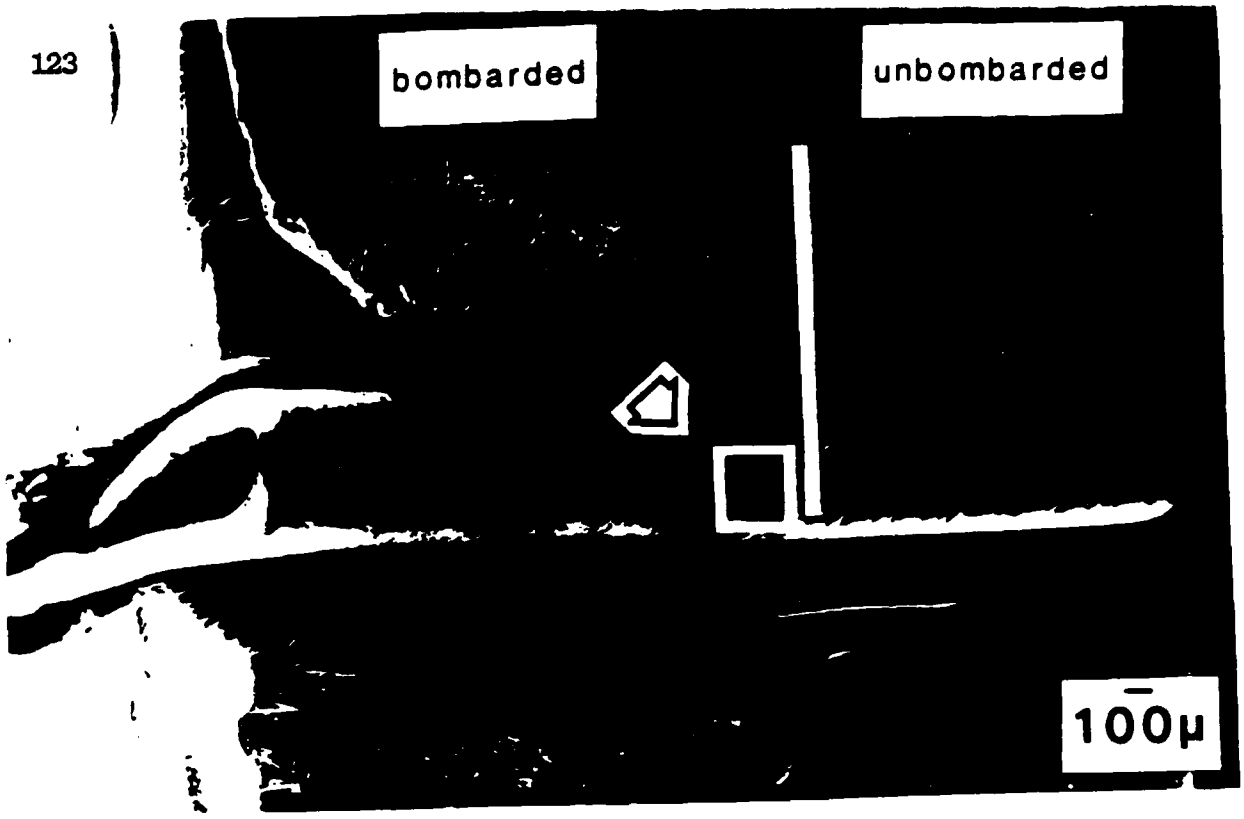
bombarded
unbombarded
100μ


Teflon stressed
10μ


Kapton sheet unstressed
1μ

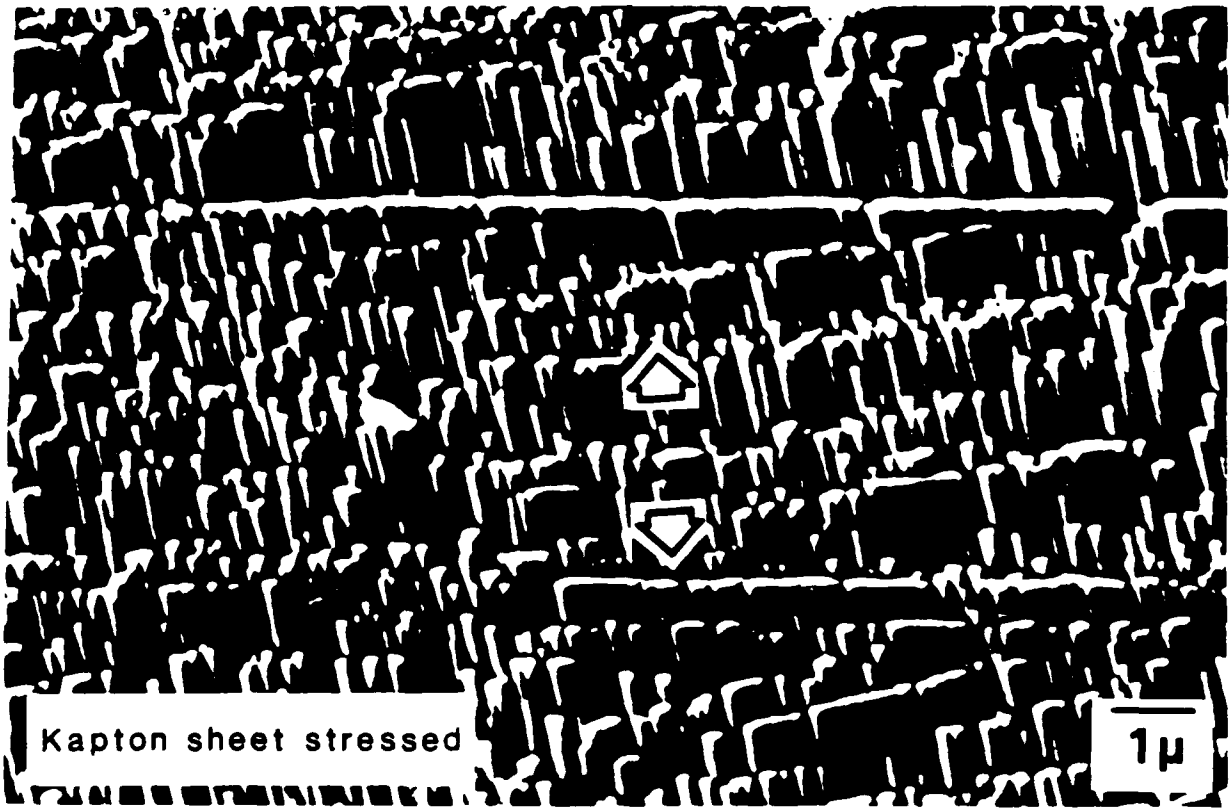
Kapton sheet stressed
1μ

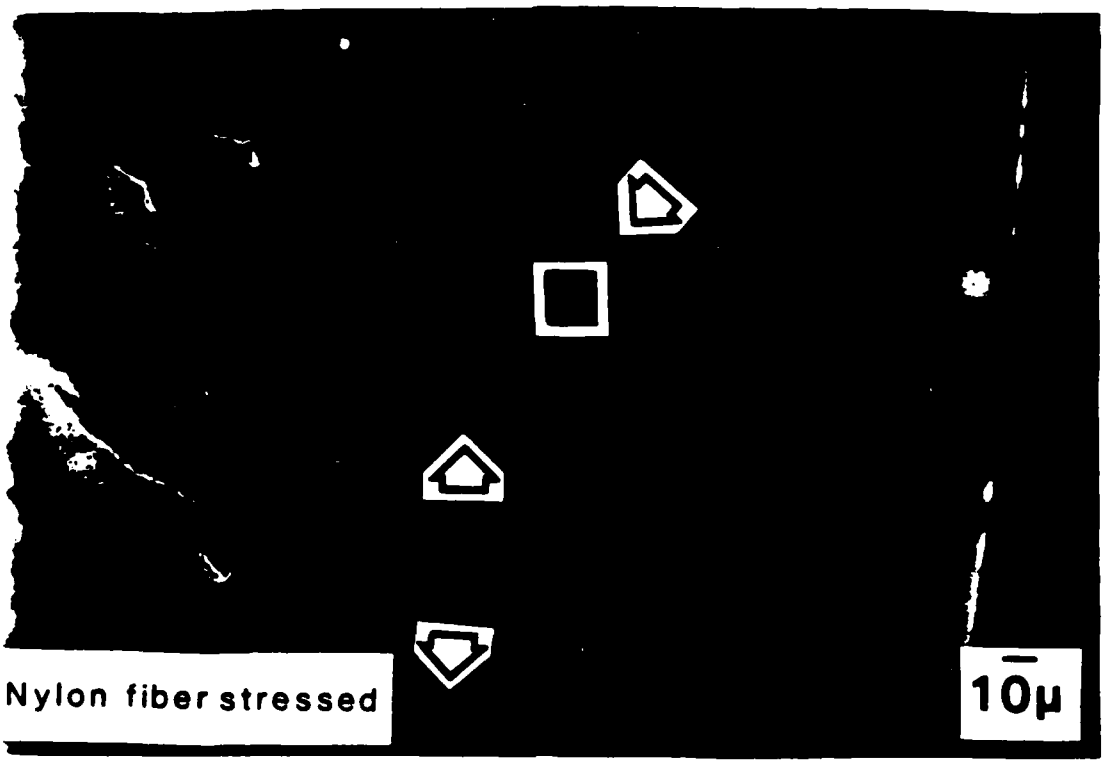
Nylon fiber stressed
10μ

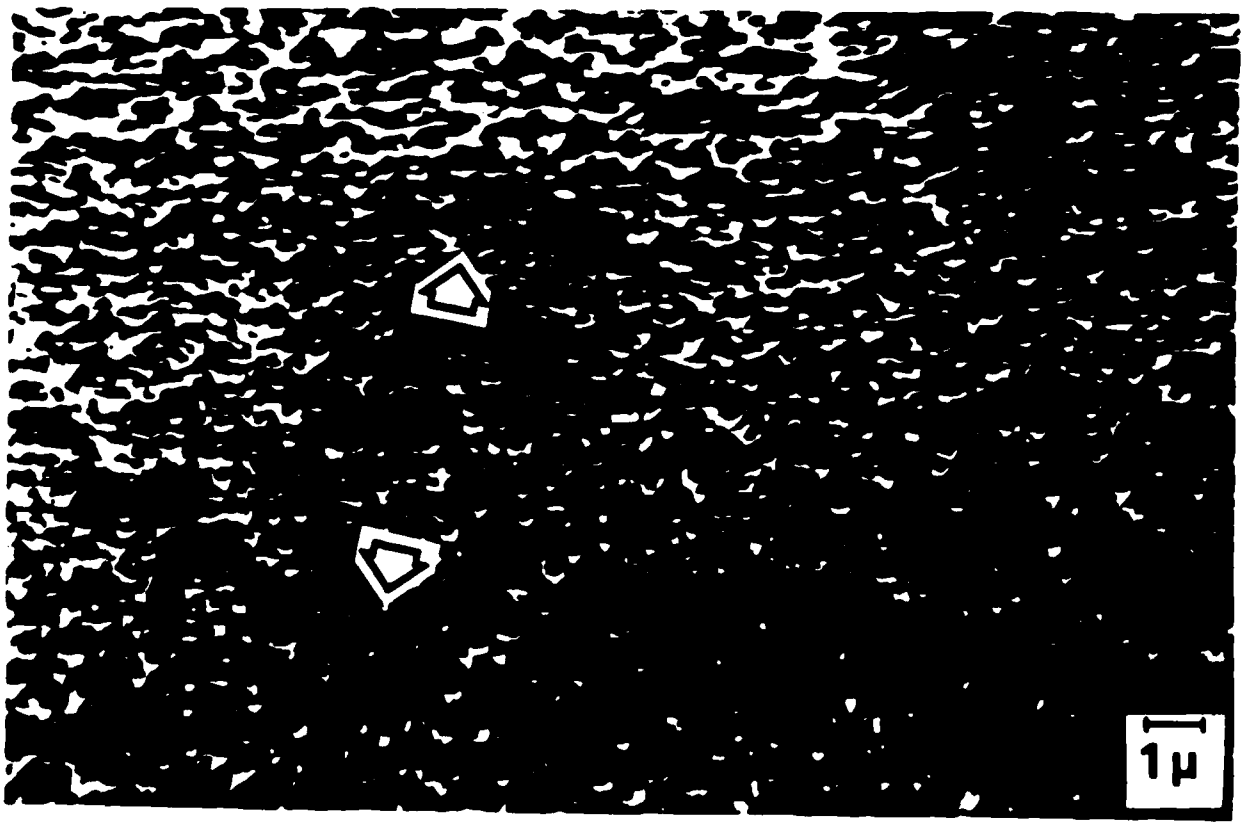
1μ

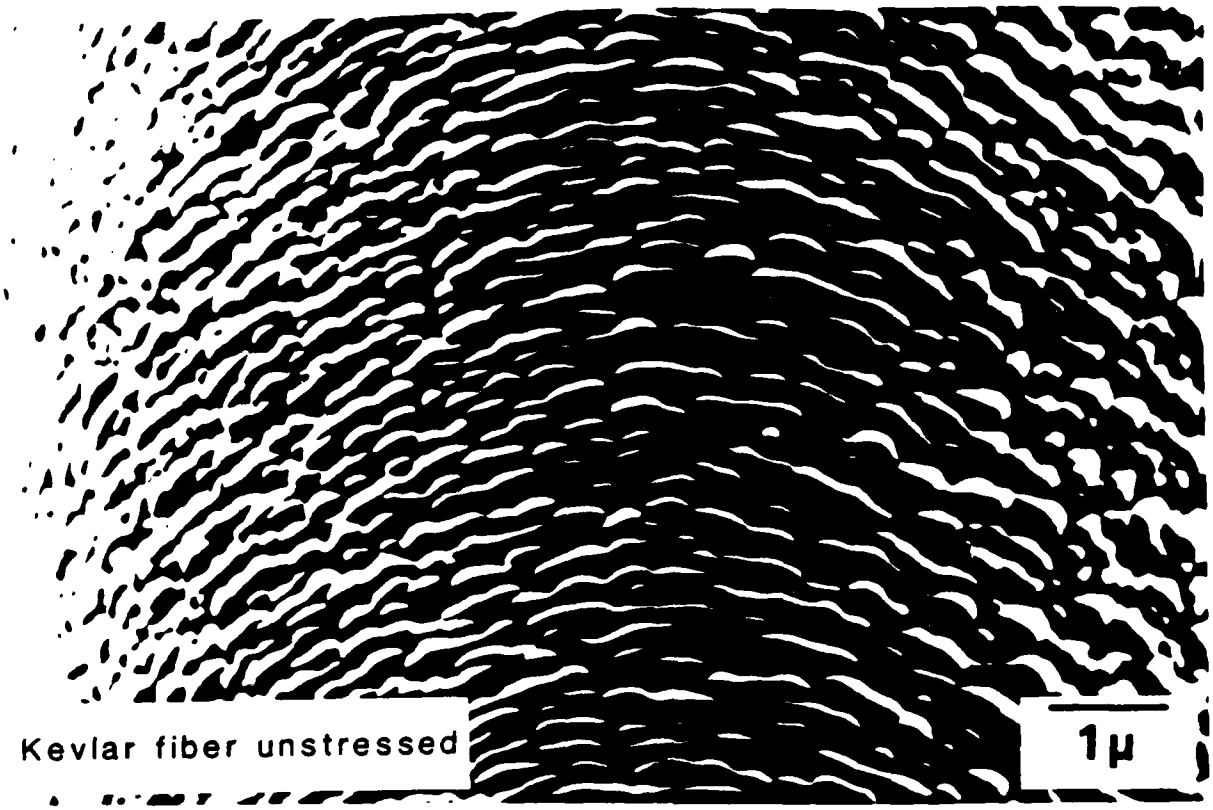
Kevlar fiber unstressed
1μ


Kevlar fiber stressed
1μ

APPENDIX I

Simultaneous Measurements of the Electron and Photon Emission Accompanying Fracture of Single Crystal MgO

S. C. Langford, J. T. Dickinson, and L. C. Jensen
Department of Physics
Washington State University
Pullman, WA 99164-2814

ABSTRACT

We investigate the simultaneous emission of electrons and photons during the deformation and fracture of two types of high purity, single crystal MgO. These crystals exhibit significant differences in optical opacity due to differences in void and precipitate concentrations. Measurements of the emission of visible photons during deformation and prior to failure of the crystals are presented, along with the time dependencies of the photon and electron emission during and after fracture. Correlations with fracture strength and fractographic features are also discussed.

I. INTRODUCTION

The emission of photons, electrons, and other species due to deformation and fracture is an interesting example of energy transfer between systems as well as a potentially useful probe of the fracture process. When due to deformation and crack growth, we refer to these emissions collectively as *fracto-emission*. MgO is an attractive material for the study of fracto-emission, because the photon and electron emissions associated with a variety of stimuli (e.g., radiation) have been intensively studied. Further, high purity MgO is readily available and well characterized mechanically and spectroscopically.

Williams and Turner reported photon emission (phE) associated with the compression of single crystal MgO.[1] During uniform deformation, phE commenced at the onset of plastic deformation and increased in an approximately linear fashion. Small peaks in phE were observed as cracks formed. An increase in phE was also observed when the strain was relieved suddenly. These emissions were attributed to defects, probably vacancy clusters, created and excited by moving dislocations. At fracture, surface defects were thought to contribute as well.

More recent work suggests that charge separation during the formation of fracture surfaces may also play an important role in the emission of photons and other species.[2-4] In addition, the emission of neutral atoms and molecules from the fracture surfaces of different single crystal MgO samples has been investigated.[5,6]

In this study, we report measurements of photon emission (phE), electron emission (EE), and possible positive ion emission (PIE) accompanying the deformation and fracture of MgO. We present results examining the photon emission prior to failure illustrating its dependence on load. We compare determinations of the instant of fracture with the phE and EE signals. We also examine in detail the phE and EE time dependencies and decay curves during and following fracture and interpret the observed kinetics in terms of primary defects known to occur in MgO. We also compare the phE and EE intensities from clear vs cloudy MgO and

suggest that the substantial differences are related to the striking differences in the intensities of the neutral molecule emission from these materials reported previously.

II. EXPERIMENT

Clear, single crystal MgO was obtained from W. & C. Spicer Ltd., and cloudy MgO from Superior Refractory, Cheltenham, England. Both sets of crystals were nominally 99.99% pure. From these crystals, samples approximately 1.6 x 6 x 12 mm were cut with a diamond saw. Some samples were broken as cut, while others were mechanically polished. The samples were mounted in a carousel assembly which moved the samples to be broken into position between the detectors and a loading mechanism. The samples were supported across a span of 6.4 mm in three point bend. The carousel assembly was mounted in an ultra high vacuum system which was maintained at a pressure of less than 10^{-6} Pa. It should be noted that the fracture event itself is typically a few us or less in duration and that the intense part of the emission lasts only tenths of a seconds. Therefore the effects of chemisorption of background gases can be ignored; at these pressures, assuming unity sticking probability, the chemisorption of a monolayer of gas would require at least tens of seconds.

phE was detected with an EMI Gencom 9924QB photomultiplier tube with bialkali phosphor and a quartz window which extends the short wavelength sensitivity down to the 200 nm region. The long wavelength sensitivity ranged up to approximately 600 nm. The EE and PIE were detected with a Galileo Electro-optics 4039 channeltron electron multiplier. Both the photomultiplier tube and electron multiplier were mounted directly in the vacuum at a distance of about 1 cm from the tensile side of the specimen. We monitored the loading force with a Kistler 9202 quartz force transducer mounted behind the loading device. The measured force included small frictional and Hooke's law components due to the supporting apparatus. The output of the force transducer was digitized and recorded every 10 ms. Simultaneously, the total numbers of phE and EE counts in the last 10 ms were recorded with synchronized

multichannel scalers. 4095 channels were available for each of these signals, providing 40 s total data aquisition time. The multichannel scalar was started just prior to the application of the load. The response of the force transducer to the change in load at fracture was much faster than the 10 ms sampling time. When desired, data could be acquired at much faster rates.

The samples were strained at a rate of 0.13 mm/s. The flexure strength, S, of these samples was estimated using the relation

$$S = (3PL)/(2bd^2) \qquad (1),$$

where S is the stress at the outer, tensile surface of the sample at fracture, P is the load at fracture, L is the support span, b is the width of the sample, and d is its thickness.

III. RESULTS

A. Typical Clear MgO

The phE, EE, and load during a test of a typical clear MgO crystal are presented in Fig. 1 using logarithmic intensity scales. phE begins soon after the onset of loading. At fracture, both phE and EE rise sharply to a peak, and thereafter decay over a period of tens of seconds.

Pre-fracture. phE generally commences soon after the onset of deformation, long before failure. Sometimes there is an initial peak in phE, probably due to transient deformation as the loading mechanism aligns with and is seated on the crystal. Our data is consistent with the observation of Williams and Turner that the deformation phE increases in a fairly linear fashion under loading at a constant rate. Changes in the loading rate were generally accompanied by congruous changes in phE. Frequently, samples showed an increase in phE immediately *before* fracture, as seen in Fig. 1.

In contrast, little EE is noted prior to fracture, except an occasional small peak at contact. No significant departure from linearity is observed in the load curve prior to fracture. Photographs of the fracture surface show features consistent with brittle fracture.

Fracture. On the time scale of most of our measurements (0.01s/channel), the duration of the fracture event was significantly less than one channel of pulse counting. To within this time resolution, however, the load measurements gave a clear indication of the time of fracture, and the phE and EE peaks (the highest single channels) were found to be *simultaneous* with the drop in load. Similar to a wide variety of materials we have studied, it is likely that the peak emission occurs during fracture.

In general, the phE and EE peak heights are not well correlated with each other. Variability of the EE peak heights may be occurring due to the dependence of our EE collection efficiency upon the geometry of the opening crack. One significant observation is that the phE peaks heights (i.e., emission during fracture) correlated very well well with flexure strength, as shown in Fig. 2. Both types of single crystal MgO studied fall on the same linear curve. The flexure strength of polished samples were not significantly greater than that of the unpolished ones. Fracture nearly always initiated at one of the edges of the sample, where mechanical polishing was least effective in removing flaws introduced by the cutting process.

Decay. The phE and EE decays typically last some tens of seconds after fracture. When the phE and EE curves of Fig. 1 are normalized at their peaks, the resulting decays are shown to be remarkably similar on this time scale. Data taken on faster time scales indicate the presence of an initial, fast decaying transient in the phE. This suggests that, apart from the transient, the emissions are the result of parallel processes. To account for the EE (which requires an escape route to the surrounding vacuum) these common processes *must be occurring at or near the surface.*

We have analyzed these slow decays in terms of a simple model based on electron-hole combination via the valence band, with retrapping. Similar models are used to describe variable order kinetics in thermally stimulated luminescence work. Curve fitting the parameters of the model to the data of Fig. 1 and similar data yields excellent agreement and shows the decay to be nearly second order.

B. Comparison of Clear and Cloudy MgO

The phE and EE from a set of clear and cloudy MgO crystals is presented for comparison in Fig. 3. In order to observe the faster cloudy crystal decays more clearly, we acquired the emission data at a faster rate (1 ms/ch).

The form of the pre-emissions from clear and cloudy crystals are much the same. However, the phE intensities from the cloudy crystals are somewhat reduced, probably due to the optical opacity of these samples.

At fracture, the phE and EE from the clear crystals is significantly higher than that from the cloudy crystals. The correlation between phE and flexure strength suggests that this is largely due to the weakness of the cloudy crystals relative to the clear ones. Differences between the EE for these two types of crystals are greater than those observed in the phE.

The most striking difference between the two materials is the much more rapid decay of both phE and EE from the cloudy samples relative to the clear samples. This suggests that a quenching process may be limiting emission from the cloudy crystals.

The rapidly decaying transient in phE decay (relative to the decay of the EE) in clear (Spicer) MgO, mentioned previously, is well displayed in Fig. 3. This transient lasts about 5 ms. A less pronounced transient may also be present in the phE decay from cloudy MgO. The existence of this phE transient suggests that a significant portion of the phE at fracture is due to processes which do not have corresponding EE branches. Processes in the bulk are an obvious possibility.

C. Intense EE from Clear MgO

Occasionally, a clear MgO crystal would display unusually high EE upon fracture, at least a factor of two or more than the average. The emissions from one of these samples are displayed in Fig. 4. The pre-emission from these crystals was not remarkable. On the other hand,

judging from the 50 or 60 seconds of post-fracture data that was collected, the EE decay from these samples would take hundreds of seconds to return to the noise level. In the case of two intense EE crystals where the load was carefully measured, one of the crystals was somewhat stronger than average, and the other crystal broke off center. Both phE and EE from crystals breaking off center tend to be higher than crystals of equivalent flexure strength, suggesting that shear stress parallel to crack motion may be a factor. Both of these crystals displayed an unusually long, smooth fracture surface along the side of the crystal toward the detector, i.e., the surface in tension.

D. Positive Ion Emission

Five samples, two clear and three cloudy, were tested for Positive Ion Emission at fracture by biasing the entrance cone of the channeltron with a high negative voltage (-3000 V). It is possible that the observed signals are not due to positive ions but to high energy electrons (greater than 3 keV) or metastable neutrals with sufficient internal energy to create a secondary electron on the entrance cone of the multiplier (requiring approximately 6 eV). We have developed methods which can resolve this ambiguity and are in the process of carrying out these experiments. Taking the liberty of calling the observed signal under these conditions Positive Ion Emission (PIE), typical EE and PIE curves are presented in Fig. 5. In order to facilitate comparison of the decays, the curves have been normalized so that their peaks coincide.

The PIE decay is fast, being essentially complete after 3 ms, with isolated single counts at later times suggesting a longer tail. In contrast to the large differences in phE and EE observed from clear and cloudy MgO, there is little if any difference in the peak PIE. In each case, the decay of PIE is much more rapid that the decay of the accompanying phE. The PIE decay is also much more rapid than any of the observed EE decays observed. This difference is relatively more pronounced in the case of clear MgO, of course. If some process is quenching phE and EE in the cloudy crystals, it does not seem to affect PIE significantly.

In each case the average *peak* PIE is a significant fraction of the average peak EE. This fraction was about 15% in the case of the clear MgO and 30% in the case of the cloudy. If these detected particles are due to high energy electrons rather than positive ions, a significant proportion of the early EE must have rather high energies *and* the energy distribution would have to drop in a few ms below 3 keV.

E. Fast Time Scale Data

Fig. 6 displays the results of phE measurements taken on progressively faster time scales. Each curve represents phE from a separate fracture experiment. A rapid rise occurs out of the slowly rising deformation luminescence previously discussed. The rise times of this faster component is on the order of five to ten microseconds. The initial decay takes about 10 us, and is followed by a decay which is obviously first order for about 20 ms. Although it is yet to be established, the peak emission is most likely occurring during fracture.

F. Fractography

The general appearance of the fracture surfaces is consistent with brittle fracture. Brittle fracture in MgO has been studied extensively.[7-10] The fracture surfaces of two clear MgO crystals in transmitted light are shown in Fig. 7. Most of the samples show clear initiation zones, with mirror, mist, and hackle regions. The initiation zones are most often at one of the sample edges, as noted above. From the initiation region, surface steps extend along the tensile half of the sample. Along the midline of the sample, the steps turn about ninty degrees, and tend to meet the compressive edge of the sample at right angles. Many surface step vees can be seen where the steps cross into the compressive side of the sample. These steps are believed to form at the boundaries of cracks proceeding on nearby (100) planes thereby revealing the path of the moving crack front.

These surfaces features reflect the state of stress at fracture and also can be related to the crack velocity[11]. In the initiation region, the crack accelerates through the mirror region until instabilities lead to repeated bifurcation of the crack. This bifurcation is responsible for the hackle surrounding the initiation mirror. The broad mirror region along the tensile side of the sample most likely results from rather stable, slow crack growth through this region. The fracture steps often jog abruptly near the midline, suggesting an interruption in the the progress of the crack. In three point bend, the midline of the sample lies on the neutral plane, a region of zero tensile stress. Thus, there is no stress to drive the crack across the midline until the crystal deforms in response to the developing crack. Further, dislocations formed on the compressive side of the crystal during deformation obstruct the growth of the crack in this region. The formation of vees in the surface steps is evidence of the crack front encountering a high density of screw dislocations in this region.[12] In many cases, the pattern of steps suggests that the crack proceeds from the midline to the back edge of the sample simultaneously along much of its width. Thus it appears that crack growth can be arrested near the midline until fracture of the tensile half of the crystal is largely complete.

The broad mirror-like region on the tensile side of the clear MgO is especially dark and smooth in those specimens yielding the highest EE. Aside from the surface steps, this region is smooth on the submicron scale, as shown in Fig. 8a. The smoothness of this feature may present an optimum geometry for electron escape and detection. Under optical illumination along the (100) direction, these areas often have a dark appearance, as shown in Fig. 7. This may be due to light scattering from extremely small surface imperfections.

Some crystals, such as that in Fig. 7a, show evidence of fracture proceeding on two parallel planes. The poorly focused region in the lower half of Fig. 7a is one of a pair of such planes. Examination of the surface steps indicate that crack growth on these planes is not parallel. There is also evidence of an obstacle to the progress of the crack in this region (shown by the arrow). Parallel crack planes have been observed in thermally shocked MgO.[13] Their presence here may be due in part to experimental geometry; the thickness of our samples is an

appreciable fraction of the support span. This geometry leads to high shear stresses, which often makes fracture unusually sensitive to bulk imperfections and sample misallignment.

Some of the mirror-like regions discussed above exhibit small inclusion-like features. These features are far more numerous in cloudy MgO than in clear.[6] The surfaces shown in Fig. 8 are typical in this regard. The inclusions are usually rather uniform in size and apparently lie in the fracture plane. We suspect that these are $Mg(OH)_2$ inclusions which have formed at subgrain boundaries. $Mg(OH)_2$ inclusions have been observed in previous studies.[14,15] Stress concentrations at subgrain boundaries, perhaps due to the inclusions themselves, would tend to make them favored fracture planes. We observe few voids at the fracture surface of our cloudy samples, suggesting that their cloudiness is due to these inclusions and not voids, as observed in certain other MgO crystals.[10] The fracture surfaces of cloudy MgO have been shown to be copious sources of O_2.[6] This O_2 seems to be associated with inclusion/crystal interfaces that serve as sinks for molecular oxygen.[6]

IV. DISCUSSION

A. Typical Clear MgO

Emission Prior to Failure. The phE we observe prior to fracture is similar to that described previously.[1,16] The defects participating in this luminescence have been the object of several photoluminescence and photoexcitation studies.[16-20] The main absorption band in deformed alkaline earth oxides is composite in character, and is attributed to excitonic transitions associated with vacancy clusters.[16,18] These excitons are localized electron-hole pairs formed when an O 2p electron from an oxygen ion of low coordination number is promoted to an Mg 3s level of a nearby magnesium ion. This conclusion is supported by the similarity of luminescence and photoexcitation spectra of powders, which possess a high density of surface oxygen ions of low coordination.[16,21-25] The luminescence we observe prior to fracture is

most likely due to excitonic transitions taking place at vacancy clusters formed during deformation. Similar processes probably take place on the newly formed surfaces during and following fracture.

The production of vacancy clusters is likely to take place by means of a jog dragging mechanism. Cathodoluminescence and secondary electron emission studies have shown that the defects responsible for these emissions are strongly localized in the region of dislocations, slip bands, and related structures.[26-33] Jogs are often formed when moving dislocations intersect, and the subsequent motion of jogged dislocations can produce vacancies. Clear evidence for this process in LiF has been provided by Andreev and Smirnov. The density changes they observed during deformation suggested that the dominate mechanism ofvacancy production was jog dragging by screw dislocations.[16] Dislocation interactions in MgO are believed to be quite similar to those in LiF.

The excitation of the defects produced in deformation is not so well understood. Dislocations are expected to accumulate charge in the process of establishing thermodynamic equilibrium with the rest of the crystal[34,35] as a consequence of the different energies of cation and anion vacancy formation. In some materials, like ZnS, the resulting electric fields may be sufficient to excite local defects.[36] However, in the alkali halides, deformation luminescence has been attributed to a more dynamic process,[37] namely the capture of electrons by moving dislocations and subsequent recombination in nearby traps. This mechanism is consistent with the much smaller dislocation charges observed in the alkali halides relative to ZnS.[38] Since MgO and LiF share the same structure and are both highly ionic, the later mechanism is the more likely in this case. As seen in Fig. 1, the increase in phE intensity with strain (at constant strain rate) is consistent with a production of defects during deformation, resulting in a greater number of defects available for excitation by moving dislocations.

As noted above, our load measurements showed no evidence of macroscopic plastic deformation prior to fracture. This raises the question of whether our phE was due to local plastic deformation near the loading nose, or whether a significant portion was from elastically

deformed regions of the crystal. phE prior to macroscopic yield has been observed in MgO loaded in compression,[16] but its intensity is much reduced relative to that during plastic deformation. Dislocation motion and multiplication is known to commence long before macroscopic plastic yield. At about two-thirds the yield stress, short slip-line segments begin to form.[39] With careful surface preparation, MgO can undergo significant plastic deformation. Studies of such crystals may help resolve this point.

As previously mentioned, no significant EE is seen in this study of MgO prior to fracture. The small bursts that were occasionally observed are attributed to microcracking or abrasion during the seating of the loading nose onto the back of the crystal. In LiF and ZnS, EE has been observed during compressive loading and has been attributed to dislocation motion.[38,40] The contrasting results between these studies and ours may be due to differences in electronic properties or local strain levels.

Emission at Failure. The intense phE and EE at fracture is probably the result of several processes. As noted above, Williams and Turner observed photoluminescence during rapid stress relaxation.[1,16] Thus some of the phE at fracture could be deformation related. Belyajev et al. have suggested that the strong dilatation of the lattice near the crack tip may result in energy level shifts.[41] This might facilitate some otherwise unlikely electronic transitions.

The fracture surfaces of MgO also show evidence of intense charge separation which may contribute to the prompt emission of electrons and photons at fracture as a result of microdischarges in the crack tip. As evidence of such electrical activity, we have detected long wavelength electomagnetic radiation accompanying fracture of MgO.[2] This breakdown may also be responsible for the creation of mobile electrons and holes which subsequently participate in a variety of emission processes.

The absence of a significant difference in the flexure strengths of polished and unpolished crystals implies that failure was not simply due to stresses exceeding the critical Griffith stress for preexisting defects. Rather, sub-critical crack growth is probably occurring as well. Clarke and Sambell[7,42] have suggested that activity on nearby slip systems can increase the local strain

at the tip of existing microcracks and supply energy for crack growth. Preexisting microcracks can then grow discontinuously until they reach the critical Griffith size, resulting in catastrophic failure. Although the surface area created during microcracking is very small, it may be possible to observe fracto-emission associated with subcritical crack growth. In cloudy MgO, we do in fact observe very rapid bursts of neutral O_2 *prior* to failure which we attribute to microcracking.

Emission After Failure. Fracture has resulted in a highly excited surface, as evidenced by the emission of particles after failure. The possible excitation mechanisms include electron bombardment of the surface, high concentrations of dislocations intersecting the surface, and chemical processes due to bond breaking at the crack tip.

In the case of microdischarge induced excitation, the emitted electrons, local acceleration due to surface charge leads to bombardment of the surface. This is supported by evidence that the defects excited in fracture are similar to those excited by particle and photon irradiation. Linke found that the TSEE peaks observed in crushed LiF agree with those observed in samples stimulated by electrons or x-rays.[41] A similar agreement between fracto-emission and electron induced emission was demonstrated by Dickinson and Jensen for polymeric systems undergoing adhesive failure.[43]

Dislocations intersecting the fracture surfaces could also result in excitations, perhaps by providing relatively high concentrations of mobile charge carriers. Direct evidence of surface charge of both signs on fresh fracture surfaces of alkali halides has been provided by Wollbrandt et al[44] using an electrostatic probe with 100 um spatial resolution.

The instantaneous stoichiometry of the fracture surface at the time of fracture is in a state of change, as evidenced by the emission of atoms and molecules.[5,6] The necessary chemistry for producing the observed neutral emission requires non-lattice surface species. Our working hypothesis is that these are initially due to "fragments" created at fracture. Another related factor is the possibility that localized heating during fracture may cause dissociation to occur *or* affect the emissions on very short time scales. Miller et al. report the observation of black body

radiation from localized hot spots during the deformation and fracture of crystalline NaCl[45] under compressive impact loading. Temperatures in excess of 300 C were observed with a duration up to 50 us. Simple energy considerations require that this heating be extremely localized. If the fracture surface reaches these temperatures, the lifetimes and mobilities of various excited species that would contribute to EE and visible phE would be modified considerably.

Relaxation of the above departures from the ground state, ideal crystal surface results in the post fracture emission. A review of known stimulated emission processes is given below, with special attention to surface processes, as these appear to dominate at times greater than a few milliseconds after fracture. We will consider first the short lived excitations which would be relevant to the faster decaying components of the emission.

Surface excitonic processes are expected to have lifetimes on the order of 1-1000 us.[21,46] Electron energy loss spectra of MgO show features that can be attributed to surface excitonic states excited by the incident electrons.[47] These surface excitons are also observed in surface photon reflectance studies.[21,25] The resulting luminescence spectrum peaks near 3.2 eV and depending on the coordination number of the participating oxygen ion, 4-6 eV photons are required to create these excitons. The excitonic luminescence is quenched by exposure to gases; this quenching is reversible to a large extent, and is believed to be collisional; i.e., the molecules must be striking the surface to produce the quenching.[21] The release of neutral gas molecules during the fracture of some types of MgO may well influence the intensities of the observed emissions.

Thermally stimulated processes such as recombination of mobile carriers at defects can lead to slower decaying emissions with non-exponential kinetics.[4] In MgO powders, Yanagisawa and Huzimura have done considerable work on UV-excited phosphorescence.[46,48] They attribute the observed phE to the recombination of electrons trapped at surface F^+ centers [surface oxygen vacancies each containing a trapped electron] with holes trapped at surface V^- centers [surface magnesium vacancies each associated with a trapped hole (an O^- ion)]. They also

observed a two component thermally stimulated luminescence (TSL) peak at about 100 C with activation energies of 0.74 and 0.84 eV, respectively. Using ESR spectroscopy, the surface F^+ center was identified as one of the participating electron defects for this luminescence. Thermal Desorption studies of oxygen from the powder surfaces indicated the need for *two* F-type centers. A candidate for this second defect is the so-called surface P^- center [a Mg-O divacancy with a trapped electron] which would behave in a similar manner as the F^+ center in luminescence processes and interactions with oxygen.[49]

The phosphorescence observed by Yanagisawa and Huzimura is quenched by small quantities of oxygen, probably due to the reaction of a molecular oxygen adsorption precursor at surface F-type centers to form a chemisorbed O^{2-} species. Thus, in contrast to the largely reversible quenching of excitonic phE noted above, this tightly bound O_2^- results in irreversible quenching. Small quantities of hydrogen gas enhances the phE intensity, however. This enhancement was attributed to the conversion of surface V^- centers to surface V^-(OH) centers. In the bulk, V^-(OH) centers are known to be considerably less stable that V^- centers, having activation energies of about 1.0 and 1.6 eV, respectively.[50] The formation of V^-(OH) centers should increase the rate of hole release and thus increase the related phE. Although they report that the phE is not strictly second order, second order kinetics was shown to apply on sufficiently long time scales, on the order of hundreds of seconds. The phosphorescence spectra they report is peaked at roughly 2.3 and 3.2 eV.

A slowly decaying EE from x-ray irradiated MgO has been reported in connection with a Thermally Stimulated Electron Emission (TSEE) study.[51] However, the mechanism of this emission is not clear. Yanagisawa and Huzimura have observed a 390 K TSEE peak from MgO powders corresponding to the TSL peak noted above.[52] The TSEE peak is also quenched by exposure to oxygen. When the powder is illuminated by light known to bleach surface V^- centers, the TSEE peak grows smaller. On this basis, and the similarity of this peak and the 400 K TSL peak, the EE was attributed to the recombination of electrons and holes from the surface F^+ and V^- centers, respectively.

Verification of excitations in the eV energy range induced by electron bombardment is provided by electron energy loss spectroscopy (EELS) and secondary electron emission spectroscopy (SEES). Henrich et al. observed a 2.3 eV energy loss peak in their study of MgO.[47] Subsequently it was identified with the surface V^- center.[53,54] Surprisingly, no features identifiable with surface F type centers were observed, even at high primary beam energies.

Certain SEES features have been found to correlate with certain types of surface damage.[55] Namba and Murata studied MgO surfaces formed by cleavage in vacuum using SEES, EELS, cathodoluminescence (CL) spectroscopy and low energy electron diffraction (LEED). Surfaces showing LEED patterns consistent with surface damage also emitted a 1.6 eV SEES signal. When the surface damage took the form of faceting, this EE was most intense along <100> directions. This peak was associated with bulk F centers on the basis of an associated CL peak at 2.4 eV. The great spatial extent of the excited F center wavefunction would facilitate hopping to nearby F centers, and finally, into the vacuum. Since the subsurface damage associated with faceting is concentrated along <100> directions, the directionality of the 1.6 eV secondary electron emission from faceted surfaces is readily accounted for. A transient bulk F^- center may also participate in this process. This damage dependent process may help account for the variability we observed in fracture induced EE.

Namba and Murata have also reported evidence of phE due to the excitation of surface F-type centers by electron bombardment. On the basis of the correspondence between surface and bulk F centers, they attributed CL peaks at 3.4 and 3.9 eV to the decay of excited F and F^+ centers, respectively. The identification of the 3.4 eV peak with recombination at surface F^+ centers is consistent with the conclusion of Yanagisawa and Huzimura in their study of phE from MgO powders. The source of weaker 2.3 eV phE observed from the powders is not yet clear.

Finally, Namba and Murata report evidence that MgO has a negative electron affinity; that is, the vacuum level lies within the band gap. Their observation of a 4.0 eV cutoff in SEES of

undamaged MgO surfaces is consistent with a vacuum level 3.8 eV from the top of the valence band. The midgap position of the vacuum level would facilitate EE due to direct transitions into the vacuum from the conduction band and excited F-type centers. Thus, we expect that at least some radiative processes occurring at MgO surfaces have electron emitting analogs.

Probable Decay Processes. In the early stages of decay, any or all of the above processes may occur. Initially, bulk processes probably contribute significantly to phE. In particular, the excitation and decay of bulk defects my moving dislocations and electron bombardment might help explain the rapid initial decay of phE relative to the EE decay.

The observed similarity of phE and EE decay after the first few milliseconds suggests that surface and near surface processes dominate. A simple trap model used by Halperin and Braner[56] to describe the process of TSL also describe the fracto-emission we observe rather well. Initially, irradiation, electron bombardment, or fracture poduces populates electron and hole traps with energies within the band gap. Subsequent thermal stimulation results in charge transport and recombination. Assuming that the long term emission we observe is due to the mechanism proposed by Yanagisawa and Huzimura, where we tentatively identify the electron traps as recombination centers and the holes as the mobile species.

The equations describing this process under isothermal conditions are:

$$-dm/dt = Amn_f, \tag{2}$$

$$-dn/dt = Bn - C(N - n)n_f, \tag{3}$$

$$dn_f/dt = dm/dt - dn/dt, \tag{4}$$

where m is the concentration of recombination sites, n is the concentration of holes in traps, N is the concentration of hole traps, and n_f is the concentration of "free" holes in the material.

Equation (2) describes the rate of electron-hole recombination, where A is the rate constant. We assume that $|dm/dt|$ is directly proportional to the phE and EE we observe, with the branching ratio between phE and EE as one of the model parameters. Equation (3) represents the thermal activation of holes from the hole traps (first term) and refilling of retrapping (second term). Equation (4) provides for the conservation of holes.

Numerical methods similar to those developed by Shenker and Chen[57] were used to integrate these equations and produce predicted phE and EE decay curves for various values of the rate constants and initial conditions. A curve fitting algorithm based on the simplex method[58] was then used to find the rate constants and initial conditions which minimized the residual sum of squares between the predicted curves and the experimentally observed decays. The "best fit" curve for the typical clear MgO decay shown in Fig. 1 is presented in Fig. 9, and the results of a similar analysis of the high EE case of Fig. 4 is presented in Fig. 10.

The agreement between the predicted and experimental curves suggests that a simple trap model can describe the overall behavior of the observed decay. The data of the high EE event show evidence of detector saturation during the first 10-30 ms of the decay. This may account for the excess of the predicted value over the experimental points in this region of Fig. 10. The agreement between the rate constants computed from the two sets of data is better when the first few data points from the high EE set are omitted from the calculations. Under these conditions, the computed thermal activation rate constants (B in Equation (3)) for the two data sets agree to within about 20%. Assuming a pre-exponential factor of 10^{10}, the computed rate constant of 8×10^{5} predicts an activation energy of about 0.2 eV. This is consistent with the values determined by Yanagisawa and Huzimura, given the uncertainty in the pre-exponential factor. Fracture at various temperatures, which we are now equipped to do, will allow a more accurate experimental determination of the activation energies involved in the fracto-emission.

In both the typical and high EE decays, the parameters determined by the curved fitting program were consistent with nearly second order decay. In this context, second order decay is one governed by a rate equation of the form

$$-dm/dt = Dm^2. \qquad (5)$$

Equation (2) reduces to this form when $n >> n_f$, $m=n$, $Am >> C(N-n)$, and $N >> n$.[59] Thus second order decay results when the number of trapped electrons and holes are equal, the number of traps is much greater than the number of trapped charge carriers, and the process of retrapping is much more probable than the process of recombination. Yanagisawa and Huzimura observed second order phosphorescence decays from some of their MgO powders.[48] This is further evidence that the processes involved in their work are similar to those in ours.

If two thermally activated processes are contributing to the free hole concentration, as in the work of Yanagisawa and Huzimura, then our model is somewhat oversimplified. However, the thermally activated processes they observed may well be hole release from surface V^- and V^- (OH) centers. Then the low OH^- concentration in our clear MgO would explain why only one thermally activated process is needed to explain our results.

Other models have been proposed to describe phosphorescence decay in other systems. Electron-hole tunneling coupled with hopping transport have been invoked to describe luminescence decay from phosphors.[60] Williams et al. have used a such a model to describe the rapid decay of a 4.9 eV luminescence induced in electron bombarded MgO.[61] Their model has the advantage of having few adjustable parameters. However, only the first 100 us of the observed decay at room temperature was described by the model, presumably due to interference from a 3.2 eV luminescence peak. In our own case, the existence of suitable surface states in sufficient numbers for the required hopping transport is in doubt.

Still other mathematical descriptions of phosphorescence decay may also be found to describe fracto-emission decay. Ferreira and Carrano de Almeida have demonstrated the existence of a correspondence between hopping transport models and trap models.[62]

Continuous time random walk models have been shown to describe fracto-emission from some polymers quite well, for instance. The choice between corresponding models must often be made on the basis of simplicity and physical plausibility. The simple trap model represented by Equations (2)-(4) has the advantage of being readily interpeted in terms of well understood surface processes.

D. Cloudy/Clear Differences.

The cloudiness of some high purity MgO crystals has been attributed to the presence of voids filled with H_2 gas at high pressure.[15,63] In a recent study of neutral emission accompanying the fracture of MgO, we observed measurable but small H_2 emission accompanying fracture .[3] This suggests that our cloudy MgO contained little H_2 at the time of fracture, or that the fracture surface did not intersect many voids, or both. However, a significant amount of O_2 was observed from cloudy MgO.[3] As the crack forms, this gas would be bombarding the fracture surfaces at a very high frequency due to the small volume in the narrow opening of the crack.

As noted above, oxygen quenches phosphorescence in MgO powders. This includes the short lived exciton decay and the long lived recombination of trapped electrons and holes. It seems likely that the fast phE and EE decay of the cloudy crystals relative to that from the clear crystals is due to the chemisorption of oxygen at surface F^+ and P^- centers. This process may be diffusion limited, as Yanagisawa and Huzimura found in their study of oxygen adsorption on MgO powders.[48] The relative phE peak heights of clear and cloudy MgO seem to be fairly well accounted for by their relative fracture strengths. If so, the collisional quenching of excitons does not seem to be important on this time scale.

Oxygen may also be involved in the quenching observed by MacLean and Duley in the photoexcitation spectra of MgO powders derived from the decomposition of $Mg(OH)_2$. They observed differences between the photoexcitation spectra of MgO powders formed from $MgCO_3$

and $Mg(OH)_2$. The emission from the ex-hydride appears to be quenched in the region of 220 nm, relative to the emission from the ex-carbonate. The difference between the two spectra was taken to be an indication of the degree of this quenching. The difference curve was similar in form to the absorption spectra of deformed single crystal MgO.[25] The absorption spectrum of surface F^+ centers is expected peak at the same energy as those in the bulk, that is, about 230 nm. Cloudy portions of melt grown MgO have been shown to be associated with hydroxyl impurities, presumably due to traces of $Mg(OH)_2$ and water associated with the starting material.[15] If MgO ex-hydride is associated with an excess of oxygen, this oxygen could quench emission from surface F-type centers. The same result would obtain if the formation of surface F-type centers were hindered in the thermal decomposition of $Mg(OH)_2$. Since excitonic transitions at nondefective sites are responsible for the greater part of the luminescence of MgO powders, the effect of quenching the luminescence at surface defect centers should be similar to the quenching observed by MacLean and Duley.

E. High EE Crystals.

As noted above, the high EE observed from certain MgO samples may be due to improved detection geometry. Although this effect is expected during crack growth, it is not so likely some milliseconds later, when the macroscopic movement of the fractured pieces should dominate over small differences in crack geometry. Another possibility is that we are seeing the effects of different kinds or degrees of surface damage. This damage may be the result of greater bending stresses, as in the case of the unusually strong high EE crystal, or greater shear stresses, as in the case of the crystal breaking off center. The off center break resulted in a far higher EE/phE ratio than normal. The extra shear stresses involved in an off-center break may affect the nature of the resulting surface damage. As noted above, Namba and Murata observed significantly different secondary electron spectra from defective and normal MgO(100) surfaces.[55] If the dark, mirror-like areas observed on the fracture surfaces are the source of

EE, this damage must be on a submicron scale. As is evident in Fig. 8, features larger than a micron are readily resolved by the SEM. The fracture steps revealed in these photographs are loci of surface damage that may be involved in damage related EE.

F. Positive Ion Emission

The signal we observe with a negatively biased Channeltron detector cannot yet be unambiguously attributed to positive ions from the fracture surface. Time of flight measurements have been used to verify the emission of positive ions from the fracture of filled elastomers and glass fibers.[64,65] In the case of a number of polymeric materials (filled and unfilled), the PIE and EE showed similar decays,[66] which is not the case in the present work. Recent observations by Klyuev et al. suggest that electrons produced during interfacial failure and fracture may have energies of tens of keV.[67] Many of these electrons would be sufficiently energetic to overcome the negative potential on the Channeltron. The resolution of this ambiguity awaits further experiment.

However, the possibility of high energy electron bombardment also suggests a mechanism for ion desorption. Desorption of O^+ ions under energetic electron bombardment has been observed in several oxides. Recently, photon stimulated desorption of O^+ ions has been observed in MgO.[68] This desorption is attributed to the Auger emission of three oxygen electrons during the decay of an excited oxygen core state. Oxygen K-level excitations require about 530 eV, well below the effective 10 keV x-ray cutoff noted by Klyuev et al., and below the -2700 bias on the front end of our channeltron. A less demanding mechanism involving an Mg core excitation has been proposed by Knotek and Feibelman.[69] They predict O^+ emission at a threshold of about 52 eV. The large band gap of MgO is expected to hinder neutralization, so that little neutral O emission is expected. The latter prediction is consistent with the paucity of O observed upon the fracture of clear MgO.[5,6]

The source of ions need not be atoms located in the lattice. The emission of neutral Mg, O, O_2, H_2O, and other species have been reported from the fracture of MgO in three point bend.[5,6] Some of these molecular species are believed to have formed on the surface as a result of chemical reactions. While adsorbed on the surface, electron bombardment could yield ion emission, again via an ESD process. However, because one would expect higher coverages of adsorbed molecules on the cloudy MgO fracture surface, then one would expect the PIE from cloudy MgO to be more intense than from the clear, which is not the case. Either of these situations require electron bombardment of the fracture surface to produce free ions. The energy distribution and time dependence of the electrons involved are not known with any certainly, although a high energy bombardment should be rather short lived. If unambiguous PIE can be established, it would serve as a probe of the fracture induced electron bombardment process.

G. Fast Time Scale Data Results

Although in these experiments no attempt was made to ascertain the precise time of fracture, we seem to be able to observe the rise in phE accompanying the catastrophic crack growth at failure. Experiments are in the planning stage to relate the various stages of failure to the rise in phE.

Coluccia et al. have estimated the luminescence lifetimes of phE from UV stimulated MgO, assuming that the observed decay was a sum of first order processes.[21] At an excitation energy of 4.52 eV, the lifetimes of the observed processes were 1, 7, and 25 us, respectively. Their apparatus was not sensitive to decays lasting much longer than 100 us. Although we have not performed a similar analysis on any of our fast time scale data, the phE decay presented in Fig. 6c is consistent with lifetimes on the order of 3-50 us. The degree of agreement encouraging, given that the fracture event itself may last a few us.

The luminescence spectra observed by Coluccia et al. are well explained by the decay of surface excitons. Although these spectra were taken under continuous irradiation, it is likely that the earliest decay processes are also dominated by exciton decay. As noted above, we expect bulk exciton decay and other processes to contribute to the emission on this time scale. However, it seems likely that surface exciton decay is a major, if not dominant, factor.

On the somewhat longer time scales of Fig. 6a and 6b, the decay becomes nearly first order, with time constants on the order of 1-3 ms. On sufficiently short time scales, phE due to electron-hole recombination via extended states is expected to yield nearly first order behavior. This suggests that we can hope to explain the bulk of the emission we see in terms of two relatively straightforward processes, exciton decay and the recombination of trapped electrons and holes.

V. CONCLUSIONS

We have measured phE and EE due to the deformation and fracture of single crystal MgO in three point bend. phE is observed before fracture, and is attributed to the creation and excitation of defects by moving dislocations. Spectroscopic analysis of this phE may determine the processes involved with more certainty. The peak phE emission at fracture was found to correlate fairly well with the flexure moduli of the fractured crystals. This suggests that the mechanical energy of deformation is being transferred in a reproducible manner. Finally, the long decay in phE and EE suggests that these emissions are due to the recombination of electrons and holes trapped at surface defects.

The dramatic differences in the emission decays from the clear and the cloudy crystals suggests that some chemical species is quenching the emissions from the cloudy crystals. Gaseous oxygen is known to quench the phosphorescence in MgO powders, and recent measurements of neutral emission from the fracture of cloudy MgO indicate that oxygen is available to the surface. Knowledge of cationic impurity concentrations alone is apparently inadequate to characterize MgO crystals for fracto-emission studies.

Several extensions of the present work are being planned in order to further clarify the processes involved in fracto-emission and to enhance the utility of fracto-emission in fracture studies. First, we plan to investigate the correlation between the growth and decay of phE and EE with the position of the crack front as it moves through the crystals. We also hope to make measurements of fracto-emission as a function of temperature. Finally, we hope to extend the range of our fracto-emission observations to crystals displaying higher strength and plasticity.

We believe that fracto-emission is a promising tool for the study of the processes accompanying fracture on the atomic scale. The emission decay provides important clues as to the identity and electronic state of fracture produced surface defects. It is also likely that the pre-fracture emission can provide information about the movement and interaction of dislocations, which are important parameters in the process of deformation and fracture. We are beginning to elucidate the connections between fracto-emission and the the atomic processes accompanying deformation and fracture.

VI. ACKNOWLEDGMENTS

This work was supported by the Ceramics and Electronics Materials Division of the National Science Foundation under Grants DMR 8210406 and DMR 8601281. We wish to thank Dr. Friedemann Freund, currently associated with NASA-Ames Research Center, for useful discussions. One of us (SCL) wishes to thank the American Vacuum Society for a Graduate Student Award which aided this research.

VII. REFERENCES

1. G. P. Williams, Jr. and T. J. Turner, Solid State Commun. 29 [3], 201-203 (1979).
2. J. T. Dickinson, L. C. Jensen, and A. Jahan-Latibari, J. Vac. Sci. Technol. A 2 [2], 1112-1116 (1984).
3. J. T. Dickinson, L. C. Jensen, and W. D. Williams, J. Am. Ceram. Soc. 68 [5], 235-240 (1985).
4. L. A. K'Singam, J. T. Dickinson, and L. C. Jensen, J. Am. Ceram. Soc. 68 [9], 510-514 (1985).
5. J. T. Dickinson, L. C. Jensen, and M. R. McKay, J. Vac. Sci. Technol. A 4 [3], 1648-1652 (1986).
6. J. T. Dickinson, M. R. McKay, and L. C. Jensen, J. Vac. Sci. Technol. A 5, July/August 1987, in press.
7. F. J. P. Clarke and R. A. J. Sambell, Philos. Mag., Series 8, 5 [55] 697-708 (1960).
8. H. G. Tattersall and F. J. P. Clarke, Philos. Mag., Series 8, 7 [84] 1977-1994 (1962).
9. R. J. Stokes, Trans. Metallurgical Soc. AIME, 224 [6] 1227-1237 (1962).
10. A. A. Bruneau and P. L. Pratt, Philos. Mag., Series 8, 7 [83] 1871-1885 (1962).
11. J. J. Mecholsky and S. W. Freiman, in **Fracture Mechanics Applied to Brittle Materials**, edited by S. W. Freiman (American Society for Testing and Materials, Philadelphia, PA, 1979), pp.136-150.
12. J. J. Gilman, Trans. Metallurgical Soc. AIME 212, 310-315 (1958).
13. G. D. Miles and F. J. P. Clarke, Philos. Mag., Series 8, 6 [72], 1449-1462 (1961).
14. A. Briggs, J. Materials Sci. 12 [3], 637-640 (1977).
15. A. Briggs, J. Materials Sci. 10 [5], 729-736 (1975).
16. R. Melton, N. Danieley, and T. J. Turner, Phys. Status Solidi A 57 [2], 755-764 (1980).
17. A. Remon and J. Piqueras, Solid State Comm. 50 [11], 983-985 (1984).
18. Y. Chen, M. M. Abraham, T. J. Turner, and C. M. Nelson, Philos. Mag. Series 8, 32 [1], 99-112 (1975).
19. Y. Chen, M. M. Abraham, L. C. Templeton, and E. Sonder, Solid State Comm. 18 [1], 61-65 (1976).
20. A. Remon and J. Piqueras, Cryst. Res. Technol. 20 [4], 582-584 (1985).
21. S. Coluccia, A. M. Deane, and A. J. Tench, J. Chem. Soc. Faraday Trans. I 74 [12], 2913-2922 (1978).
22. A. Zecchina, M. G. Lofthouse, and F. S. Stone, J. Chem. Soc. Faraday Trans. I 71 [7], 1476-1490 (1975).
23. S. Coluccia, A. J. Tench, and R. L. Segall, J. Chem. Soc. Faraday Trans. I 75 [7], 1769-1779 (1979).
24. E. Garrone, A. Zecchina, and F. S. Stone, Philos. Mag. B 42 [5], 683-703 (1980).
25. S. G. MacLean and W. W. Duley, J. Phys. Chem. Solids 45 [3], 227-235 (1984).
26. C. Ballesteros, J. Piqueras, J. Llopis, and R. Gonzalez, Phys. Status Solidi A 83 [2], 645-649 (1984).
27. R. Gonzalez, J. Llopis, and C. Ballesteros, Philos. Mag. B 50 [5], 599-606 (1984).
28. J. Llopis, J. Piqueras, and L. Bru, J. Materials Sci. 13 [6], 1361-1364 (1978).
29. J. Llopis and J. Piqueras, Phys. Status Solidi A 49 [1], K9-K12 (1978).
30. J. Llopis, J. Piqueras, and C. Ballesteros, Phys. Status Solidi A 70 [2], 739-746 (1982).
31. J. Llopis, C. Ballesteros, J. Piqueras, A. Remon, and R. Gonzalez, Phys. Status Solidi A 78 [2], 679-684 (1983).
32. M. A. Orchando and J. Llopis, J. Appl. Phys. 58 [8], 3174-3179 (1985).
33. E. Macho, J. Llopis, A. Remon, C. Ballesteros, and J. Piqueras, Phys. Status Solidi A 82 [1], 111-117 (1984).
34. K. L. Kliewer and J. S. Koehler, Phys. Rev. 140 [4A], 1226-1240 (1965).

35. Kurt Lehovec, J. Chem. Phys. 21 [7], 1123-1128 (1953).
36. S. I. Bredikhin and S. Z. Shmurak, Sov. Phys. JETP 49 [3], 520-525 (1979).
37. A. V. Poletaev and S. Z. Shmurak, Sov. Phys. Solid State 26 [12], 2147-2152 (1984).
38. M. I. Molotskii, Sov. Phys. Solid State 25 [1], 67-69 (1983).
39. R. J. Stokes, T. L. Johnston, and C. H. Li, Trans. Metallurgical Soc. AIME 215, 437-444 (1959).
40. A. V. Poletaev and S. Z. Shmurak, Sov. Phys. JETP 60 [2], 376-379 (1984).
41. E. Linke, J. Wollbrandt, and U. Bruckner, Radiation Protection Dosimetry 4 [3-4], 194-196 (1983).
42. J. Wollbrandt, U. Bruckner, and E. Linke, Phys. Status Solidi A 77, 545 (1983).
43. F. J. P. Clarke, R. A J. Sambell, and H. G. Tattersall, Philos. Mag., Series 8, 7 [75], 393-413 (1962).
44. J. T. Dickinson and L. C. Jensen, J. Polym. Sci., Polym. Phys. Ed. 23 [5], 873-888 (1985).
45. P. J. Miller, C. S. Coffey, and V. F. DeVost, J. Appl. Phys. 59 [3], 913-916 (1986).
46. Y. Yanagisawa and R. Huzimura, J. Phys. Soc. Jpn. 53 [1], 66-69 (1984).
47. V. E. Henrich, G. Dresselhaus, and H. J. Zeiger, Phys. Rev. B 22 [10], 4764-4775 (1980).
48. Y. Yanagisawa and R. Huzimura, J. Phys. Soc. Jpn. 50 [1], 209-216 (1981).
49. B. Henderson and J. E. Wertz, **Defects in the Alkaline Earth Oxides**, (Taylor and Francis, London, 1977), p. 137.
50. W. C. Mackrodt and R. F. Stewart, J. Phys. C 12 [23], 5015-5035 (1979).
51. W. Maenhout-Van der Vorst, Radiation Protection Dosimetry 4 [3-4], 254-256 (1983).
52. Y. Yanagisawa and R. Huzimura, Radiation Protection Dosimetry 4 [3-4] 260-262 (1983).
53. P. R. Underhill and T. E. Gallon, Solid State Commun. 43 [1], 9-11 (1982).
54. J. W. He and P. J. Moller, Chem. Phys. Lett. 129 [1], 13-16 (1986).
55. H. Namba and Y. Murata, J. Phys. Soc. Jpn. 53 [5], 1888-1898 (1984).
56. A. Halperin and A. A. Braner, Phys. Rev. 117 [2], 408-415 (1960).
57. D. Shenker and R. Chen, J. Comput. Phys. 10, 272-283 (1982).
58. M. S. Caceci and W. P. Cacheris, Byte Magazine 9 [5], 340-362 (1984).
59. R. Chen and Y. Kirsh, **Analysis of Thermally Stimulated Processes**, (Pergamon Press, London, 1981), p. 32.
60. D. G. Thomas, J. J. Hopfield, and W. M. Augustyniak, Phys. Rev. 140 [1A], 202-220 (1965).
61. R. T. Williams, J. W. Williams, T. J. Turner, and K. H. Lee, Phys. Rev. B 20 [4], 1687-1699 (1979).
62. G. F. Leal Ferreira and L. E. Carrano de Almeida, Phys. Rev. B 19 [12], 6601-6603 (1979).
63. B. Henderson and J. E. Wertz, **Defects in the Alkaline Earth Oxides**, (Taylor and Francis, London, 1977), pp. 131-133.
64. J. T. Dickinson, L. C. Jensen, and M. K. Park, J. Materials Sci. 17, 3173-3178 (1982).
65. J. T. Dickinson, L. C. Jensen, and M. K. Park, Appl. Phys. Lett. 41 [9], 827-829 (1982).
66. J. T. Dickinson, L. C. Jensen, and M. K. Park, Appl. Phys. Lett. 41 [5], 443-445 (1982).
67. V. A. Klyuev, A. G. Lipson, Yu. P. Toporov, A. D. Aliev, and A. E. Chalykh, Sov. Tech. Phys. Lett. 10 [9], 480-482 (1984).
68. R. L. Kurtz and R. Stockbauer, private communication.
69. M. L. Knotek and P. J. Feibelman, Surface Sci. 90 [1], 78-90 (1979).

FIGURE CAPTIONS

Fig. 1. phE, EE, and load during deformation and after fracture of a typical, clear MgO crystal. The sampling time is 10 ms per channel. The phE and EE data show simultaneous peaks about 0.5 s after fracture due to electrical noise generated when the electric motor loading the sample was shut off.

Fig. 2. Plot of phE peak height vs. flexure strength. The line is a least squares fit to the experimental points. Events in which fracture occurred off center are not shown, but generally fall well above the line.

Fig. 3. A comparison of phE and EE from clear and cloudy MgO. The sampling time is 1 ms per channel.

Fig. 4. phE, EE, and load for a crystal of clear MgO displaying particularly strong EE. The fracture occurred somewhat off center.

Fig. 5. Typical PIE and EE decays from clear and cloudy MgO. The triangles represent PIE counts and the dots EE counts. The PIE and EE curves have been normalized at their peaks to facilitate comparison of the decays. The arrow indicates the time of fracture. The PIE and EE data were collected during and after separate fracture events.

Fig. 6. phE from clear MgO, showing the phE decay on three successively faster time scales: a) 25 us/channel; b) 1 us/channel; c) 50 ns/channel. The data were taken during three separate fracture events.

Fig. 7. Composite photographs of the fracture surfaces of two clear MgO crystals. Crystal (a) yielded the typical emissions of Fig. 1 and crystal (b) yielded the high EE emission of Fig. 4. During loading, the upper portion of each crystal was in tension and the lower portion was in compression. The arrow in (a) shows where the progress of crack growth along the tensile side of the crystal was impeded.

Fig. 8. SEM photographs of clear (a) and cloudy (b) MgO fracture surfaces. Both photographs were taken in macroscopically smooth areas of the fracture surface.

Fig. 9. The typical emission decay of Fig. 1 and the decay curve predicted by Equations (2)-(4) with a "best fit" choice of parameters. Only a representative selection of data points is shown.

Fig. 10. The high EE emission decay of Fig. 4 and the decay curve predicted by Equations (2)-(4) with a "best fit" choice of parameters. Only a representative selection of data points is shown.

EMISSION FROM CLEAR MgO - TYPICAL

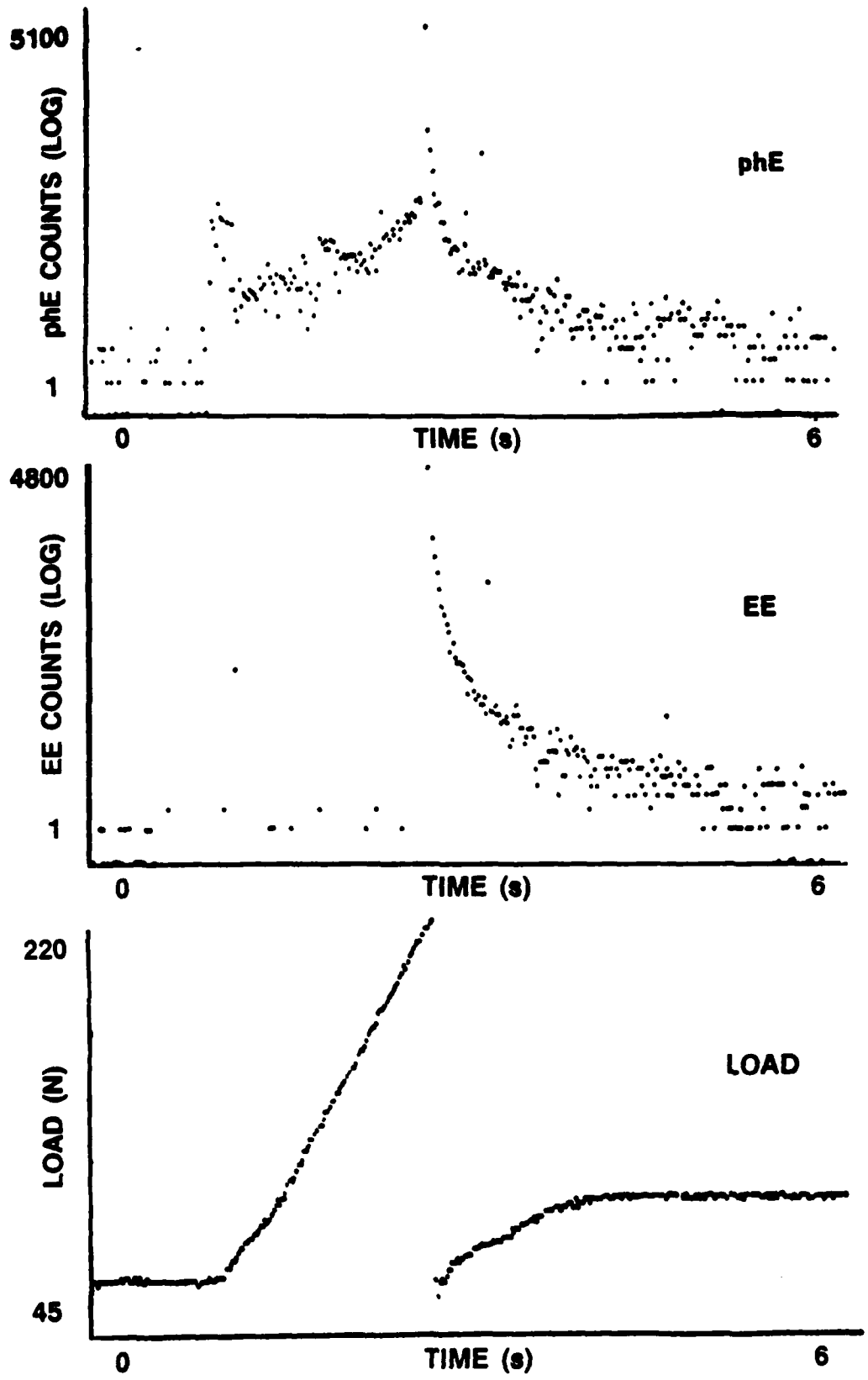

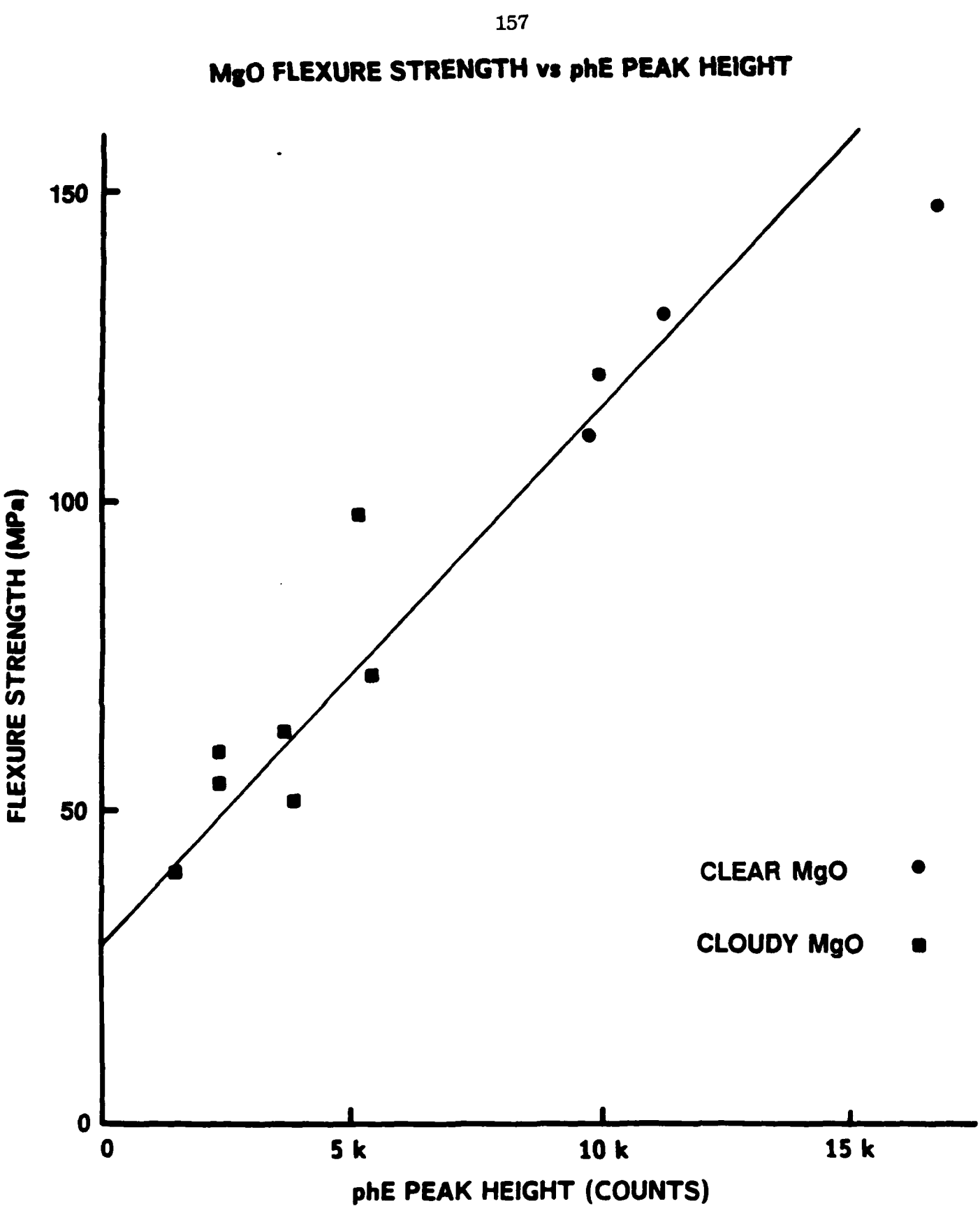
MgO FLEXURE STRENGTH vs phE PEAK HEIGHT
150
100
50
0
FLEXURE STRENGTH (MPa)
0
5 k
10 k
15 k
phE PEAK HEIGHT (COUNTS)
CLEAR MgO
CLOUDY MgO

2

COMPARISON OF CLEAR AND CLOUDY MgO - phE

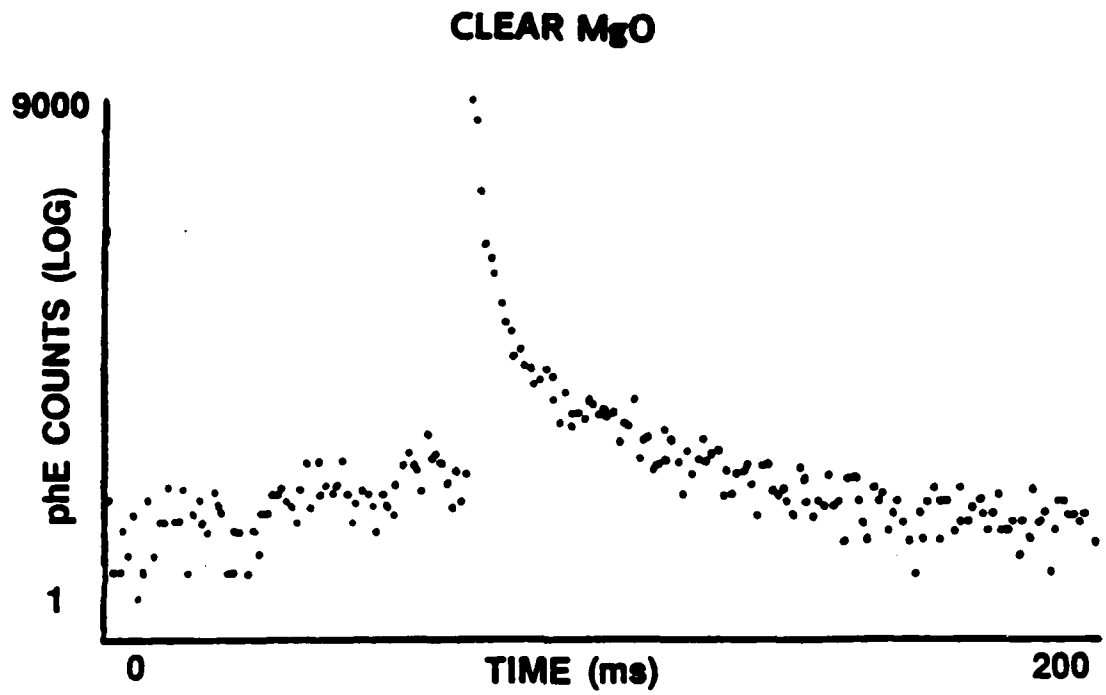

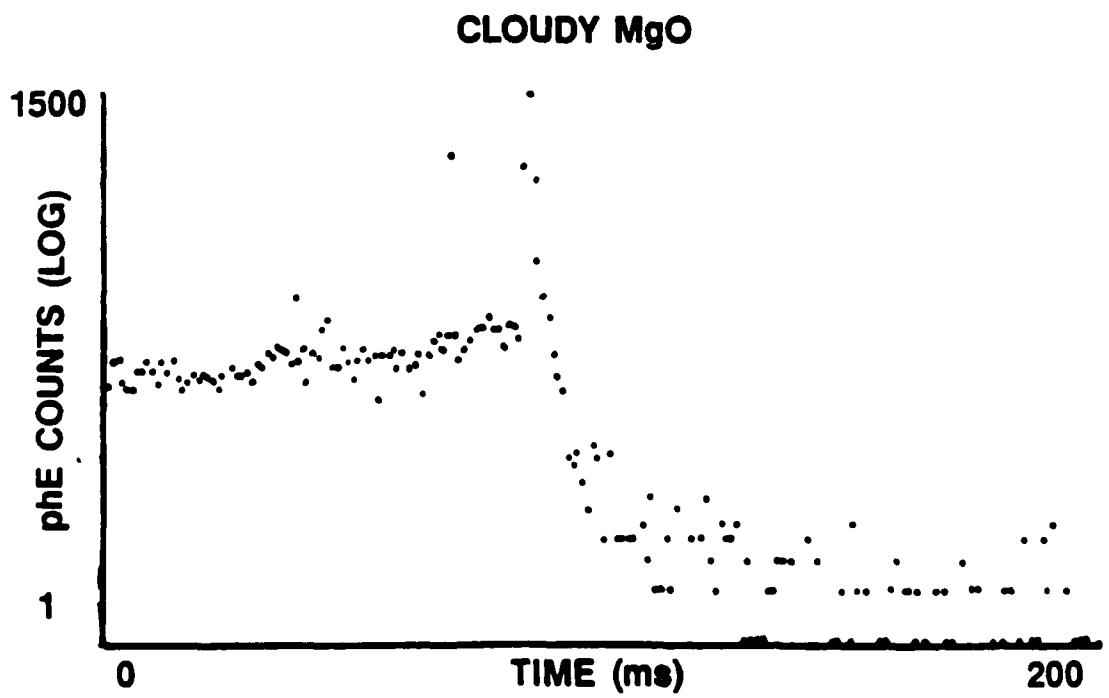

3 left

COMPARISON OF CLEAR AND CLOUDY MgO - EE

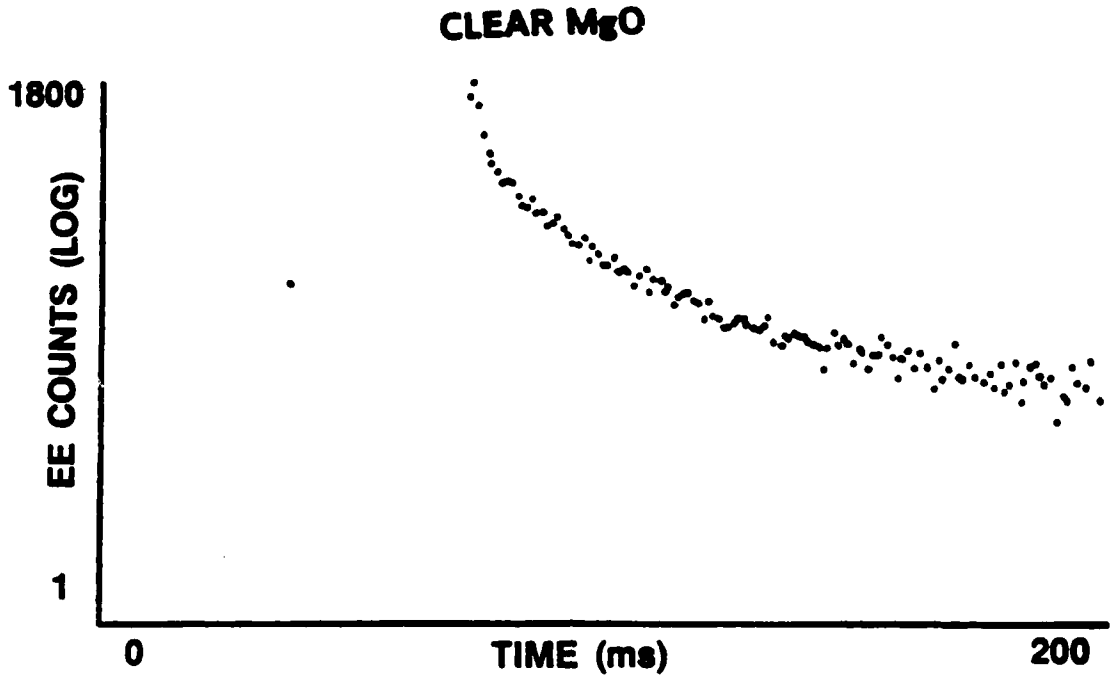

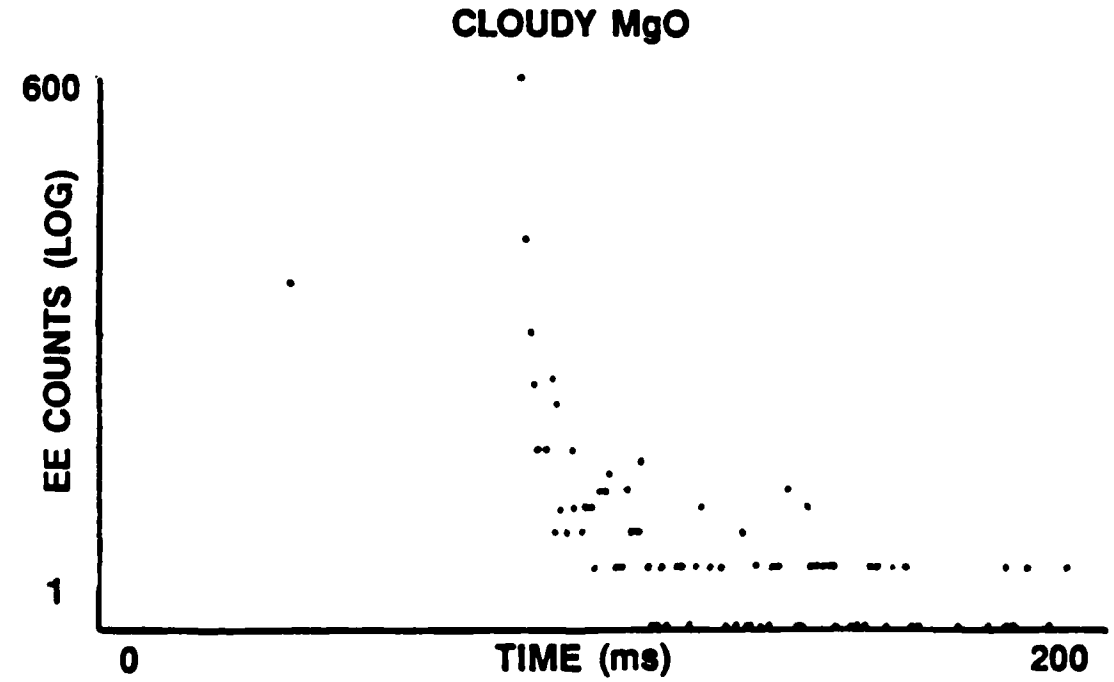

3 right

EMISSION FROM CLEAR MgO - HIGH EE CASE

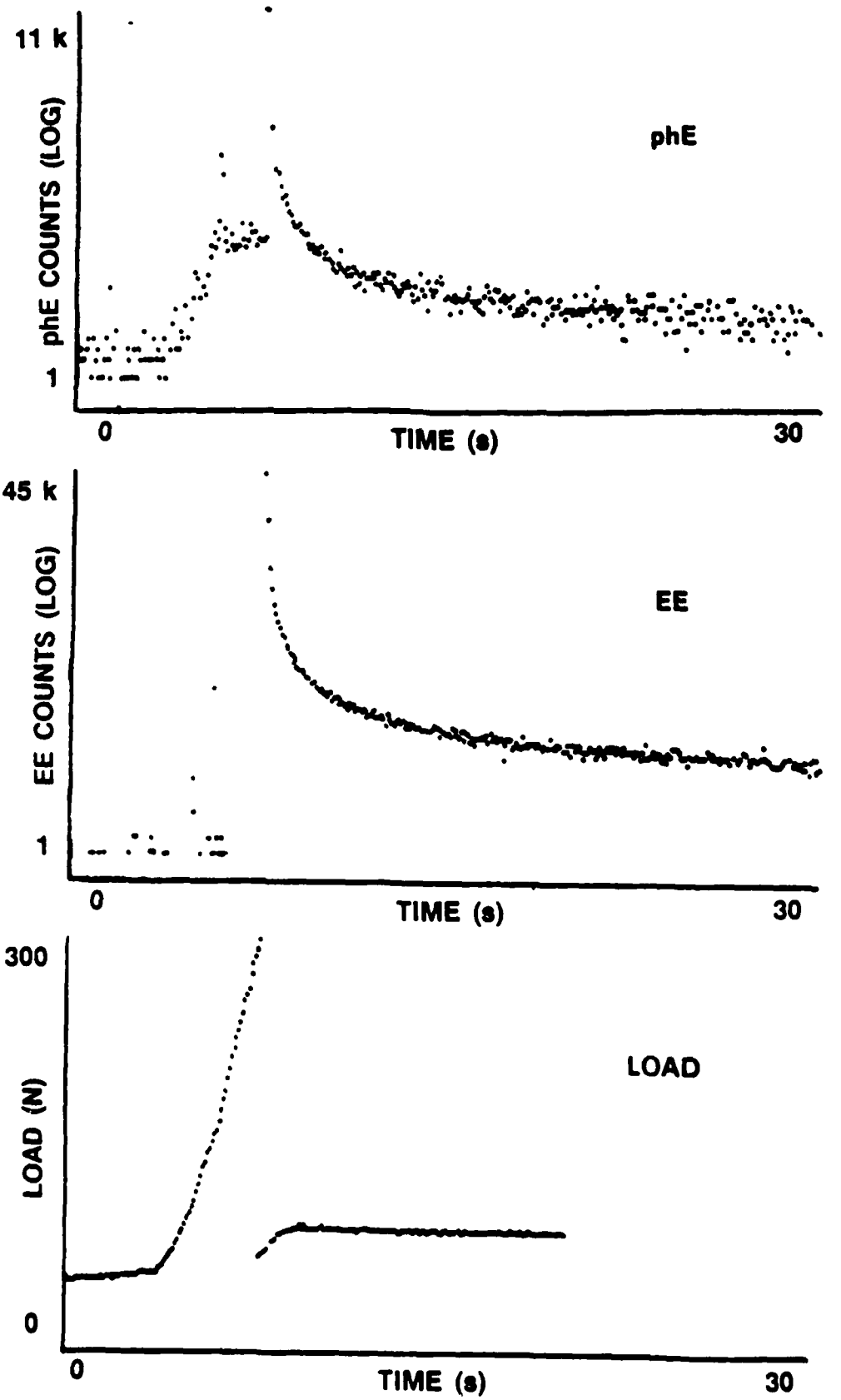

phE FROM CLEAR MgO - FAST TIME SCALES

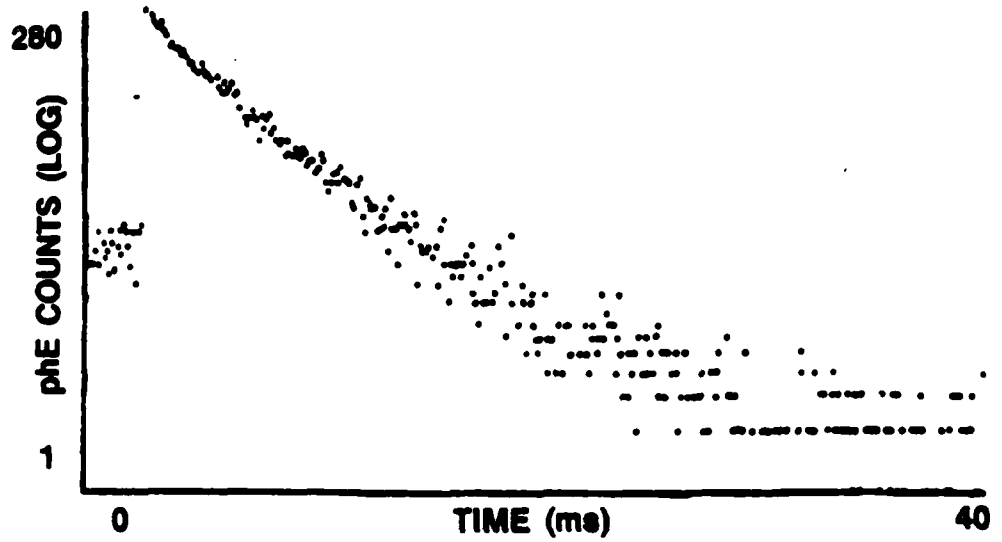

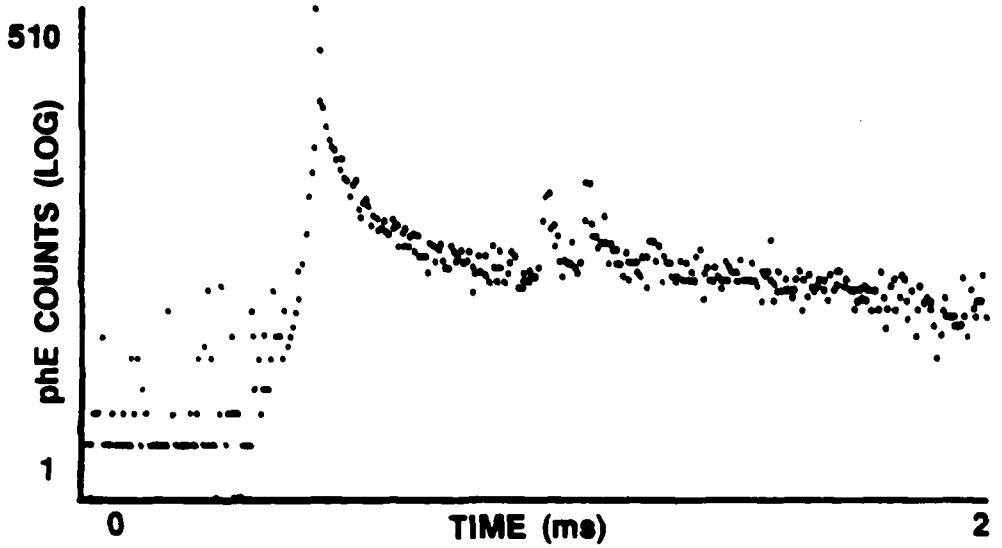

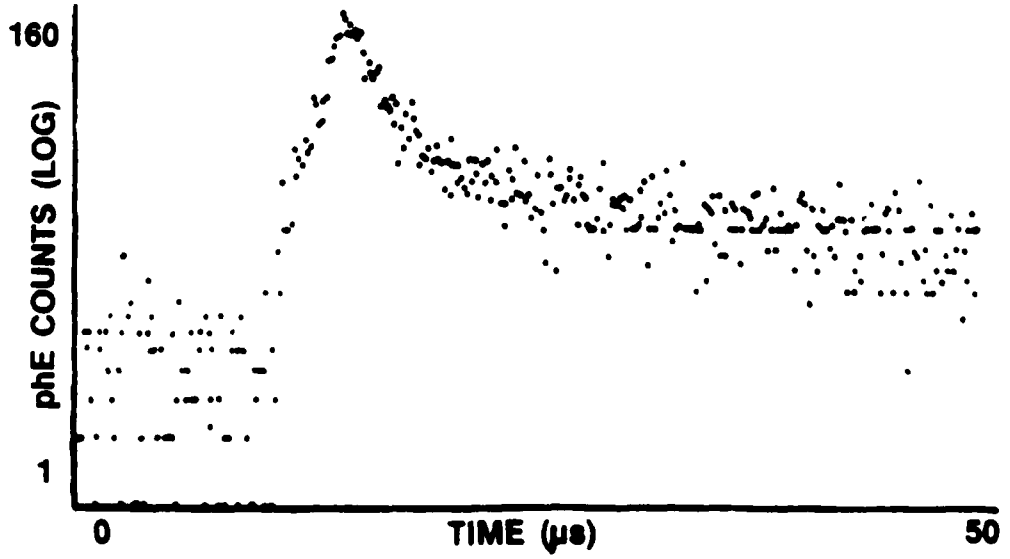

TYPICAL PIE AND EE DECAYS FROM CLEAR AND CLOUDY MgO

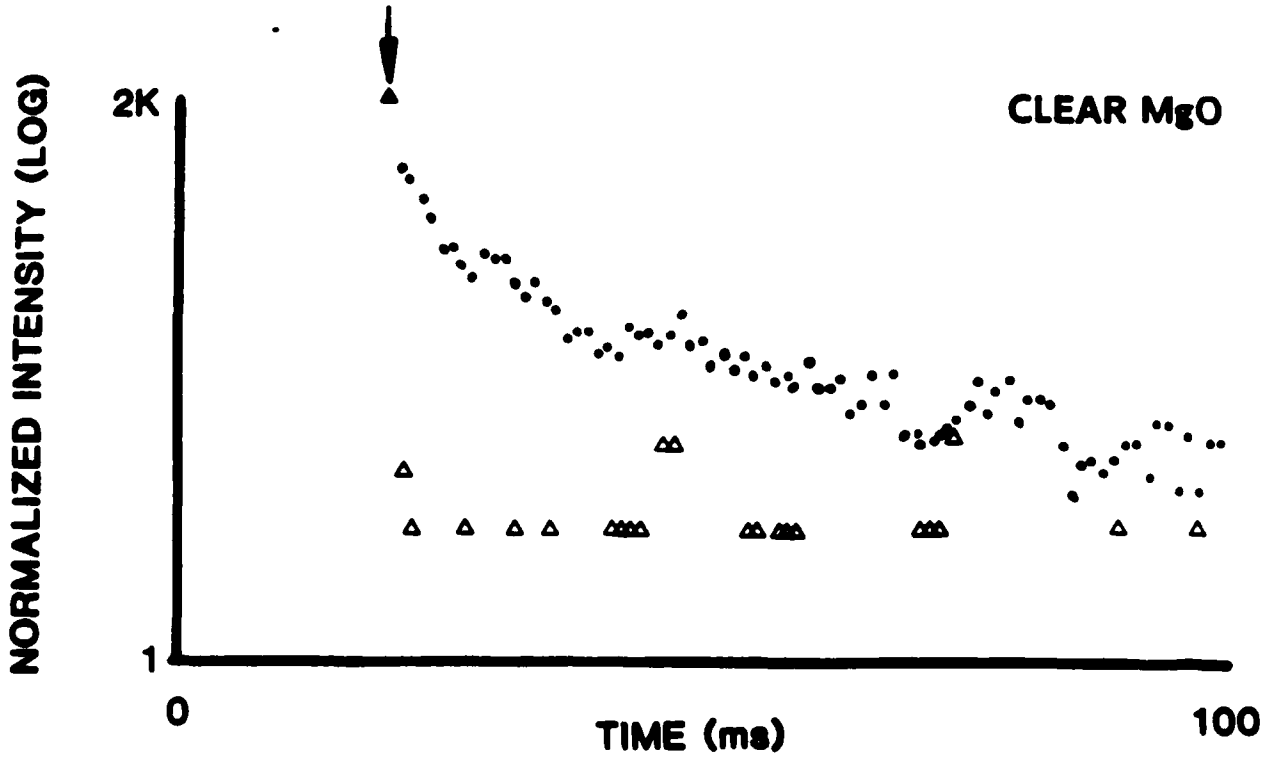

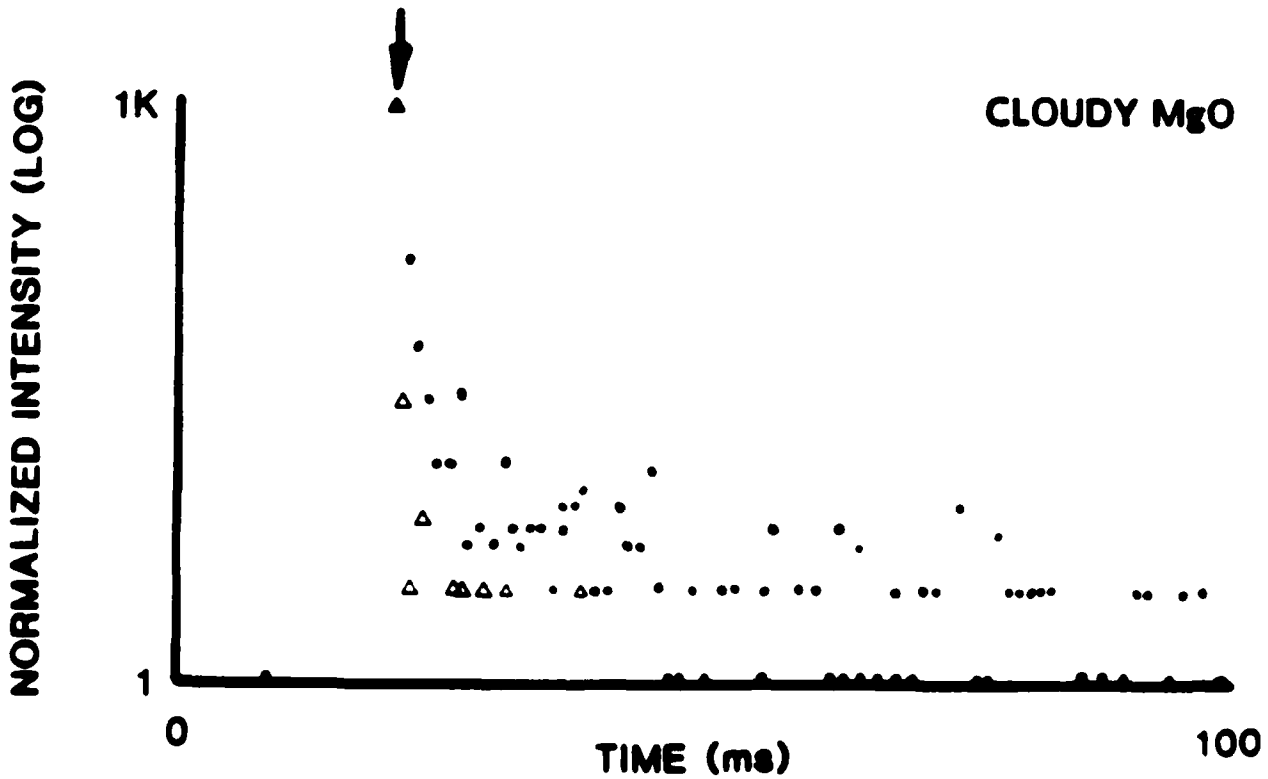

PHOTOGRAPHS OF TYPICAL AND HIGH EE FRACTURE SURFACES

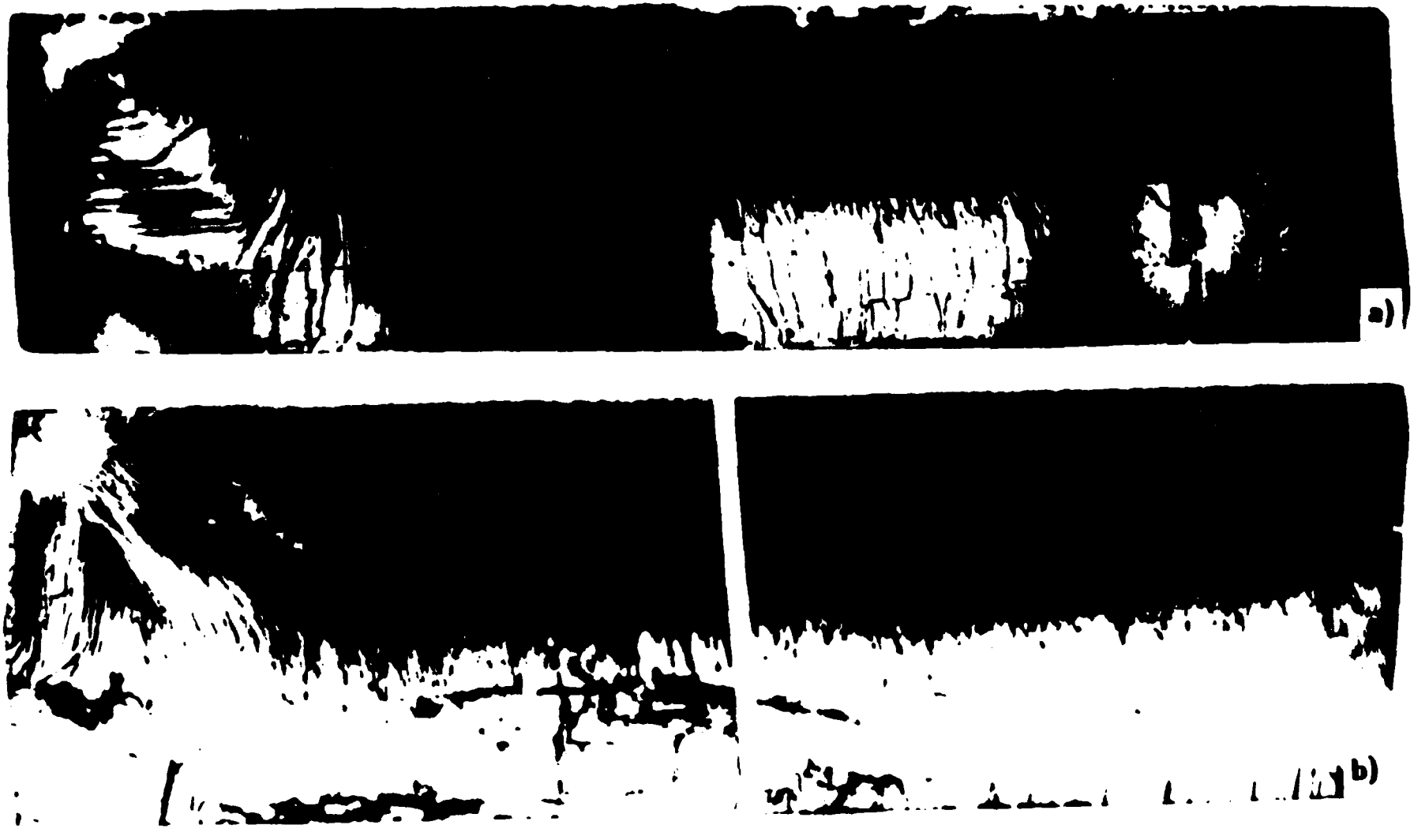

SEM PHOTOGRAPHS OF FRACTURE SURFACES

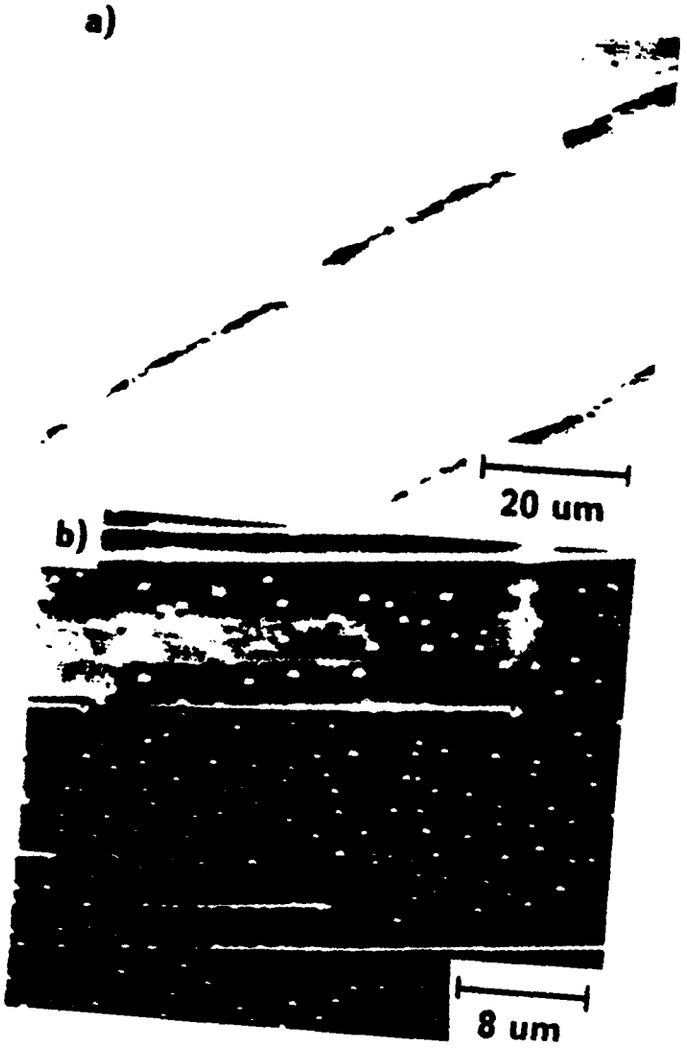

CURVE FIT TO EMISSION DECAY-- TYPICAL CLEAR MgO

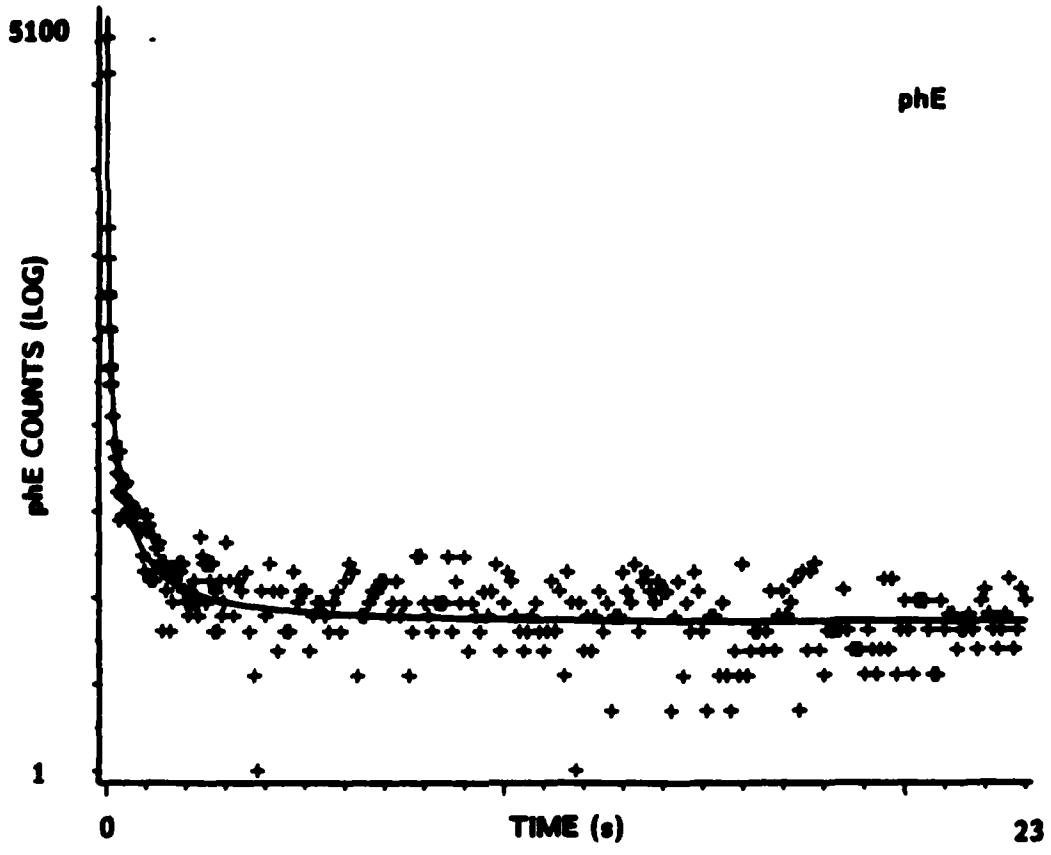

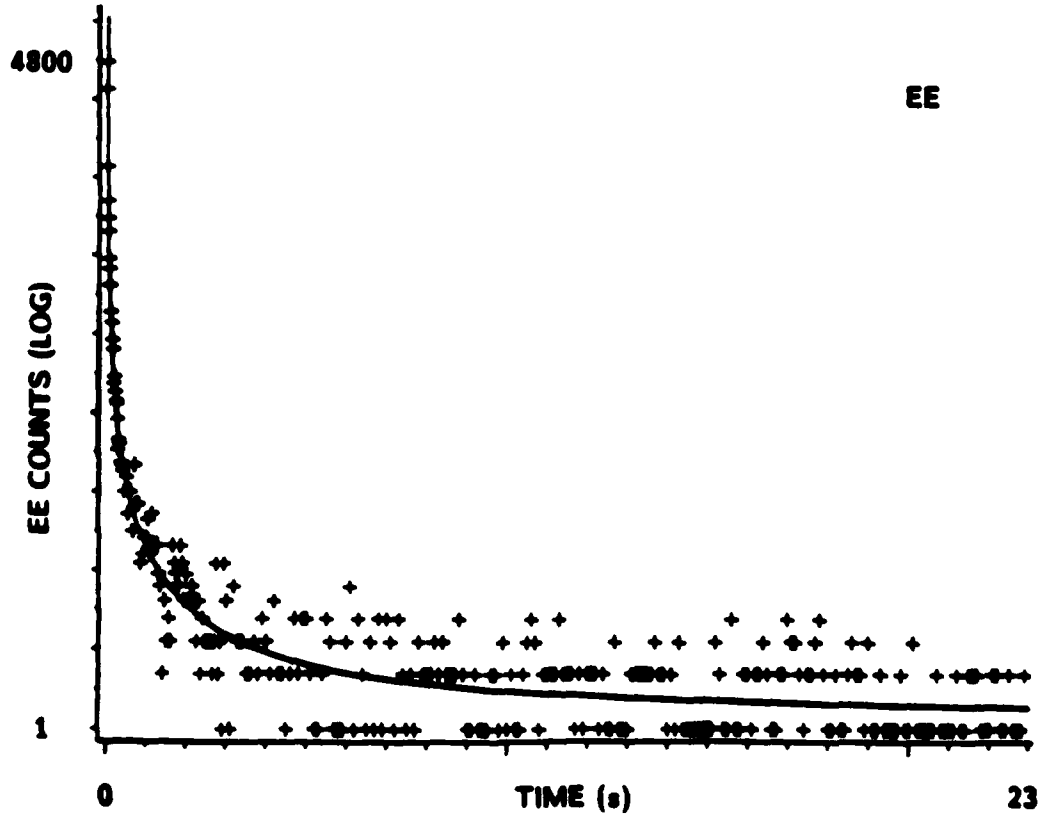

CURVE FIT TO EMISSION DECAY-- HIGH EE CASE

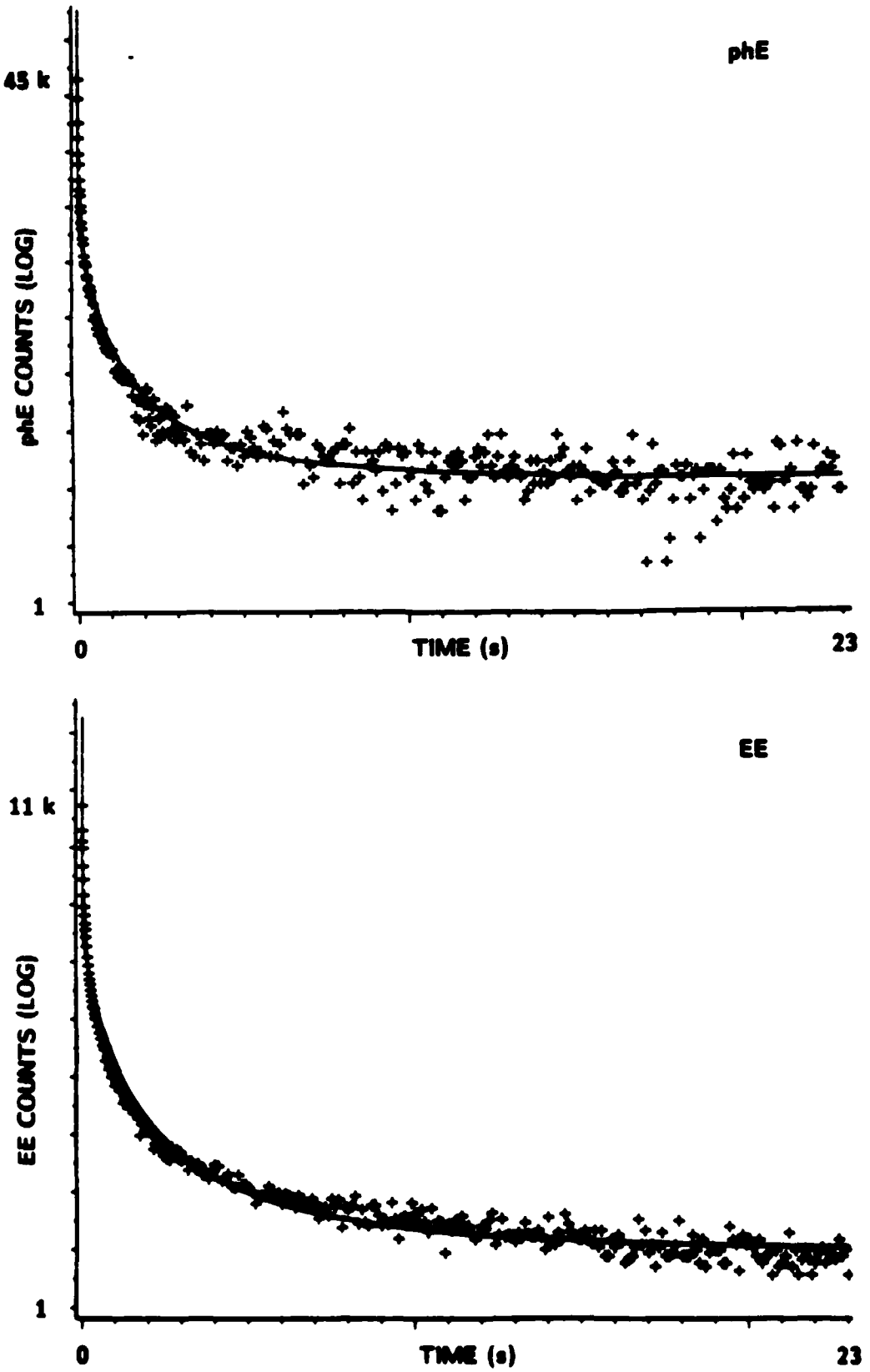

APPENDIX II.

RECENT PRESENTATIONS AND PUBLICATIONS

INVITED TALKS:

"Fracto-Emission from Inorganic Solids," Department of Materials Science, Penn State, April, 1985.

"Atomistics of Fracture," Johnson Space Center, Houston, TX, June, 1985.

Atomistics of Fracture," ONR Workshop on Fracture and Deformation of Polymers, Great Oak Harbor, MD, June, 1985.

"Fracture of Composites and the Emission of Particles," Owens/Corning Technical Center, Gainville, OH, August, 1985.

"Fracto-Emission Accompanying Adhesive Failure," National AIChE Meeting, Seattle, WA, August, 1985.

"Fracto-Emission from Composites," McDonnell Douglas Research Laboratories, St. Louis, MO, September, 1985.

"The Emission of Particles from Fracture of Single Crystals," Army Research & Development Center, Picatinny, NJ, September, 1985.

"The Physics of Fracture," AT&T Bell Labs, Murray Hill, NJ, September, 1985.

"Fracto-Emission from Filled and Unfilled Elastomers," Goodyear Tire Co., Akron, OH, September, 1985.

"Fracto-Emission from Ceramics," Battelle Northwest, Richland WA, October, 1985.

"The Emission of Particles Accompanying the Fracture of Composites," Gordon Conference on Composites, Santa Barbara, CA, January, 1986.

"Chemistry Induced by Fracture in Crystalline Materials," ONR Workshop on Fracture and Deformation, NSWC, January, 1986.

"Electrostatic Effects from the Fracture of Model Rocket Propellents," Redstone Arsenal, Huntsville, AL, January, 1986.

"Physical Phenomena Accompanying Fracture," Department of Materials Science, Michigan State University, April, 1986.

"Fracto-Emission from Polymers," Prague International Conference on Epoxy Resins, Prague, Czechoslovakia, July, 1986.

"Fracto-Emission as a Probe of Energetic Processes Accompanying Fracture," Energetic Material Initiation Fundamentals Workshop, Los Alamos National Labs, October, 1986.

"Fracto-Emission from Crystals, Polymers, and Interfaces," Department of Physics, Texas Tech. University, November, 1986.

"Radiation Induced Crack Initiation and Fracture in Polymers," Department of Electrical Engineering, Texas Tech. University, November, 1986.

"Fracto-Emission from Polymers, Crystals, and Interfaces," International Society for Optical Engineering O-E LASE '87, Los Angeles, January, 1987.

"The Emission of Particles and Light Accompanying the Fracture of Minerals", Geology Dept., WSU, March, 1987.

"Radiation Induced Damage of Optical Coatings", Symposium on Adhesives, Sealants, and Coatings for Space and Harsh Environments, National ACS Meeting, Denver, April, 1987.

"Fracto-Emission Accompanying the Deformation and Failure of Crosslinked Polymers and Interfaces", Symposium on Chemistry, Properties, and Applications of Crosslinking Systems", National ACS Meeting, Denver, April, 1987.

"Bombardment Induced Crack Initiation and Crack Growth in Polymers and Polymer Surfaces", Symposium on Adhesives, Sealants, and Coatings for Space and Harsh Environments, National ACS Meeting, Denver, April, 1987.

"Fracto-Emission from Minerals", U.S. Bureau of Mines, Denver, April, 1987.

"Fracto-Emission from Crystals, Polymers, and Interfaces", Univ. Washington Materials Science Dept., April, 1987.

"Particle Emission Accompanying Fracture", Michigan Technological University, Physics Department, April, 1987.

"Fracto-Emission Studies", ONR Workshop on Dynamic Deformation, Fracture, and Transient Combustion, Great Oak Harbor, MD, May, 1987.

PROFESSIONAL PAPERS:

"Electron Beam Induced Fracture of Glass Fibers," American Ceramics Society, Cincinnati, OH, May 1985.

"Atom and Molecular Emission Accompanying Fracture of Crystalline Inorganic Solids," American Ceramics Society, Cincinnati, OH, May 1985.

"Fracto-Emission Accompanying Failure of Metal/Glass Interfaces," American Ceramics Society, Cincinnati, OH, May 1985.

"Neutral Emission from the Fracture of Inorganic Crystals," American Ceramics Soc. Pacific Coast meeting, Irvine, CA, October, 1985.

"Fracto-Emission: Particles from the Fracture of Solids," 2nd International Conf. on Fundamentals of Fracture, Oak Ridge, Tenn., Nov. 1985.

"Atom and Molecule Emission Accompanying Fracture of Crystalline Solids," American Vacuum Society, Houston, TX, Nov. 1985.

"Electron Beam Induced Fracture of Polymers," American Vacuum Society, Houston, TX, Nov. 1985.

"Neutral Emission Accompanying the Fracture of MgO," American Physical Society, Las Vegas, NV, March, 1986.

"The Tear Energy of an Elastomer Under Electron Bombardment," American Physical Society, Las Vegas, NV, March, 1986.

"Electron Induced Crack Growth in Polymers," American Physical Society, Las Vegas, NV, March, 1986.

"Atom and Molecule Emission From Fracture of Single Crystal MgO," American Ceramics Society, Chicago, April, 1986.

"Failure of Pressure Sensitive Adhesives: Dependence of Photons and Radiowave Emissions on the Interface Properties," SAMPE Symposium, Las Vegas, April, 1986.

"Changes in Surface Morphology and Microcrack Initiation in Polymers under Simultaneous Exposure to Stress and Fast Atom Bombardment," ASTM Conference on Radiation Effects, Seattle, WA, June, 1986.

"Electron Beam Induced Fracture in Polymers," Symposium on Environmental Effects in Materials, Battelle PNW Laboratories, Richland, WA, August, 1986.

"Fracto-Emission Accompanying the Deformation and Failure of Composites and Adhesive *Joints*," *18th International* SAMPE Technical Conference, October, 1986.

"Bombardment Induced Crack Initiation and Crack Growth in Polymers," 18th International SAMPE Technical Conference, October, 1986.

"Neutral Particle Emission from the Fracture of Inorganic Materials, American Ceramics Soc. Pacific Coast meeting, Seattle, October, 1986.

"The Emission of Atoms and Molecules from the Fracture of MgO," American Vacuum Society. Baltimore, October, 1986.

"Radiation Induced Crack Initiation and Crack Growth," American Vacuum Society, Baltimore, October, 1986.

"Emission of Atoms and Molecules from Fracture of Inorganic Single Crystals," Am. Cer. Soc. National Meeting, Pittsburgh, 1987.

"Neutral Atom and Molecule Emission from the Fracture of Alkali Silicate Glasses," Am. Cer. Soc. National Meeting, Pittsburgh, 1987.

PUBLICATIONS:

J. T. Dickinson, A. Jahan-Latibari, and L. C. Jensen, "Fracto-Emission from Single Fibers of Kevlar-49," J. Mat. Sci. 20, 1835 (1985).

J. T. Dickinson, A. Jahan-Latibari, and L. C. Jensen, "Electron Emission and Acoustic Emission from the Fracture of Graphite/Epoxy Composites," J. Mat. Sci. 20, 229 (1985).

J. T. Dickinson, L. C. Jensen, and S. Bhattacharya "Fracto- Emission from the Failure of Metal/Epoxy Interfaces," J. Vac. Sci. Technol. A3, 1398 (1985).

J. T. Dickinson, W. D. Williams, and L. C. Jensen, "Fracto- Emission from Lead Zirconate-Titanate," J. Am. Cer. Soc., 68 235 (1985).

J. T. Dickinson, X. A. Shen, and L. C. Jensen, "Peeling of Pressure Sensitive Adhesives," Proceedings of the 30th National SAMPE Symposium, 1985.

E. E. Donaldson, X. A. Shen, and J. T. Dickinson, "Photon and Radiowave Emission from Peeling Pressure Sensitive Adhesives in Air," Proceedings of the 30th National SAMPE Symposium, 1985.

M. H. Miles, J. T. Dickinson, and L. C. Jensen, "Fracto- Emission from Single Crystals of PETN," J. Appl. Phys. 57, 5048 (1985).

J. T. Dickinson, A. Jahan-Latibari, and L. C. Jensen, "Fracto-Emission from Fiber-Reinforced and Particulate Filled Composites," in Polymer Composites and Interfaces, ed. by N. G. Kumar and H. Ishida (Plenum Publishers, New York), Review Article, 1985.

J. T. Dickinson and L. C. Jensen, "Fracto-Emission from Filled and Unfilled Polybutadiene," J. Poly. Sci.: Poly. Phys. Edition 23, 873 (1985).

J. T. Dickinson, M. J. Dresser, and L. C. Jensen, "Time Correlation of Ion and Electron Emission from Surfaces Following Fracture," in Desorption Induced by Electronic Transitions (DIET II), W. Brenig and D. Menzel, ed., Springer-Verlag, Berlin, (1985).

L. A. K'Singam, J. T. Dickinson, and L. C. Jensen, "Electron and Photon Emission Accompanying Failure of Metal/Glass Interfaces," J. Am. Ceramics Soc. 68, 510 (1985).

J. T. Dickinson, M. L. Klakken, M. H. Miles, and L. C. Jensen, "Electron Beam Induced Fracture of Polymers," J. Poly. Sci.: Poly. Phys. Ed. 23, 873 (1985).

E. E. Donaldson, J. T. Dickinson, and X. A. Shen, "Time and Size Correlations of Photon and Radiowave Bursts from Peeling Pressure Sensitive Adhesives in Air," J. Adhesion 19, 267 (1986).

J. T. Dickinson, L. C. Jensen, and M. R. McKay, "Emission of Atoms and Molecules Due To Fracture of Single Crystal MgO," J. Vac. Sci. Technol. 4A, 1648 (1986).

J. T. Dickinson, L. C. Jensen, and M. L. Klakken, "Electron Beam Induced Fracture of Kevlar Single Fibers," J. Vac. Sci. Technol. 4A, 1501 (1986).

E. E. Donaldson and J. T. Dickinson, "Autographs of Adhesive Failure: Direct Recording of Photon Emission on Photographic Film," Proceedings of the 31st International Symposium, SAMPE (1986).

J. T. Dickinson, S. Bhattacharya, and L. C. Jensen, "Fracto-emission from Neat Epoxy Resin" (review article), Die Makromolekulare Chemie 7 129 (1987).

J. T. Dickinson and M. A. Loudiana, "Radiation Induced Damage of Optical Coatings", Proceedings of the ACS Division of Polymeric Materials: Science and Engineering 56, 680 (1987).

J. T. Dickinson, "Fracto-Emission Accompanying the Deformation and Failure of Crosslinked Polymers and Interfaces", Proceedings of the ACS Division of Polymeric Materials: Science and Engineering 56, 264 (1987).

J. T. Dickinson, "Bombardment Induced Crack Initiation and Crack Growth in Polymers and Polymer Surfaces", Proceedings of the ACS Division of Polymeric Materials: Science and Engineering 56, 282 (1987).

J. T. Dickinson, L. C. Jensen, and M. R. McKay, "Neutral Molecule Emission from the Fracture of Crystalline MgO," submitted to J. Vac. Sci. Technol.

J. T. Dickinson, K. Tonyali, M. L. Klakken, and L. C. Jensen, "Crack Initiation and Crack Growth in Polymers Induced by Electron Bombardment," submitted to J. Vac. Sci. Technol.

J. T. Dickinson, M. L. Klakken, and L. C. Jensen, "Bombardment Induced Crack Initiation and Crack Growth in Polymers," Proceedings of the 18th International Technical Conference, SAMPE, October, 1986, pp 983-992.

J. T. Dickinson, L. C. Jensen, and W. D. Williams, "Fracto- Emission Accompanying the Deformation and Failure of Composites and Adhesive Joints," Proceedings of the 18th International Technical Conference, SAMPE, October, 1986, pp 390-400.

A. S. Castro, R. Corey, J. T. Dickinson, R. V. Subramanian, and Y. Eckstein, "Correlation of Photon and Acoustic Emission with Failure Events in Model Composites," Composites Sci. & Technol., to be published.

R. Michael, S. Frank, D. Stulik, and J. T. Dickinson, "Changes in Surface Morphology and Microcrack Initiation in Polymers under Simultaneous Exposure to Stress and Fast Atom Bombardment," Proceedings of 1986 ASTM Conference on Radiation Effects in Materials, Seattle, WA (1986), to be published.

M. A. Loudiana, J. T. Dickinson, A. Schmid, and E. J. Ashley, "Electron Enhanced Sorption of Fluorine by Silver Surfaces," Appl. Surf. Sci., to be published.

F. Freund, J. T. Dickinson, R. M. Knobel, and F. Struwe, "Degassing of Olivine and the Synthesis of Organic Molecules," submitted to Geochim. Cosmochim. Acta.

S. C. Langford, J. T. Dickinson, and L. C. Jensen, "Simultaneous Measurements of the Electron and Photon Emission Accompanying Fracture of Single Crystal MgO," submitted to J. Appl. Phys.

J. T. Dickinson and L. C. Jensen, "Fracto-Emission from Polymers, Crystals, and Interfaces," to appear in Proceedings of O-E/LASE '87, The International Society for Optical Engineering, SPIE, Bellingham, WA.

J. T. Dickinson and E. E. Donaldson, "Autographs from Peeling Pressure Sensitive Adhesives: Direct Recording of Fracture Induced Photon Emission," submitted to J. Adhesion.

Ser 432/84/211DYN
Revised January 1985

(DYN)

DISTRIBUTION LIST

Dr. R.S. Miller
Office of Naval Research
Code 432P
Arlington, VA 22217
(10 copies)

Dr. J. Pastine
Naval Sea Systems Command
Code 06R
Washington, DC 20362

Dr. Kenneth D. Hartman
Hercules Aerospace Division
Hercules Incorporated
Alleghany Ballistic Lab
P.O. Box 210
Washington, DC 21502

Mr. Otto K. Heiney
AFATL-DLJG
Elgin AFB, FL 32542

Dr. Merrill K. King
Atlantic Research Corp.
5390 Cherokee Avenue
Alexandria, VA 22312

Dr. R.L. Lou
Aerojet Strategic Propulsion Co.
Bldg. 05025 - Dept 5400 - MS 167
P.O. Box 15699C
Sacramenta, CA 95813

Dr. R. Olsen
Aerojet Strategic Propulsion Co.
Bldg. 05025 - Dept 5400 - MS 167
P.O. Box 15699C
Sacramento, CA 95813

Dr. Randy Peters
Aerojet Strategic Propulsion Co.
Bldg. 05025 - Dept 5400 - MS 167
P.O. Box 15699C
Sacramento, CA 95813

Dr. D. Mann
U.S. Army Research Office
Engineering Division
Box 12211
Research Triangle Park, NC 27709-2211

Dr. L.V. Schmidt
Office of Naval Technology
Code 07CT
Arlington, VA 22217

JHU Applied Physics Laboratory
ATTN: CPIA (Mr. T.W. Christian)
Johns Hopkins Rd.
Laurel, MD 20707

Dr. R. McGuire
Lawrence Livermore Laboratory
University of California
Code L-324
Livermore, CA 94550

P.A. Miller
736 Leavenworth Street, #6
San Francisco, CA 94109

Dr. W. Moniz
Naval Research Lab.
Code 6120
Washington, DC 20375

Dr. K.F. Mueller
Naval Surface Weapons Center
Code R11
White Oak
Silver Spring, MD 20910

Prof. M. Nicol
Dept. of Chemistry & Biochemistry
University of California
Los Angeles, CA 90024

Mr. L. Roslund
Naval Surface Weapons Center
Code R10C
White Oak, Silver Spring, MD 20910

Dr. David C. Sayles
Ballistic Missile Defense
Advanced Technology Center
P.O. Box 1500
Huntsville, AL 35807

(DYN)

DISTRIBUTION LIST

Mr. R. Geisler
ATTN: DY/MS-24
AFRPL
Edwards AFB, CA 93523

Naval Air Systems Command
ATTN: Mr. Bertram P. Sobers
NAVAIR-320G
Jefferson Plaza 1, RM 472
Washington, DC 20361

R.B. Steele
Aerojet Strategic Propulsion Co.
P.O. Box 15699C
Sacramento, CA 95813

Mr. M. Stosz
Naval Surface Weapons Center
Code R10B
White Oak
Silver Spring, MD 20910

Mr. E.S. Sutton
Thiokol Corporation
Elkton Division
P.O. Box 241
Elkton, MD 21921

Dr. Grant Thompson
Morton Thiokol, Inc.
Wasatch Division
MS 240 P.O. Box 524
Brigham City, UT 84302

Dr. R.S. Valentini
United Technologies Chemical Systems
P.O. Box 50015
San Jose, CA 95150-0015

Dr. R.F. Walker
Chief, Energetic Materials Division
DRSMC-LCE (D), B-3022
USA ARDC
Dover, NJ 07801

Dr. Janet Wall
Code 012
Director, Research Administration
Naval Postgraduate School
Monterey, CA 93943

Director
US Army Ballistic Research Lab.
ATTN: DRXBR-IBD
Aberdeen Proving Ground, MD 21005

Commander
US Army Missile Command
ATTN: DRSMI-RKL
Walter W. Wharton
Redstone Arsenal, AL 35898

Dr. Ingo W. May
Army Ballistic Research Lab.
ARRADCOM
Code DRXBR - IBD
Aberdeen Proving Ground, MD 21005

Dr. E. Zimet
Office of Naval Technology
Code 071
Arlington, VA 22217

Dr. Ronald L. Derr
Naval Weapons Center
Code 389
China Lake, CA 93555

T. Boggs
Naval Weapons Center
Code 389
China Lake, CA 93555

Lee C. Estabrook, P.E.
Morton Thiokol, Inc.
P.O. Box 30058
Shreveport, Louisiana 71130

Dr. J.R. West
Morton Thiokol, Inc.
P.O. Box 30058
Shreveport, Louisiana 71130

Dr. D.D. Dillehay
Morton Thiokol, Inc.
Longhorn Division
Marshall, TX 75670

G.T. Bowman
Atlantic Research Corp.
7511 Wellington Road
Gainesville, VA 22065

Ser 432/84/211DYN
Revised January 1985

(DYN)

DISTRIBUTION LIST

R.E. Shenton
Atlantic Research Corp.
7511 Wellington Road
Gainesville, VA 22065

Brian Wheatley
Atlantic Research Corp.
7511 Wellington Road
Gainesville, VA 22065

Mike Barnes
Atlantic Research Corp.
7511 Wellington Road
Gainesville, VA 22065

Mr. G. Edwards
Naval Sea Systems Command
Code 62R32
Washington, DC 20362

Dr. Lionel Dickinson
Naval Explosive Ordinance
Disposal Tech. Center
Code D
Indian Head, MD 20340

C. Dickinson
Naval Surface Weapons Center
White Oak, Code R-13
Silver Spring, MD 20910

Prof. J.T. Dickinson
Washington State University
Dept. of Physics 4
Pullman, WA 99164-2814

Prof. John Deutch
MIT
Department of Chemistry
Cambridge, MA 02139

M.H. Miles
Dept. of Physics
Washington State University
Pullman, WA 99164-2814

Dr. E.H. deButts
Hercules Aerospace Co.
P.O. Box 27408
Salt Lake City, UT 84127

Dr. T.F. Davidson
Vice President, Technical
Morton Thiokol, Inc.
Aerospace Group
110 North Wacker Drive
Chicago, Illinois 60606

David A. Flanigan
Director, Advanced Technology
Morton Thiokol, Inc.
Aerospace Group
110 North Wacker Drive
Chicago, Illinois 60606

Mr. J. Consaga
Naval Surface Weapons Center
Code R-16
Indian Head, MD 20640

Dr. L.H. Caveny
Air Force Office of Scientific
Research
Directorate of Aerospace Sciences
Bolling Air Force Base
Washington, DC 20332

Naval Sea Systems Command
ATTN: Mr. Charles M. Christensen
NAVSEA-62R2
Crystal Plaza, Bldg. 6, Rm 806
Washington, DC 20362

W.G. Roger
Code 5253
Naval Ordance Station
Indian Head, MD 20640

Mr. R. Beauregard
Naval Sea Systems Command
SEA 64E
Washington, DC 20362

Dr. Donald L. Ball
Air Force Office of Scientific
Research
Directorate of Chemical &
Atmospheric Sciences
Bolling Air Force Base
Washington, DC 20332

Ser 432/84/211DYN
Revised January 1985

(DYN)

DISTRIBUTION LIST

Dr. Anthony J. Matuszko
Air Force Office of Scientific Research
Directorate of Chemical & Atmospheric Sciences
Bolling Air Force Base
Washington, DC 20332

Dr. Michael Chaykovsky
Naval Surface Weapons Center
Code R11
White Oak
Silver Spring, MD 20910

J.J. Rocchio
USA Ballistic Research Lab.
Aberdeen Proving Ground, MD 21005-5066

G.A. Zimmerman
Aerojet Tactical Systems
P.O. Box 13400
Sacramento, CA 95813

B. Swanson
INC-4 MS C-346
Los Alamos National Laboratory
Los Alamos, New Mexico 87545

Dr. James T. Bryant
Naval Weapons Center
Code 3205B
China Lake, CA 93555

Dr. L. Rothstein
Assistant Director
Naval Explosives Dev. Engineering Dept.
Naval Weapons Station
Yorktown, VA 23691

Dr. M.J. Kamlet
Naval Surface Weapons Center
Code R11
White Oak, Silver Spring, MD 20910

Dr. Henry Webster, III
Manager, Chemical Sciences Branch
ATTN: Code 5063
Crane, IN 47522

Dr. A.L. Slafkosky
Scientific Advisor
Commandant of the Marine Corps
Code RD-1
Washington, DC 20380

Dr. H.G. Adolph
Naval Surface Weapons Center
Code R11
White Oak
Silver Spring, MD 20910

U.S. Army Research Office
Chemical & Biological Sciences Division
P.O. Box 12211
Research Triangle Park, NC 27709

G. Butcher
Hercules, Inc.
MS X2H
P.O. Box 98
Magna, Utah 84044

W. Waesche
Atlantic Research Corp.
7511 Wellington Road
Gainesville, VA 22065

Dr. John S. Wilkes, Jr.
FJSRL/NC
USAF Academy, CO 80840

Dr. H. Rosenwasser
AIR-320R
Naval Air Systems Command
Washington, DC 20361

Dr. Joyce J. Kaufman
The Johns Hopkins University
Department of Chemistry
Baltimore, MD 21218

Dr. A. Nielsen
Naval Weapons Center
Code 385
China Lake, CA 93555

(DYN)

DISTRIBUTION LIST

K.D. Pae
High Pressure Materials Research Lab.
Rutgers University
P.O. Box 909
Piscataway, NJ 08854

Dr. John K. Dienes
T-3, B216
Los Alamos National Lab.
P.O. Box 1663
Los Alamos, NM 87544

A.N. Gent
Institute Polymer Science
University of Akron
Akron, OH 44325

Dr. D.A. Shockey
SRI International
333 Ravenswood Ave.
Menlo Park, CA 94025

Dr. R.B. Kruse
Morton Thiokol, Inc.
Huntsville Division
Huntsville, AL 35807-7501

G. Butcher
Hercules, Inc.
P.O. Box 98
Magna, UT 84044

W. Waesche
Atlantic Research Corp.
7511 Wellington Road
Gainesville, VA 22065

Dr. R. Bernecker
Naval Surface Weapons Center
Code R13
White Oak
Silver Spring, MD 20910

Prof. Edward Price
Georgia Institute of Tech.
School of Aerospace Engineering
Atlanta, GA 30332

J.A. Birkett
Naval Ordnance Station
Code 5253K
Indian Head, MD 20640

Prof. R.W. Armstrong
University of Maryland
Dept. of Mechanical Engineering
College Park, MD 20742

Herb Richter
Code 385
Naval Weapons Center
China Lake, CA 93555

J.T. Rosenberg
SRI International
333 Ravenswood Ave.
Menlo Park, CA 94025

G.A. Zimmerman
Aeroject Tactical Systems
P.O. Box 13400
Sacramento, CA 95813

Prof. Kenneth Kuo
Pennsylvania State University
Dept. of Mechanical Engineering
University Park, PA 16802

T.L. Boggs
Naval Weapons Center
Code 3891
China Lake, CA 93555

Ser 432/84/340
Revised January 1985

(DTM)

DISTRIBUTION LIST

Dr. C.S. Coffey
Naval Surface Weapons Center
Code R13
White Oak
Silver Spring, MD 20910

D. Curran
SRI International
333 Ravenswood Avenue
Menlo Park, CA 94025

E.L. Throckmorton
Code SP-2731
Strategic Systems Program Office
Crystal Mall #3, RM 1048
Washington, DC 20376

Dr. R. Martinson
Lockheed Missiles and Space Co.
Research and Development
3251 Hanover Street
Palo Alto, CA 94304

C. Gotzmer
Naval Surface Weapons Center
Code R-11
White Oak
Silver Spring, MD 20910

G.A. Lo
3251 Hanover Street
B204 Lockheed Palo Alto Research Lab
Palto Alto, CA 94304

R.A. Schapery
Civil Engineering Department
Texas A&M University
College Station, TX 77843

J.M. Culver
Strategic Systems Projects Office
SSPO/SP-2731
Crystal Mall #3, RM 1048
Washington, DC 20376

Prof. G.D. Duvall
Washington State University
Department of Physics
Pullman, WA 99163

Dr. E. Martin
Naval Weapons Center
Code 3858
China Lake, CA 93555

Dr. M. Farber
135 W. Maple Avenue
Monnovia, CA 91016

W.L. Elban
Naval Surface Weapons Center
White Oak, Bldg. 343
Silver Spring, MD 20910

G.E. Manser
Morton Thiokol
Wasatch Division
P.O. Box 524
Brigham City, UT 84302

R.G. Rosemeier
Brimrose Corporation
7720 Belair Road
Baltimore, MD 20742

Ser 432/84/340
Revised January 1985

Administrative Contracting
Officer (see contract for
address)
(1 copy)

Director
Naval Research Laboratory
Attn: Code 2627
Washington, DC 20375
(6 copies)

Defense Technical Information Center
Bldg. 5, Cameron Station
Alexandria, VA 22314
(12 copies)

Dr. Robert Polvani
National Bureau of Standards
Metallurgy Division
Washington, D.C. 20234

Dr. Y. Gupta
Washington State University
Department of Physics
Pullman, WA 99163